

**Analysis of Oligosaccharides**  
*via*  
**Ion Mobility-Mass Spectrometry**

Inaugural-Dissertation  
to obtain the academic degree  
Doctor rerum naturalium (Dr. rer. nat.)

submitted to the Department of Biology, Chemistry, Pharmacy  
of Freie Universität Berlin

by

Christian Manz  
from Schwerte, Germany

2022



The work reported in this thesis was performed from June 2017 to March 2022, at the Freie Universität Berlin and the Fritz Haber Institute of the Max Planck Society in Berlin, under the supervision of Prof. Dr. Kevin Pagel.

First Reviewer: Prof. Dr. Kevin Pagel  
Freie Universität Berlin

Second Reviewer: Prof. Dr. Christoph Schalley  
Freie Universität Berlin

Date of defense: 10.11.2022



# Eidesstattliche Erklärung

Hiermit erkläre ich an Eides statt, dass ich die vorliegende Dissertation selbstständig verfasst und keine als die angegebenen Hilfsmittel genutzt habe. Alle wörtlich oder inhaltlich übernommenen Stellen habe ich als solche gekennzeichnet. Ich versichere außerdem, dass ich die vorliegende Dissertation nur in diesem und keinem anderen Promotionsverfahren eingereicht habe und dass diesem Promotionsverfahren keine endgültig gescheiterten Promotionsverfahren vorausgegangen sind.

Berlin, März 2022

Christian Manz



# Abstract

Complex carbohydrates, also referred to as glycans, are ubiquitous in nature and represent one of the major classes of biopolymers. In contrast to peptides and oligonucleotides whose structure is directly related to specific genes, glycans are not directly encoded in the DNA. Instead, their structure is the result of a dynamic biosynthetic pathway that is heavily affected by environmental factors. Consequently, glycans are extremely diverse and exhibit branched sites, as well as a complex regio- and stereochemistry.

A common way to address this complexity is liquid chromatography (LC) in combination with spectroscopic and mass spectrometric (MS) detection. It allows for high throughput measurements and can identify the general building block composition of a glycan, but it often fails to unambiguously assign the linkage between building blocks. The type of linkage, however, is a key factor for the three-dimensional structure of the glycan and therefore its biological functions. A promising alternative, which is sensitive to the globular structure of a glycan, is ion mobility-mass spectrometry (IM-MS). In addition to the separation based on the mass-to-charge ( $m/z$ ) ratio, IM-MS allows to distinguish ions based on their size, shape, and charge. LC-MS and IM-MS both showed enormous potential for the analysis of glycans as standalone techniques, each providing a different level of information. However, there are very few examples of combining both approaches into a consistent LC-IM-MS workflow.

In this thesis, it was investigated if IM-MS can be hyphenated to classical LC-MS workflows to enable a comprehensive structural elucidation of complex *N*-glycans. As sample preparation for LC-MS usually includes the modification of the reducing end of the glycan, the first step was to study the effect of these derivatizations on the quality of IMS separation. The problem was addressed by the systematic study of a set of six isomeric fucose-containing blood group antigens that are derivatized with the most common fluorescent tags using IMS. The quality of the separation was evaluated by comparing the CCS values of all species in positive and negative ion mode as well as with adduct ions. Afterwards, the application of LC-IMS-MS for the investigation of complex *N*-glycans was

demonstrated. For this purpose, the glycans from human alpha-1-acid glycoprotein (hAGP) were investigated to identify the sialylation ( $\alpha$ 2,3- vs  $\alpha$ 2,6-linked residues) and fucosylation (core vs terminal) patterns. It was shown that IMS enables the structural elucidation of even highly sialylated glycans up to tetraantennary species without changing the sample preparation and within a single LC run. The main parameters that are obtained from LC-IMS-MS measurements are retention times, mass-to-charge-ratios, and drift times, which represent a powerful dataset to identify glycan isomers. However, retention times in LC and drift times in IMS depend significantly on instrumental parameters and are difficult to compare between experiments. We therefore introduced an internal calibration method for the conversion of retention times into universal glucose units (GU) and drift times into collisional cross-sections (CCS). It was shown that the internal calibration approach enabled a faster, more accurate analysis for both LC and IMS without loss in calibration accuracy or informational content.

Overall, the addition of IMS into classical LC-MS workflows is straightforward and only requires minor adaptations in sample preparation and data treatment. It enables a fast and accurate identification of structural motifs and complements the informational content of LC-MS experiments. LC-IM-MS therefore represents a powerful combinational approach for the comprehensive analysis of complex *N*-glycans.

# Zusammenfassung

Komplexe Kohlenhydrate, auch als Glykane bezeichnet, sind in der Natur allgegenwärtig und stellen eine der Hauptklassen von Biopolymeren dar. Im Gegensatz zu Peptiden und Oligonukleotiden, deren Struktur in direktem Zusammenhang mit bestimmten Genen steht, sind Glykane nicht direkt in der DNA kodiert. Stattdessen ist ihre Struktur das Ergebnis einer dynamischen und komplexen Biosynthese, der stark von Umweltfaktoren beeinflusst wird. Folglich sind Glykane äußerst vielfältig und weisen verzweigte Stellen sowie eine komplexe Regio- und Stereochemie auf.

Ein gängiger Weg, um dieser Komplexität zu begegnen, ist die Flüssigchromatographie (LC) in Kombination mit spektroskopischer und massenspektrometrischer (MS) Detektion. Es ermöglicht Messungen mit hohem Durchsatz und kann die allgemeine Zusammensetzung eines Glykans identifizieren, kann jedoch häufig die Verknüpfung zwischen Bausteinen nicht eindeutig zuordnen. Die Art der Verknüpfung ist jedoch ein Schlüsselfaktor für die dreidimensionale Struktur eines Glykans und damit mitverantwortlich für seine biologischen Funktionen. Eine vielversprechende Alternative, die sensitiv für die globuläre Struktur eines Glykans ist, ist die Ionenmobilitäts-Massenspektrometrie (IM-MS). Zusätzlich zur Trennung auf Basis des Masse-zu-Ladungsverhältnis ( $m/z$ ) ermöglicht IM-MS die Unterscheidung von Ionen basierend auf ihrer Größe, Form und Ladung. LC-MS und IM-MS zeigten beide großes Potenzial für die Analyse von Glykanen als eigenständige Techniken, die jeweils eine andere Informationsebene liefern. Es gibt jedoch nur sehr wenige Beispiele für die Kombination beider Ansätze zu einem konsistenten LC-IM-MS Arbeitsablauf.

In dieser Arbeit wurde untersucht, ob IM-MS mit klassischen LC-MS Arbeitsabläufen verknüpft werden kann, um eine umfassende Strukturaufklärung komplexer N-Glykane zu ermöglichen. Da die Probenvorbereitung für LC-MS normalerweise die Modifikation des reduzierenden Endes am Glykan beinhaltet, bestand der erste Schritt darin, die Auswirkung dieser Derivatisierungen auf die Qualität der IMS-Trennung zu untersuchen. Das Problem wurde durch die systematische Untersuchung eines Satzes von sechs

isomeren Blutgruppen Antigenen angegangen, die mit den gängigsten Fluoreszenzmarkern derivatisiert wurden und anschließend mittels IMS gemessen wurden. Die Qualität der Trennung wurde durch den Vergleich der CCS-Werte aller Spezies im positiven und negativen Ionenmodus sowie mit Addukt-Ionen bewertet. Anschließend wurde die Anwendung von LC-IMS-MS zur Untersuchung komplexer N-Glykane demonstriert. Zu diesem Zweck wurden die Glykane aus menschlichem alpha-1-acid Glykoprotein (hAGP) untersucht, um das Sialylierungs- ( $\alpha$ 2,3- vs.  $\alpha$ 2,6-Verknüpfung) und Fucosylierungsmuster (am reduzierenden Ende vs. terminal) zu identifizieren. Es konnte gezeigt werden, dass IMS die Strukturaufklärung selbst hochsialylierter Glykane bis hin zu tetraantennären Spezies ohne Änderung der Probenvorbereitung und innerhalb eines einzigen LC-Laufs ermöglicht. Die Hauptparameter, die aus LC-IMS-MS-Messungen erhalten werden, sind Retentionszeiten, Masse-zu-Ladungsverhältnisse und Driftzeiten, die eine hohe Informationsdichte zur Identifizierung von Glykanisomeren darstellen. Retentionszeiten in LC und Driftzeiten in IMS hängen jedoch erheblich von instrumentellen Parametern ab und sind zwischen Experimenten nur schwer zu vergleichen. Wir haben daher ein internes Kalibrierverfahren eingeführt, das die Umrechnung von Retentionszeiten in universelle Glucoseeinheiten (GU) und von Driftzeiten in Kollisionsquerschnitte (CCS) ermöglicht. Es wurde gezeigt, dass dies eine schnellere und genauere Analyse sowohl für LC als auch für IMS ohne Verlust der Kalibrierungsgenauigkeit oder des Informationsgehalts ermöglicht. Insgesamt ist die Integration von IMS in klassische LC-MS-Workflows unkompliziert und erfordert nur geringfügige Anpassungen bei der Probenvorbereitung und Datenverarbeitung. Es ermöglicht eine schnelle und genaue Identifizierung von Strukturmotiven und ergänzt den Informationsgehalt von LC-MS-Experimenten. LC-IMS-MS stellt daher einen leistungsstarken kombinatorischen Ansatz für die umfassende Analyse komplexer N-Glykane dar.

# Contents

<b>1 Introduction</b>	<b>1</b>
1.1 Motivation .....	1
1.2 Outline of the Thesis .....	3
<b>2 Fundamentals and Methods</b>	<b>5</b>
2.1 Structure of Glycans .....	5
2.1.1 Monosaccharides and the Formation of a Glycosidic Bond .....	5
2.1.2 N- and O-linked Glycosylation.....	9
2.2 Glycan Analysis <i>via</i> Liquid Chromatography and Mass Spectrometry .....	12
2.2.1 General Aspects .....	12
2.2.2 Derivatization of Glycans.....	13
2.2.3 Chromatographic Separation.....	17
2.2.4 Mass Spectrometric Detection .....	20
2.3 Glycan Analysis <i>via</i> Ion Mobility-Mass Spectrometry .....	22
2.3.1 Fundamentals of Ion Mobility .....	22
2.3.2 Types of Ion Mobility Separations .....	24
2.3.3 Examples of Ion Mobility Separations in Glycan Analysis .....	28
2.4 Combination of Liquid Chromatography and Ion Mobility-Mass Spectrometry ..	32
<b>3 Separation of Isomeric Glycans by Ion Mobility Spectrometry – the Impact of Fluorescent Labelling</b>	<b>33</b>
3.1 Introduction.....	33
3.2 Experimental Details .....	34
3.3 Results and Discussion .....	36
3.3.1 ABO and Lewis Blood Group System .....	36
3.3.2 Labelling of Glycans.....	37
3.3.3 Ion Mobility Separation of Labelled Glycans .....	39
3.3.4 Comparison of Isomeric Labelled Glycan Isomers.....	41
3.3.5 The Impact of Labelling on Fucose Migration.....	44
3.4 Conclusion .....	45

<b>4</b>	<b>Determination of Sialic Acid and Fucose Isomers from Released N-glycans</b>	
	<b>Using Ion Mobility Spectrometry</b>	<b>47</b>
4.1	Introduction .....	47
4.2	Experimental Details.....	49
4.3	Results and Discussion.....	51
4.3.1	Direct Injection IM-MS Analysis of Released Glycans.....	51
4.3.2	HILIC-MS Characterisation of N-Glycans Released from hAGP.....	55
4.3.3	Quantitative Assignment of Sialic Acid Isomers based on LC-IM-MS ...	56
4.3.4	Assignment of Fucosylated Complex N-glycans .....	59
4.4	Conclusion.....	63
<b>5</b>	<b>Dextran as Universal Calibrant for N-Glycan Analysis by Liquid</b>	
	<b>Chromatography Coupled to Ion Mobility-Mass Spectrometry</b>	<b>65</b>
5.1	Introduction .....	65
5.2	Experimental Details.....	66
5.3	Results and Discussion.....	69
5.3.1	External GU calibration.....	69
5.3.2	Internal GU calibration.....	70
5.3.3	CCS calibration.....	73
5.4	Conclusion.....	75
<b>6</b>	<b>Summary and Future Perspective</b>	<b>77</b>
	<b>References</b>	<b>81</b>
	<b>Appendix A Sialic Acid and Fucose Determination</b>	<b>97</b>
	<b>Appendix B Internal Dextran Calibration</b>	<b>102</b>
	<b>List of Publications</b>	<b>108</b>

# 1 Introduction

## 1.1 Motivation

There are four major biomolecular classes (proteins, DNA, lipids, and glycans) and each of them takes over important biological functions. Proteins and DNA, however, are especially valued for their fundamental role in the development of life as we know it and thus, they are termed the first and second revolution in evolution. Each molecular machine (*e.g.*, a protein or enzyme) is encoded in an individual genetic template and the absolute number of genes is often used as indicator for the complexity of life. But the number of genes of eukaryotes is not much higher compared to simple bacterial lifeforms, so how can the gigantic gap in complexity be explained?

Scientists nowadays claim that glycosylation—the addition of glycans to other biopolymers—should be considered the third revolution in evolution because it allows for the creation of multiple novel molecular structures from within one genetic template. In contrast to peptides and oligonucleotides whose structure is directly related to specific genes, glycans are not directly encoded in the DNA. Instead, their structure is the result of a dynamic and complex biosynthetic pathway, which is affected by a variety of genetic and environmental factors.<sup>1</sup> Glycosylation can adapt to these factors and thereby has a huge impact on the biopolymers they are bound to. Changes in glycosylation can induce alterations in the overall structure (such as folding) and even functionalize the glycoconjugate for novel purposes.

As glycosylation is sensitive to the environment in the cell, it reflects the overall cellular status in health and disease.<sup>2</sup> Changes in the glycosylation can therefore serve as indicator for pathogenic processes such as cancer and make glycans a key player in diagnostic and therapeutic research.<sup>3-5</sup> But the understanding of structure-function relationships for glycosylated structures is still lacking behind the understanding for proteomics or genomics. The main reason for that lies in their complexity: a very large number of different glycans can be made by varying number, order and type of monosaccharide building blocks.<sup>6, 7</sup> This results in many three-dimensional structures that differ

tremendously in their biological function. The development of novel analytical tools for the analysis of complex glycans is therefore the most important task to improve our understanding of the physiological processes that are regulated by glycans.

Historically, analytical techniques for glycan analysis originate from proteomics and genomics and include (among others) nuclear magnetic resonance spectroscopy (NMR)<sup>8</sup> and X-ray crystallography as well as capillary electrophoresis (CE)<sup>9</sup>, high performance liquid chromatography (HPLC)<sup>10</sup> and mass spectrometry (MS)<sup>11, 12</sup>. While NMR and X-ray crystallography provide extremely high resolution for glycan structures, they are usually limited by the required sample purity, volume, and the low throughput.

As a consequence, recent glycomics studies adopt combinational approaches of LC or CE with MS detection that require low volumes of sample and offer potential for automatic measurements in a high throughput fashion.<sup>13, 14</sup> As glycans usually occur in complex mixtures, LC separation is necessary to simplify the complex sample matrix and thereby isolate each compound for improved identification. The very polar glycans are not retained on commonly employed reversed phase (RP) columns, therefore specialised stationary phase such as porous graphitic carbon (PGC) or hydrophilic interaction chromatography (HILIC) are applied. Derivatized glycans are subsequently detected *via* UV or fluorescence and can often be directly identified based on their elution order and prior knowledge on the biosynthetic pathway. The resolving power for isomeric glycans, however, is limited and often multiple species elute at the same time, rendering it impossible to determine the structure of unknown samples. Therefore, LC separation is often coupled to MS as the spectrometric detection allows for sensitive measurements and an unambiguous assignment of glycans with the same retention time, but different mass. The fragmentation of the glycan precursor in the gas phase (MS/MS) even allows to define the general building block composition. LC-MS established itself as gold standard for glycan analysis due to its high throughput and detailed information on the glycan structure.

The level of detail, however, is usually limited to the general composition and structure of the glycan. The type of linkage in between the different building blocks (which defines

their three-dimensional structure and therefore is important for their biological function) often remains elusive.

An alternative to LC-MS recently came up in the form of ion mobility-mass spectrometry (IMS).<sup>15, 16</sup> IMS is an electrophoretic gas-phase technique that can separate glycan isomers based on their mass, size, shape and charge.<sup>17, 18</sup> IMS enables to distinguish linkage isomers and can be applied to intact glycans as well as to fragment ions<sup>19-21</sup>. Although the measurements are usually limited in throughput and can hardly be automated, the separation of glycans in the gas phase is expected to be more universal as it does not depend on the nature of the stationary phase as opposed to conventional LC.

LC-MS<sup>22-25</sup> and IMS<sup>19-21</sup> both showed great potential for the analysis of glycans as standalone techniques, each providing a different level of information. However, there are very few examples of combining both approaches into a consistent LC-IM-MS workflow. IMS can be directly hyphenated with LC-MS with minor adaptations of existing instrumental setups, thereby offering an additional and orthogonal dimension of separation in a suitable timescale. Such a ready-to-use instrumental setup could therefore help to fill the informational gap left behind by LC-MS by fully unravelling the monosaccharide composition and the type of linkage in between them. We envision that LC-IM-MS has the potential to serve as a universal analysis tool for the structural elucidation of glycans and glycoconjugates.

## 1.2 Outline of the Thesis

This thesis is dedicated to the direct hyphenation of LC-MS and IMS into a consistent workflow for glycan analysis. To establish the theoretical foundation of the exposed work, **chapter 2** starts with an introduction into structural aspects of glycosylation and subsequently introduces in more detail analytical techniques used here to elucidate their complex structure.

The analysis of glycans very often includes the modification of the glycan structure to improve the separation in the LC and/or MS dimensions. Most commonly, glycans are modified at the reducing end with a fluorescent label to enable spectroscopic detection

and easier quantification. Although fundamental for the analysis *via* LC-MS, there is very little information about the use of fluorescent labels in combination with IMS. Therefore, in **chapter 3**, the influence of commonly applied fluorescent labels on the quality of mobility separations is evaluated. In addition, the impact of a variety of adducts and the influence of ion polarity on the resolution of glycan separations in IMS is described.

In **chapter 4**, the application of LC-IMS-MS for the investigation of complex *N*-glycans is demonstrated. For this purpose, the glycans from human alpha-1-acid glycoprotein (hAGP) are investigated to determine the level and type of sialic acids. Sialic acids can appear as  $\alpha$ 2,3- and  $\alpha$  2,6-linked residues and represent an important biomarker in therapeutic research. It is examined if the addition of IMS into the classical LC-MS workflow can replace commonly applied enzymatic digestions and thereby improve and simplify routine *N*-glycan analysis. The workflow is further assessed on the separation and quantitation of other important structural glycan motifs.

In addition to sample preparation and LC-IM-MS measurements, also data analysis requires substantial adaptations to allow for a meaningful integration of IMS into the LC-MS workflow. The main parameters that are obtained from LC-IMS-MS measurements are retention times, mass-to-charge-ratios, and drift times, which represent a powerful dataset to identify glycan isomers. However, retention times in LC and drift times in IMS depend significantly on instrumental parameters and are prone to shifting, which makes it hard to compare with databases. In **chapter 5**, we tackle this challenge and introduce an internal calibration method for the conversion of retention times into universal glucose units (GU) and drift times into collisional cross-sections (CCS).

Finally, **chapter 6** concludes the thesis und discusses future prospects for instrumental developments as well as *N*-glycan analysis in general.

## 2 Fundamentals and Methods

### 2.1 Structure of Glycans

#### 2.1.1 *Monosaccharides and the Formation of a Glycosidic Bond*

The term carbohydrates goes back more than a century and is literally derived from naturally occurring “hydrates of carbon”, expressed in the general chemical formula  $C_x(H_2O)_n$ . Nowadays the term also involves the derivatives of the originally formula which contain other functional groups and heteroatoms like nitrogen and sulphur. The terms glycans, sugars and carbohydrates are used for this class of biomolecules and no sharp distinction in nomenclature exists.<sup>7</sup> Therefore, the different terms will be used interchangeably in this work.

The biomass on earth is mostly made up from carbohydrates, be it in the form of short mono- or disaccharides such as table sugar and milk sugar or as long, regular polysaccharides such as cellulose and starch. In addition to their enormous importance as energy suppliers and as structural polymers, sugars also play a crucial role in a number of physiological processes.<sup>26</sup> Here, mostly complex and branched structures assume essential functions such as sensors in biological communication processes. They are often attached to other biomolecules such as proteins or lipids and thereby significantly influence their function and structure.<sup>27</sup> Due to the large number of different biological functions of carbohydrates, it is essential to not only know their composition, but also their fine structure to understand structure-function associated properties.

Monosaccharides are the smallest building blocks from which larger carbohydrates are built up. Because of their different chemical functionalities, one divides monosaccharides into aldoses (polyhydroxyaldehydes) and ketoses (polyhydroxyketones). Aldoses carry an aldehyde group at the terminal C atom of the chain, whereas ketoses have a keto group on the second carbon atom of the carbon chain. As sugars mostly differ in the relative orientation of individual OH groups, a chemical representation of the stereochemistry of

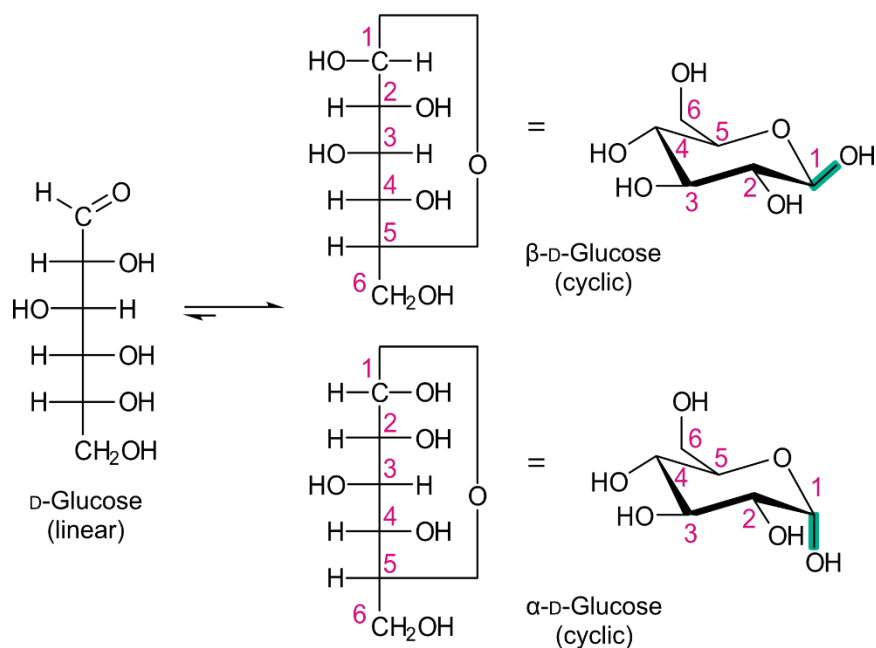


**Figure 1:** Visual representation of d-Glucose in the Fischer Projection and after cyclization. The configuration of the naturally occurring d-glucose is defined based on the orientation of the hydroxyl group at the penultimate carbon (C5), depending on whether it is displayed on the left (l-configuration) or right side (d-configuration). The cyclization happens between C1 and C5 and represents the preferred structural form of monosaccharides. When the ring is closed, a new stereocentre is formed. Depending on the reference atom C5, it can either be labelled  $\alpha$  for a trans position or  $\beta$  for a cis position.

sugars, known today as Fischer projection, was invented in the 1890s. The Fischer projection is based on a perpendicular arrangement of the longest carbon chain, where the most oxidized carbon atom (i.e., the aldehyde function in aldoses and the keto group in ketoses) is placed on top of the carbon chain (**Figure 1**). This projection does only allow to distinguish between D- and L- enantiomers of sugars but enables a simplified identification of all kinds of monosaccharides based on the orientation (left or right direction) of the hydroxyl residues. Each monosaccharides contains at least one asymmetric carbon atom in its chain and its total number is equal to the number of internal carbons bound to a hydroxyl group ( $n-2$  for aldoses and  $n-3$  for ketoses with  $n$  carbon atoms). The total number of stereoisomers corresponds to  $2^k$ , where  $k$  equals the number of asymmetric carbon atoms. This complexity can be shown by an aldose with six carbon atoms and the general formula  $\text{C}_6\text{H}_{12}\text{O}_6$ : It contains four asymmetric carbon atoms and therefore sixteen possible isomeric monosaccharides can be formed. In nature,

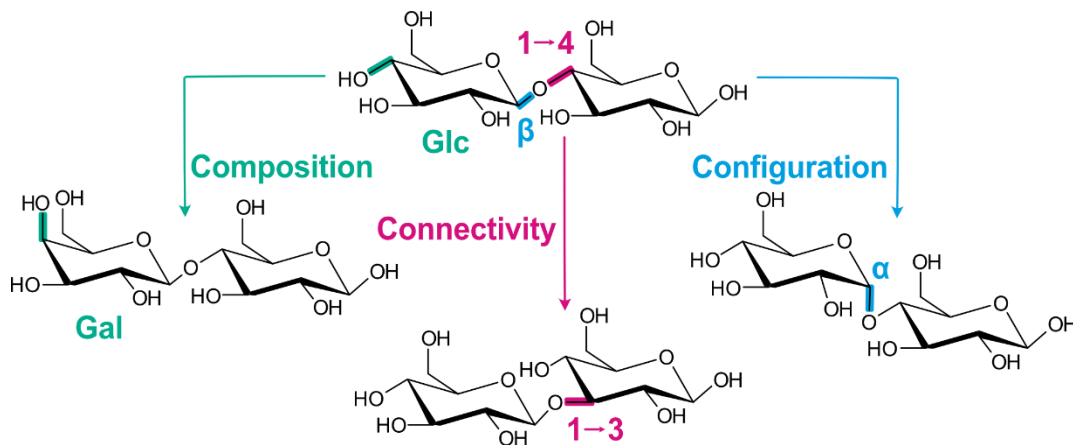


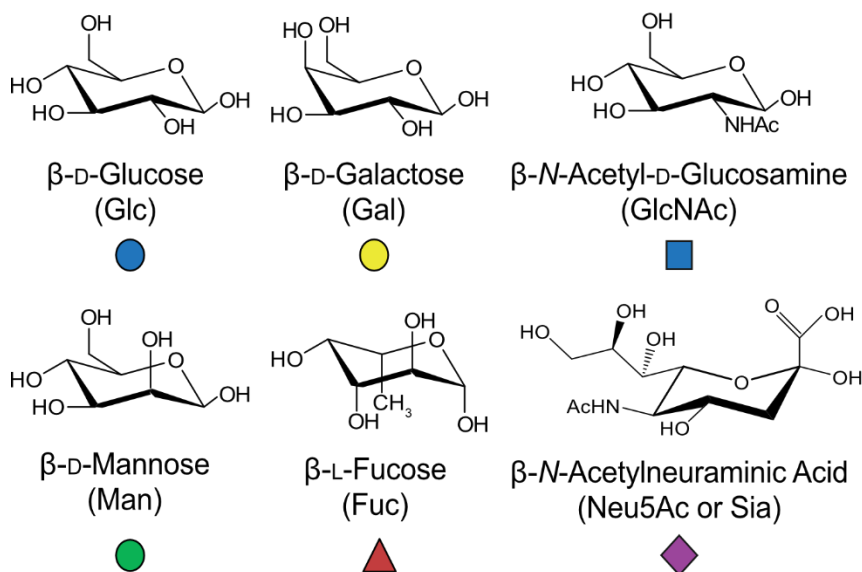
**Figure 2:** Main characteristics that define a carbohydrate structure. Carbohydrates can differ in their composition, e.g., the type of monosaccharides, in the connectivity between two monosaccharides, as well as in the configuration of the anomeric centre resulting in a large variety of isomers.

monosaccharide are rarely found as open chain but are frequently present in a ring conformation as the result of an enthalpically favoured cyclization reaction. For hexoses, this reaction includes the binding of the hydroxyl group at position 4 or 5 with the aldehyde at C-1, leading to a five membered ring, called furanose, or a six membered ring, called pyranose, respectively.<sup>28</sup> Pyranose rings are usually structurally preferred due to less torsional strain. Furthermore, the cyclization reaction leads to the creation of a new stereogenic centre at C-1, called the anomeric centre.<sup>29</sup> Depending on the configuration of the reference atom at C-5, the resulting monosaccharide configuration is either called  $\alpha$  for a *trans*-relationship or  $\beta$  for a *cis*-relationship, but is interchangeable due to the equilibrium between linear and cyclic form in a process called mutarotation.

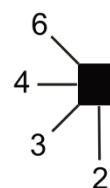
Two monosaccharides can react together to form a glycosidic bond—this is the fundamental linkage between all monosaccharide building blocks. The glycosidic bond is formed between the C1 (anomeric centre) of one monosaccharide and a hydroxyl group of another under condensation. The result gives rise to an extreme diversity of complex structures which can be categorized *via* three important structural parameters: composition, connectivity, and configuration (**Figure 2**).

The composition defines the type of monosaccharide building blocks used, such as glucose (Glc), galactose (Gal) or N-acetylglucosamine (GlcNAc). In the human body, there are nine

## A - Composition



## B - Connectivity



## C - Configuration

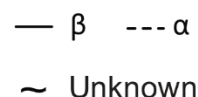


**Figure 3:** SNFG nomenclature of carbohydrates. Sugars are represented by different geometrical shapes and colours, while regio- and stereochemistry is indicated by the type and orientation of the linkage. There are nine common monosaccharides present in vertebrates and the six building blocks important for this work are shown in SNFG nomenclature.

common monosaccharides present, but once incorporated into bigger glycan structures, these monosaccharides can be further modified and epimerized to result in a much greater variety. Furthermore, many of these building blocks only differ in the orientation of a single hydroxyl group, such as glucose and galactose that are C4 epimers. The connectivity describes the regiochemistry of the glycosidic bond and is important for the three-dimensional structure of the oligosaccharide. As typical monosaccharides contain multiple free hydroxyl groups, different connectivities can result in an extremely high diversity of different linkages and branched structures.<sup>7</sup> In addition, while forming the glycosidic bond, the anomeric carbon atom is converted from a hemiacetal into a full acetal and thereby creates a new, permanent stereocentre. The stereochemistry of the acetal is described as  $\alpha$  or  $\beta$  configuration.

Due to their enormous structural complexity, the structure of glycan molecules cannot be easily accessed by their structural formula. For linear molecules such as peptides and DNA, it is possible to utilize a letter code to simplify their nomenclature<sup>30,31</sup>, but this seems impractical for the branched structure of glycans. Instead, a visual representation is used to simplify the complex structure of carbohydrates. This visual representation is provided

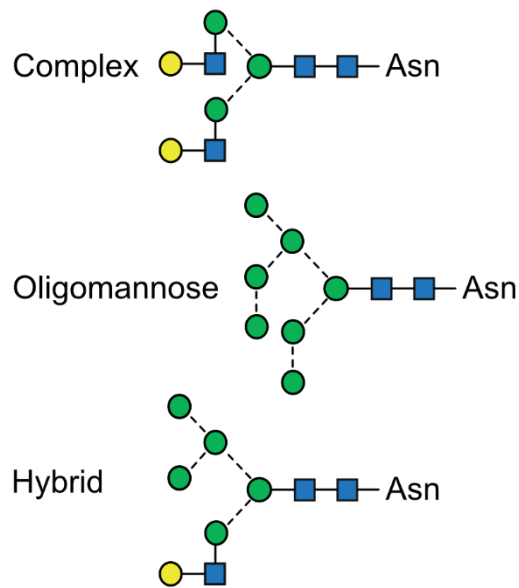
by the symbol nomenclature for glycans (SNFG) as presented in **Figure 3**.<sup>32, 33</sup> The SNFG depicts monosaccharides in different geometrical shapes and colours to illustrate same-mass isomers and epimers. The reducing end of a glycan is drawn on the right side and different regio- and stereoisomers are indicated by the type and angle of the lines that connect the monosaccharides. This allows the identification of the composition, connectivity, and configuration of even larger, complex glycans. A mixture of structural formulas and SNFG nomenclature is used within this work. Whenever it is important to access the chemical structure of glycans in more detail, they are illustrated as plain structural formula, while more general representations are pictured in SNFG style.

### 2.1.2 *N- and O-linked Glycosylation*

Monosaccharides can be combined in almost infinite ways to create oligo- and polysaccharides. But in vertebrates there are specific core structures which fulfil very different biological functions and allow to categorize them. Probably the best studied category are *N*-linked glycans. As the name suggests, they are linked *via* an amine-bond to an asparagine residue of a glycoprotein. *N*-glycosylation can only occur at specific asparagine side chains with the consensus sequence asparagine-X-serine/threonine/cysteine, where X can be any amino acid except proline. *N*-linked glycans share a common core structure composed of two *N*-acetylglucosamine (GlcNAc) and three mannose building blocks (Man).<sup>34</sup> The extensions of this core structure are classified in three *N*-glycan types: (1) the oligomannose-type, in which exclusively Man residues extend the core structure; (2) the complex-type, in which “antennae” starting with a GlcNAc extend the core; and (3) the hybrid-type, which is a combination of both oligomannose- and complex-type (**Figure 4**).

In contrast to the rather clean categories for *N*-glycans, *O*-glycosylation is not well understood. An *O*-glycan is linked to a glycoprotein by an *O*-glycosidic bond to the side chains of either serine or threonine, but there is no clear consensus sequence which would enable the prediction of the glycosylation site. Further there are no exact rules for *O*-glycans in terms of composition and structure. Up to eight different core structures are known and each of these cores can be extended in a variety of ways which can lead to very

### A - Types of N-Glycans



### B - Structural Motifs

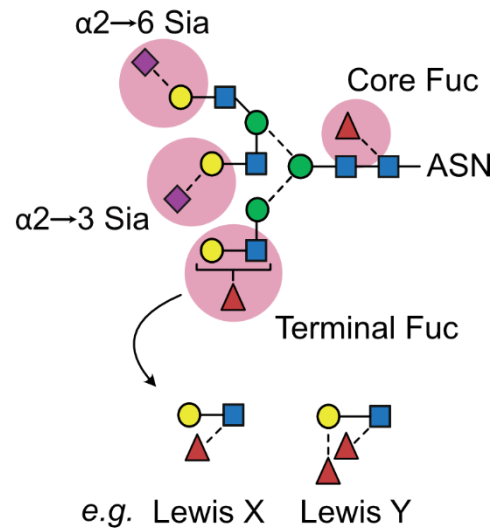


**Figure 4:** Classification of *N*-glycans and typical structural motifs. (A) All *N*-glycans share the same pentasaccharide core that consists of two GlcNAc and three Man building blocks and is amine-bonded to an asparagine residue. Based on the extension of this core structure, *N*-glycosylation can be categorized into three types: The complex-type contains “antenna”-like structures starting with an GlcNAc extension; the oligomannose-type in which exclusively Man building blocks extend the core structure in a variety of different ways and the hybrid-type which represents a combination of both, oligomannose- and complex-type. (B) Complex- and Hybrid-type *N*-glycans can further be decorated by a variety of structural motifs which functionalize the molecule. The addition of  $\alpha 2,3$ - or  $\alpha 2,6$ -linked sialic acid residues can increase the half-life of a glycoconjugate and serve as sensor to communicate with other biomolecules. The absence of core fucosylation can significantly increase antibody-dependent cell-mediated cytotoxicity (ADCC), while terminal fucosylation commonly serves as antigen motifs such as blood group epitopes (e.g., Lewis X and Lewis Y).

heterogeneous structures with hundreds of different chains being present on one glycoprotein.<sup>1</sup> *O*- and *N*-glycosylation have in common that their core structures can be decorated with specific structural motifs which can consist of one or more monosaccharide building blocks. These extensions functionalize the glycan structure and are important for the biological activity. Besides so-called *bisecting* GlcNAc residues and LacNAc extensions which are common for complex and hybrid type *N*-glycans, the level of sialylation and fucosylation are important keys for all types of glycosylation.<sup>35, 36</sup> Sialic acid residues commonly terminate the glycan structures and most often occur as  $\alpha 2,6$ - or  $\alpha 2,3$  linked residues (**Figure 4B**). They are bound to a terminal galactose building block and therefore usually stick outside of the three-dimensional glycan structure. The specific linkage of

these sialic acid isomers is an important factor to alter the role of glycoproteins in biological events, and changes in the sialic acid pattern are usually observed as a result of a pathogenic process.<sup>37, 38</sup> The main factor here is the number of charges (that is proportional to the number of carboxyl groups) that are prominently located on the outside of the glycoconjugate. The high acidity of the sialic acid residues can increase the half-life of sialylated species in serum and can further cause charge-mediated promotion or prohibition of binding events.<sup>39</sup> Monitoring the presence and the ratio of sialic acid linkage isomers can therefore be used to investigate cell-virus interactions (*e.g.* influenza)<sup>40</sup> or to directly find biomarkers related to many diseases such as cancer.<sup>41</sup>

A comparable situation can be observed for the fucosylation pattern. Complex *N*-glycans predominantly contain core fucosylation where the fucose residue is linked to the GlcNAc at the reducing end *via* an  $\alpha$ 1,6 linkage. The absence of core fucosylation can significantly enhance antibody-dependent cell-mediated cytotoxicity (ADCC) and represents a key biomarker for the analysis of glycosylated antibodies.<sup>42, 43</sup> Besides core fucosylation, *N*- and *O*-glycans can contain terminal/ antenna fucosylation which is linked to either a terminal galactose or GlcNAc at the non-reducing end. The variety here is much greater compared to the core fucosylation and gives rise to multiple epitope structures (**Figure 4B**). A prominent example are blood group antigens such as Lewis antigens.<sup>2, 44</sup> Lewis antigens are known to mediate the interaction between tumour cells and endothelium and their up- and downregulation has been reported in many types of cancers<sup>45</sup> and disease-related miscarriages<sup>46</sup>.

The monitoring of the general glycan structure, as well as the screening of specific motifs such as sialic acid or fucose pattern are particularly important for medical diagnostic or therapeutic applications. But the enormous variety of structural motifs and their similarity due to their isomeric character makes glycan analysis a challenging field.

## 2.2 Glycan Analysis *via* Liquid Chromatography and Mass Spectrometry

### 2.2.1 General Aspects

The field of glycan analysis experienced a significant growth in recent years and many different techniques and methods have been developed to unravel the complex nature of glycan structures.<sup>4</sup> Monitoring alterations in the *N*- and *O*-glycosylation profile helped to understand various diseases<sup>3, 5, 47</sup> and enabled the production of tailor-made therapeutics.<sup>48</sup> For this purpose, high throughput screening methods, such as LC-MS, found their way as routine measurement in clinical environment and the characterisation of glycosylation became an important quality attribute in the development of glycoconjugate-based drugs.<sup>49-51</sup>

Most of the information about glycan structures and their specific motifs originates from experiments performed on released glycoforms, while little information is gained from glycoproteins directly. To cleave the glycan from a glycoprotein, there are two methods available: either *via* chemical treatment or *via* enzymatical digestion. Enzymatic methods are very popular for the release of *N*-glycans as one single enzyme is able to cleave the glycosidic bond between the core GlcNAc and the asparagine of a glycoprotein for all types of *N*-glycans.<sup>52</sup> Peptide:*N*-glycosidase F (PNGase F) is widely available, simple to use and achieves high yields of glycan release which is one of the main reasons why *N*-glycan analysis is more advanced than *O*-glycan analysis.<sup>12</sup> As *O*-glycans do have a greater variety in core structures, no single enzyme is available for the release of all *O*-linked glycans and some types of glycans cannot be cleaved enzymatically at all. Therefore chemical release *via*  $\beta$ -elimination is the preferred way.<sup>53</sup> Although very efficient, the chemical release is not very specific and usually also induces *N*-glycan release as well as unwanted degradation reactions.

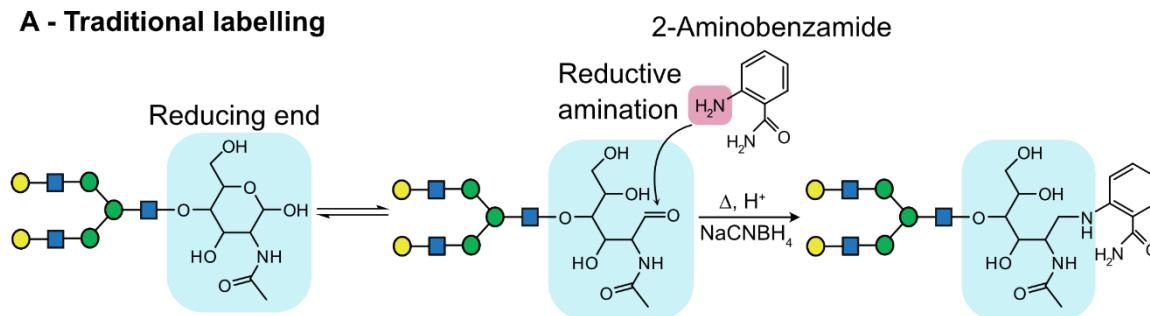
For the structural characterisation of released glycans, many established methods originating from protein and DNA characterisation are available, but of these LC-based

techniques have become the method of choice.<sup>54</sup> They can be readily coupled to either optical or MS detection and require only small amounts of sample which benefits the analysis of biomolecules such as glycans. The analysis of *N*- and *O*-glycans, however, remains challenging as glycans are much more hydrophilic than peptides and oligonucleotides which hampers the use of traditionally employed reversed-phase LC (RPLC). The hydrophilicity of glycans also complicates the coupling to MS when utilizing electrospray ionization (ESI), as ESI inherently favours hydrophobic analytes.<sup>55</sup> Furthermore, glycans lack suitable chromophores for spectroscopic detection *via* UV or fluorescence. To overcome this problem, several types of derivatization chemistry can be used to modify and increase the overall hydrophobicity of *N*-linked glycans and improve their detection in both MS and spectroscopic methods.

### 2.2.2 Derivatization of Glycans

One of the most common employed derivatizations is the addition of aromatic labels at the reducing end of the glycan which allow spectroscopic detection *via* UV or fluorescence.<sup>56</sup> Reducing end labels react selectively at the anomeric centre of the monosaccharide at the reducing end in a 1:1 stoichiometry. These types of derivatization therefore do not only enable an efficient detection *via* spectroscopic or mass spectrometric means, but also quantification.<sup>57</sup> An overview of the most common reducing end modifications is shown in **Figure 6**. Traditionally, this type of modification is introduced by reductive amination and requires a label containing a primary amine group. In this reaction, the primary amine of the label reacts in a condensation reaction with the aldehyde group at the reducing end of the glycan, resulting in an imine which is subsequently reduced by a reducing agent to yield a stable secondary amine. The yield of such derivatizations is very high and usually reaches nearly 100%, but due to the excess amount of label and reducing agent, it requires an additional purification step before analysis. Popular labels (among many others) are 2-aminobenzamide (2-AB), 2-aminobenzoic acid (2-AA) and most recently procainamide hydrochloride (ProA).<sup>58</sup> All of these labels share a common aromatic core with a primary amine attached in *ortho* or *para* position to the respective functionality individual for each label. The type of functionality

### A - Traditional labelling



### B - Alternative labelling

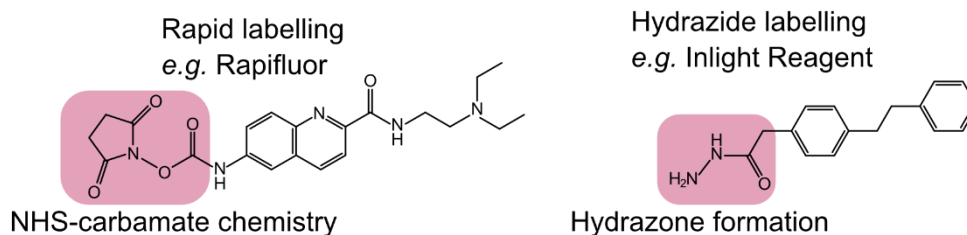


**Figure 5:** Linkage-specific derivatization of sialic acid residues. The reaction with a weak nucleophile such as isopropylamine leads to the conversion of  $\alpha$ 2,6-linked sialic acid residues to the corresponding alkylamide, while  $\alpha$ 2,3-linked sialic acid isomers form lactones under dehydration. The products of this reaction exhibit a mass difference of 59 Da and can therefore directly be differentiated by mass spectrometry.

has a huge influence on the intensity of UV/ fluorescence detection and can further affect the separation efficiency in the chromatographic dimension. Although 2-AB has weak fluorescence intensity and leads to only moderate separation of *N*-glycans in typically applied HILIC separations, it is still the most popular choice for *N*-glycan analysis as it was one of the first labels applied for glycan derivatization and many database entries are available for this type of labelled glycans. 2-AA has similar fluorescence properties but differs from 2-AB as it features a carboxylic acid which makes it more attractive for ion exchange separations or capillary electrophoresis. Procainamide recently emerged as promising alternative, as it provides high intensity fluorescence signals in combination with a great MS response.<sup>59</sup> It contains a tertiary amine group that can be readily protonated in the ESI process and improves the ionization efficiency of ProA-labelled glycans when measured in positive ion mode. As reductive amination usually takes up to 2-3 hours of reaction time, alternative types of reducing end labels have been developed to speed up the reaction (see **Figure 6**). So-called rapid or instant labels do not react *via* traditional reductive amination, but use a different chemistry from the aforementioned labels.<sup>60</sup> Rapid or instant labels contain an activated form of the primary amine which is

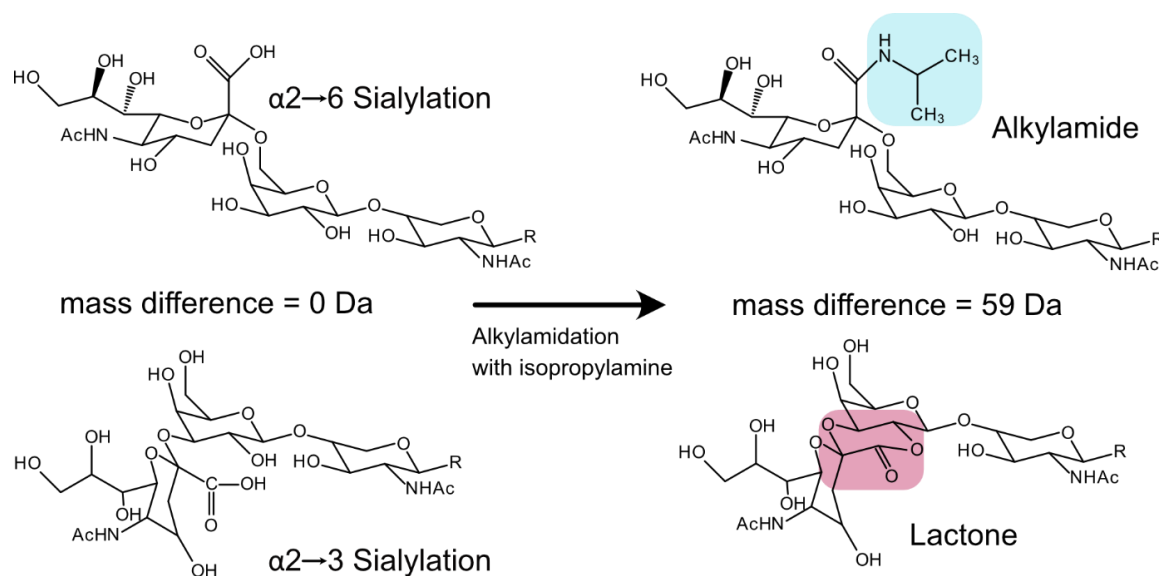


**Figure 6:** Typical workflow for *N*-glycan release from the glycoprotein and the subsequent reducing end modification. *N*-glycans are released from the glycoprotein *via* enzymatic digestion with PNGase F with a free reducing end. (A) Traditional labelling approaches react *via* reductive amination at the reducing end of the released glycan (the example reaction shows the reaction with 2-aminobenzamide, 2-AB). The traditional labelling approach takes up 2-3 hours and requires a reducing agent to produce the stable amine bond. (B) Alternative labelling approaches use different chemistries. While rapid labels such as Rapifluor™ react *via* NHS-carbamate chemistry within 5-10 minutes, hydrazide tags such as InLight™ are bound to the reducing end *via* hydrazone formation. The reaction time for the hydrazone formation takes up to 2 hours but does not require additional clean up steps.

modified with N-hydroxysuccinimide carbamate to result in a “rapid tagging functional group”. These functions can react rapidly with glycosylamine-containing *N*-glycans directly after their enzymatic release and result in a urea linkage.<sup>61</sup> These types of reactions originate from peptide labelling and became more popular for *N*-glycan analysis due to their fast reaction times. The reaction happens within minutes (5-10 minutes) and is therefore significantly shorter compared to the reaction time of reductive amination (2-3 hours) but is only accessible for *N*-glycosylation as *O*-glycans do not exhibit the required glycosylamine after enzymatic digestion. Furthermore, a purification step to remove excess label and salts is still necessary. To circumvent the purification step, it is possible to use hydrazide labels which form stable hydrazones without the need for reducing agents. Although hydrazide tagging is a rather slow reaction (hours), the amount of salt is drastically reduced and that enables the direct measurement of the sample after derivatization.<sup>62</sup> This type of labelling is popular for MALDI imaging experiments as the

clean-up of tissue slices can be very difficult, but recently hydrazide tagging gained some attention for LC-MS as it is possible to include stable isotope labels ( $^{13}\text{C}$ ).<sup>63</sup> The inclusion of light and heavy isotopic labels allows very precise quantitation experiments *via* MS without the need for optical detection.

Besides the aforementioned modifications at the reducing end of the glycan, there is a variety of other derivatization chemistries to modify other parts of the glycan. Most often, these modifications aim to mask the polar hydroxyl groups for a more efficient ionization or to stabilize labile functional groups such as sialic acid monosaccharides. An unspecific way to achieve both features is permethylation.<sup>64, 65</sup> In permethylation, the hydroxyl, amino, and carboxylic acid groups located on the glycan structure are chemically modified to their corresponding methyl-ether, thereby decreasing the overall hydrophilicity of the molecule. This facilitates separation on reversed phase columns and benefits ESI ionization while stabilizing labile functional groups on the glycan. The chemical reaction, however, utilizes very toxic reagents and is therefore not suitable for high throughput applications. More selective modifications can not only help to stabilize labile functions of the molecule but can be utilized for identifying isomeric features. A prominent example is the selective derivatization of  $\alpha 2,3$ - and  $\alpha 2,6$ -linked sialic acid residues.<sup>39, 66</sup> The differentiation is not straightforward *via* conventional means, as they exhibit the same mass and the negative charge on the acid moiety further prevents efficient ionization in positive ion mode and separation in the chromatographic dimension. Recently, several unique derivatization methods have been developed where  $\alpha 2,3$ - and  $\alpha 2,6$ -linked sialic acid residues are modified to exhibit different masses.<sup>39, 66</sup> They utilize the different reactivity of  $\alpha 2,3$ - and  $\alpha 2,6$ -linked sialic acid residues to attach an external nucleophile: While  $\alpha 2,6$ -linked sialic acid residues react readily with weak nucleophiles,  $\alpha 2,3$ -linked sialic acids form lactones under dehydration. **Figure 5** shows an example reaction with isopropylamine as nucleophile that leads to the selective alkylamidation of  $\alpha 2,6$ -linked sialic acid residues. There is a variety of different nucleophiles available that differ in reaction yield and specificity as well as in the fundamental chemistry (amidation *vs* esterification). Although such reactions are able to create distinguishable functional groups with a distinct mass difference, the mechanism (and thereby the varying reaction

yields) is not well understood and the resulting lactones are not stable for extended period of times.<sup>67</sup> Studies on possible two step reactions (to stabilize the lactones) are ongoing and could lead to a more routine application of the chemical modification for glycan analysis.<sup>68</sup>

All of the presented derivatization chemistries, reducing end modifications as well as general modifications to mask hydroxy or carboxyl functions of the glycan, lead to an increase of hydrophobicity of the glycan structure.<sup>56</sup> These can benefit ESI ionization and increase retention on reversed phased LC, but RPLC is usually not sufficient to resolve all glycan isomers. Therefore, in the last decade several specialised separation techniques have been developed for the analysis of *N*- and *O*-glycans.

### 2.2.3 Chromatographic Separation

The highest resolution to separate glycan isomers can be achieved by porous graphitic carbon (PGC) chromatography.<sup>69</sup> It has unique retention properties for non-polar and polar analytes due to its special surface chemistry. The chemical surface of PGC behaves similar to alkyl-bonded silica gels (like C8 or C18 columns) and retains non-polar molecules strongly but extends the possibilities of RPLC when facing polar analytes. The retention mechanism is based on a variety of factors and mainly depends on the size, shape and electron distribution of the analyte.<sup>70</sup> This provides a unique retention behaviour which is able to separate stereoisomers, diastereomers and other very closely related compounds.<sup>71, 72</sup> In addition, the carbon material offers a high stability over the entire pH range of 0-14 and is compatible to almost all solvents and solvent additives. Although PGC offers a broad range of possibilities to separate non-polar and polar analytes, its strong retention for very polar analytes can also lead to irreversible binding to the stationary phase. This results in extremely unstable and shifting retention times, making it less robust for routine analysis. Contemporary studies are trying to compensate with lengthy wash routines,<sup>70</sup> but currently PGC is mainly used for the analysis of very demanding compounds such as *O*-glycans.<sup>73</sup> The analysis of *N*-glycans, however, is mainly based on more reliable methods such as HILIC chromatography.

HILIC is a variant of normal phase separation consisting of a polar surface (bare silica or modified with ionizable functional groups such as amide-, amine- or sulfobetaine-groups) and reversed-phase type eluents with at least 2% water. The mobile phase forms a water-rich layer on the surface of the polar stationary phase and creates a liquid-liquid extraction system with the organic solvent in the middle of the column. The separation mechanism is mainly based on a partition effect of the analyte that separates compounds based on their polarity and degree of solvation. In addition, molecules can interact with the functional groups of the column surface *via* weak electrostatic interactions, resulting in ion exchange separation in addition to the polar partition effect.<sup>74</sup> Although HILIC does not provide the resolution power of PGC, it is more reproducible and allows an efficient coupling to MS due to the high proportion of organic solvent in the mobile phase. HILIC is therefore routinely used for the separation of *N*-glycans and is widely used in many laboratories.<sup>75</sup>

Besides HPLC-based separation, electrophoretic separations (such as capillary electrophoresis) came up as powerful analysis tool for glycan analysis.<sup>9</sup> In CE, analytes migrate in a submillimetre diameter capillary through an electrolyte solution under the influence of an electric field. Analytes are separated based on their ion mobility and/or partitioning into an alternate phase *via* non-covalent interactions. This electrophoretic separation technique can be much faster than conventional LC experiments depending on experimental conditions. In addition the resolution for the separation of glycan isomers is very high, but the coupling to MS remains difficult.<sup>76</sup> Recent studies promise an easier coupling which makes CE an interesting alternative in the near future.<sup>77</sup>

While chromatographic as well as electrophoretic separations allow to distinguish between isomeric structures, sequencing of the analyte remains a challenge. In general, MS detection in combination with MS/MS fragmentation is the preferred way and can deliver detailed information on the structure of a glycan. But there are some ways to identify unknown structures in combination with only spectroscopic detection such as fluorescence or UV: The most straightforward way is the direct comparison with known standards. It is fast and allows to unambiguously identify certain species but only in the case a suitable standard is available. This is a particular challenge for *N*- and *O*-glycans as

glycans exhibit very complex structures that are not template-driven, and which hampers the extraction from natural sources.<sup>78</sup> Furthermore, glycans are present as highly diverse mixtures, which makes separation and isolation of the isomers additionally challenging. A similar picture can be drawn for the chemical synthesis of glycans. It is very elaborate and relies on a mixture of enzymatical methods and solid phase synthesis.<sup>79, 80</sup> Although the process for glycan synthesis is advancing in big steps, it is still too early to reliably imitate all glycan structures from natural *N*- and *O*-glycosylation.<sup>81</sup> Structural elucidation *via* comparison with known standards is therefore restricted to rather simple structures and cannot cover the broad range of glycan complexity yet.

The preferred way for glycan sequencing is the sequential digestion with suitable enzymes. Exoglycosidases specifically cleave individual monosaccharides from the non-reducing end of the glycan structure. If a glycan is sequentially digested with different exoglycosidases, it is possible to determine the monosaccharide composition and linkage.<sup>82</sup> This method provides very detailed information on the structure of the glycan, but due to the multiple reaction and measurement steps it is very time-consuming and costly, limiting its overall ability for high throughput analysis of unknown samples. Furthermore, not all glycans can be cleaved enzymatically which represents a big problem, particularly for *O*-glycans. For *N*-glycosylated analytes, however, sequential exoglycosidase treatment represents the method of choice to determine sialic acid residues and fucose position as well as for general sequencing of unknown compounds. If a glycan structure is elucidated, the respective retention time (from HILIC or PGC chromatography) can be stored in suitable databases to simplify future identifications.<sup>83, 84</sup> Retention times in HPLC-based experiments, however, are prone to shifting and depend significantly on external factors such as temperature, solvent and condition/age of the column. To generalize shifting retention times, they can be converted into relative drift times by an external standard. LC-based as well as CE-based techniques utilize a homopolymeric glucose standard, often called dextran ladder, for that purpose.<sup>69, 85, 86</sup> The external standard is measured in parallel to the actual analyte and allows to align the data to make it more comparable. This is done by converting the retention times into glucose units (GU) according to established calibration processes. In contrast to shifting retention

times, GU values can serve as reliable indicator to identify unknown structures and can be implemented in databases. There are, however, some limitation in comparability of the GU values. As different reducing end modifications or chemical derivatizations of the glycan have a significant influence on their overall polarity, they also affect the retention time. This makes it necessary to have a unique database for each label/ derivatization, hampering the utilization of modern labels with more advantageous features (e.g., instant label) and favouring traditional labels with well-advanced databases such as 2-AB. Another limitation of the structural elucidation *via* GU values is the resolution of the chromatographic systems. Although many isomers can be separated by HILIC or PGC, it is common for glycans (especially for relatively large glycans such as N-glycans) to exhibit very similar or even overlapping retention times, resulting in almost equal GU values. In this regard, MS has become an irreplaceable technique for the structural characterisation of glycans *via* LC-MS or LC-FLD-MS.

#### 2.2.4 *Mass Spectrometric Detection*

MS-based techniques are frequently used in proteomics and found its way for glycan analysis due to its outstanding sensitivity. Glycans are mainly brought into the gas phase by two prominent ionization methods: MALDI<sup>87</sup> and ESI<sup>88</sup>. MALDI was preferred in the beginning of the glycomics field due to its high throughput capabilities and is still popular today due to the possibility to create 2-dimensional images of tissue slices.<sup>89</sup> Nowadays, however, ESI has become the dominant ion source as it can be hyphenated to LC and CE which is often necessary to compensate for the complex glycan matrix. Both types of ionization generate mostly intact and thus non-fragmented analyte ions. While MALDI predominantly yields in singly charged ions, ESI ionization can result in a distribution of multiple charge states which can be beneficial for the detection of large molecules in a limited  $m/z$  range. In positive ion mode, glycans ionized by ESI can occur as protonated ions as well as complexated by metal cations such as sodium, potassium, or lithium. In negative ion mode, deprotonated ions or anion-adducted species can be observed. The type of charge state and adduct are dependent on the ESI conditions such as pH, salts and

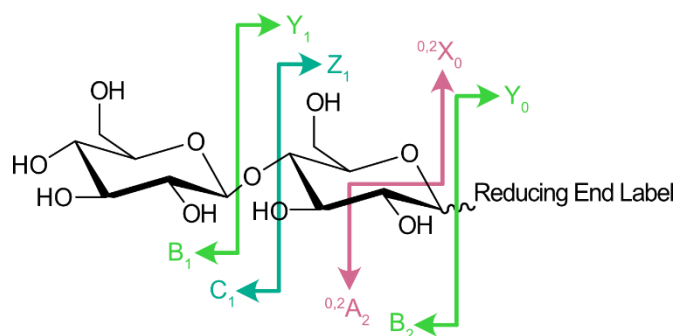


**Figure 7:** Nomenclature for the MS/MS fragmentation of glycans according to Domon and Costello. Fragments resulting from the cleavage of a glycosidic bond are labelled B, Y, Z and C, depending on the position of the cleavage. Cross-ring fragments are assigned with the letters A and X. Numbers in subscript indicate the position of the cleavage, counted from the terminal end of the glycan for ABC fragments and from the reducing end for XYZ fragments. Numbers in superscript label the position of the cross-ring cleavage inside of a monosaccharide building block.

detergents and thus directly connected to the solvent gradient and additives coming from the hyphenated LC system. A simple mass spectrum of intact sugars reveals only the number of hexoses or pentoses as the most common naturally occurring monosaccharides are diastereomers and therefore have the same molecular mass. This limited information, however, is enough to draw conclusions on the general monosaccharide composition. In combination with the GU values obtained from the chromatographic separation, it is possible to identify many typical complex *N*-glycans.<sup>69, 84</sup> The exact determination of the connectivity between each monosaccharide, however, requires more experiments and is especially important for the unambiguous identification of specific structural motifs such as the sialylation and fucosylation patterns. For clarification, one can activate the precursor ion and thus induce fragmentation to elucidate its structure.<sup>12, 16</sup> A specific fragment pattern is formed that depends on the energy of the fragmentation, the charge of the ion, and the type of adduct. The nomenclature of the glycan fragments is based on the common peptide nomenclature and goes back to the definition by Domon and Costello (**Figure 7**).<sup>90</sup> If the charge remains on the part of the sugar with the reducing end, these fragments are then labelled X, Y and Z. Fragments with the charge at the non-reducing end are labelled A, B, or C. An index indicates the broken glycosidic bond starting from the terminus or non-reducing end of the fragment. Glycans can be fragmented in different ways in the mass spectrometer. One of the most common methods is collision induced

dissociation (CID). Molecular ions are accelerated into a collision cell filled with a neutral buffer gas such as argon, nitrogen, or helium. A large number of collisions between the charged molecular ions and the neutral gas particles leads to slow heating and subsequent fragmentation of the ion. The smaller fragment ions generated are indicative of certain structural properties of the precursor molecule and often allow unambiguous identification.<sup>91</sup> While positive ion mode MS/MS experiments preferentially result in cleavage of the glycosidic bond between two monosaccharides,<sup>92</sup> negative ion mode activation of sugars results in characteristic cross-ring cleavages.<sup>93-95</sup> MS/MS spectra in the positive mode therefore often contain a smaller number of fragments and allow conclusions about the composition and, to a limited extent, also about the connectivity. In contrast, MS/MS spectra in the negative mode are often much more complex and expensive to evaluate. However, the increased information content of the cross-ring fragments allows clearer statements about the connectivity and configuration of the glycans. Besides, when fragments form, rearrangement reactions and therefore erroneous structural assignments can occur — as in the case of fucose rearrangement.<sup>96,97</sup> The reaction and the underlying mechanism are not yet fully elucidated yet, but recent studies showed that the reaction is proton-driven<sup>98</sup> and the fucose residue is shifting only to certain functional motifs such as N-acetylated side chains or primary or secondary amines.<sup>99</sup> In general, LC-MS in combination with MS/MS is a powerful method to elucidate the structure of many complex glycan structures, but it does not allow for the complete sequencing of the compound. In addition, the example of fucose rearrangement further shows the limitation of LC-MS for specific glycan motifs and the urgent need for orthogonal methods to support the structural elucidation of isomeric glycans.

## 2.3 Glycan Analysis *via* Ion Mobility-Mass Spectrometry

### 2.3.1 *Fundamentals of Ion Mobility*

As glycan isomers usually exhibit the same mass and often very identical fragmentation spectra, it can be helpful to add an additional separation dimension to reduce ambiguity in structural characterisation. In this regard, ion mobility spectrometry (IMS) established

itself as potent gas-phase electrophoretic separation technique and has gained a lot of popularity.<sup>15, 16, 100</sup> It has a variety of civil and military applications ranging from the detection of explosives at airports<sup>101</sup> to diagnostic functions in hospitals<sup>102</sup>, while scientific applications regularly use the technique to study and characterize biomolecules in the gas phase.<sup>103-105</sup> The general separation principle of IMS is described here, while a more detailed explanation of different IMS platforms is given in the next chapter.

In IMS, an ionized sample is injected into a drift cell, which is filled with a neutral buffer gas like nitrogen or helium. The ions are guided through the cell by a weak, electric field and undergo collisions with the buffer gas on their way. Thereby, ions are separated according to their mobility  $K$ , which is dependent on charge, size, and shape of the species. Small and compact ions have a higher mobility than larger, extended molecules and therefore traverse the drift cell faster.<sup>106, 107</sup> IMS separation can be readily hyphenated to MS due to their similar mechanics in terms of orthogonality and time requirements. While MS separates ions based on their mass-to-charge ratio ( $m/z$ ), IMS can separate ions based on their size and shape. Furthermore, the recording of MS spectra is much faster (in the order of microseconds) than IMS separations (in the millisecond regime) which allows the averaging of many MS spectra within a single IMS separation cycle. This enables the implementation of IMS in typical MS workflows without additional costs. The combination of both techniques yields a multi-dimensional measurement method that stands out due to a low detection limit and response time.

A fundamental assumption for many IMS separations is that separations take place under so-called low-field limit.<sup>108</sup> The low-field describes that the motion of the ions through the drift cell is only affected by their internal energy and not by the directional motion of the applied electric field. Within the low-field limit, ion-neutral collisions with the buffer gas are essentially thermal, and therefore the mobility  $K$  is independent of the electric field:

$$K = \sqrt{\frac{18\pi}{\mu k_B T} \frac{ze}{16N} \frac{1}{CCS}} \quad (1)$$

Equation 1 is the fundamental ion mobility equation, usually referred to as Mason-Schamp equation.<sup>109, 110</sup> Here,  $ze$  is the ion charge,  $N$  the buffer gas number density,  $\mu$  is the reduced

mass of the buffer gas and the ion,  $k_B$  is the Boltzmann constant and  $T$  is the effective temperature. Additionally, the equation contains the rotationally averaged collisional cross-sections (CCS) which describes the area of an ion which is able to interact with a buffer gas. It depends on the conformational shape of a molecule without being dependent on instrumental parameters, thus it can be compared to theoretical values obtained from X-ray crystallography, NMR spectroscopy, or model structures. The universal character of CCS values makes it comparable across different IMS platforms and allows the storage in suitable databases to facilitate the identification of unknown analytes.

### 2.3.2 *Types of Ion Mobility Separations*

Although the working principles of IMS were known for many years, the first commercial IM-MS platform was introduced in 2006.<sup>111, 112</sup> Over the years, a variety of instruments with significant different design of ion mobility cells were developed. In the following section, three popular types of IMS platforms for glycan analysis are introduced and briefly discussed. The separation principles of all three types mainly differs in the geometry of the applied electric field, thus a general overview of the working principles together with a schematic representation of the ion movement inside the respective IMS cells is presented in **Figure 8**. The first commercially available IM-MS instrument was the so-called Synapt (Waters Corporation) in 2006 which is based on a travelling wave ion mobility cell (TWIMS, **Figure 8A**).<sup>111, 112</sup> TWIMS is a time-dispersive method that utilizes traversing pulses to guide ions through the drift cells. These sinusoidal waves are used to separate the ions in a mobility-dependent matter. Species with a high mobility are able to maintain their position on each wave, while ions with lower mobility experience roll-over events, thereby reaching lower average velocities. As a result, however, ions follow complex trajectories while travelling through the drift cell and to date no analytical model can accurately describe or predict the ions' motion through the cell.<sup>113, 114</sup> Thus, CCS values cannot be directly determined from TWIMS measurements and instead calibration with reference substances of known CCSs is required.<sup>115</sup> Such calibrations are straightforward and can be done *via* calibrated single field methods<sup>116</sup>, but it requires suitable calibrants with similar physicochemical properties and  $m/z$  range as the actual analyte. A significant

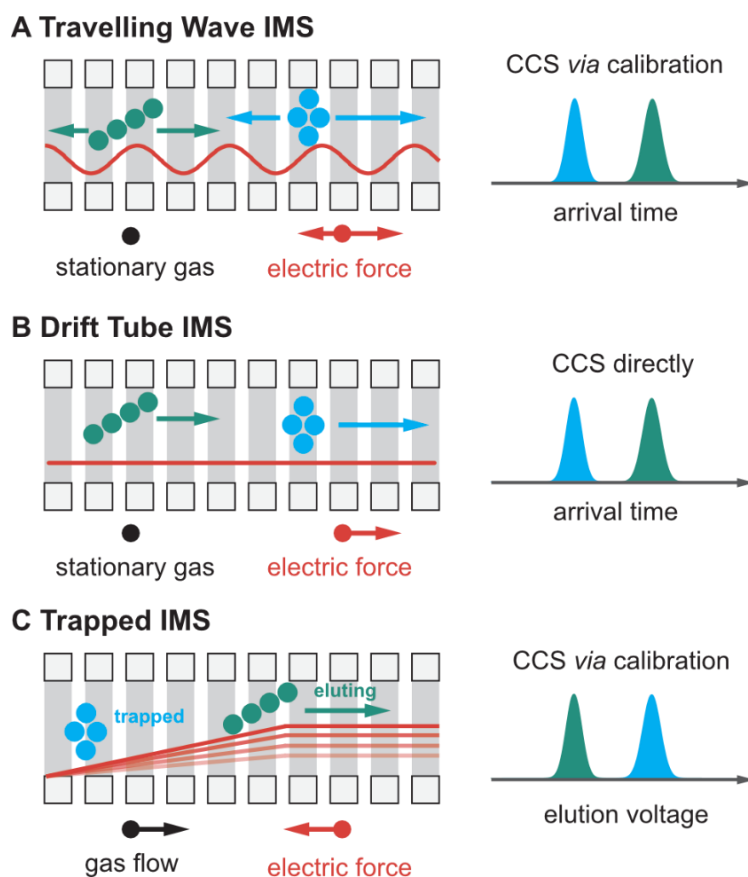


**Figure 8:** Schematic overview of the drift cells of three popular ion mobility platforms. For the IMS types (A) TWIMS, (B) DTIMS and (C) TIMS the specific motion of the ion through the drift cell and the applied electric field gradient are schematically presented.

(DTIMS, **Figure 8B**) is the simplest form of IMS and is based on a constant linear electric field generated by a coated tube or a stack of ring electrodes. After the ions are injected into the drift cell, the molecules collide with a stationary, neutral buffer gas such as helium or nitrogen as described in the chapter before. Due to the uniform electric field, the mobility of the ions is reverse proportional to the CCS. Absolute CCS values can therefore directly be derived from the recorded drift times, *e.g. via* a traditional stepped-field approach.<sup>116</sup> Direct CCS determination *via* DTIMS is generally more accurate than estimated CCS by other IMS platforms<sup>116</sup> and is not dependent on suitable calibration agents, making DTIMS a popular alternative in glycan analysis. One disadvantage of DTIMS, however, is the limited resolution. The resolution of the DTIMS instrument is

advantage of TWIMS over other IMS platforms is the compact architecture and the flexibility of the electric field.<sup>117</sup> It can deviate from linear geometries of the drift cell to generate cyclic arrangements, resulting in extremely long pathways (and thus resolution) and allowing for the separation of very similar isomers such as glycan anomers.<sup>118</sup>

In 2013, the first commercially available drift tube instrument (DTIMS) was introduced by Agilent Technologies.<sup>119</sup> Drift tube ion mobility spectrometry

directly proportional to the length of the drift tube and increasing the length to improve sample separation in the gas phase may become impractical beyond a certain limit.<sup>120</sup>

Most recently, Bruker introduced the newest development in the field of ion mobility technology in the form of the so-called timsTOF.<sup>121, 122</sup> This instrument separates ions in a trapped ion mobility drift cell (TIMS, **Figure 8C**) according to their gas-phase mobilities. The IMS separation can be divided into two steps: trapping and elution. In the trapping step, ions are dragged through the drift cell by a fast axial gas flow while facing a linear electric field that decelerates their movement. Depending on their mobility, each ion reaches a steady state that balances the effects of gas flow and electric field. Ions with low mobilities are carried far to the end of the gradient of the electric, while ions with high mobilities are focused near the entrance of the ion mobility cell. In the second step, ions are eluted selectively from the drift cell by a stepwise decrease of the magnitude of the electric field gradient.<sup>123</sup> This technique separates ions with outstanding resolution in a relatively compact drift cell and has a duty cycle of almost 100% due to the adjustable electric field gradients.<sup>124</sup> In principle, TIMS can be understood as a reversed drift tube which would allow the direct determination of absolute CCS, but the high gas velocities and pressure impede accurate readouts. Therefore calibration procedures with known calibrant standards (similar to TWIMS) are preferred to estimate CCS values.<sup>125</sup>

In this thesis, a commercial travelling wave Synapt G2-S (Waters, Manchester) instrument is used for the investigations (**Figure 9**). A detailed discussion about technical aspects of the instrument can be found elsewhere.<sup>111, 112</sup> Here, only the distinctive features of the instrument in general as well as an overview over the general workflow is briefly presented. The instrument is equipped with a nano-electrospray ionization source (nESI) which can be used to spray the analyte solution from metal-coated glass capillaries by applying a high voltage of 1-2 kV. The needles are home-fabricated, and the opening of the tip can be adjusted to diameters of 1-10  $\mu\text{m}$  to allow for very low natural flow rates in the nL/min range. This is essential to reduce sample consumption as biological samples are often limited. After ionization, the analyte is transferred to the high vacuum region of the instrument and reaches a quadrupole which allows for  $m/z$  selection of a precursor ion before the actual IMS separation. This region is divided into three parts (so-called

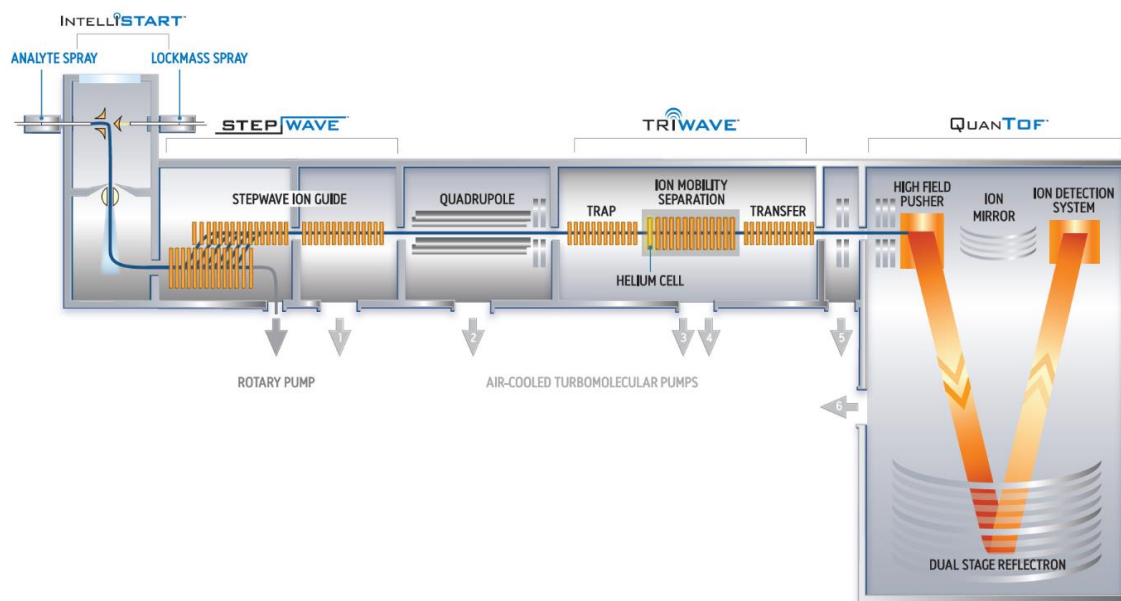


**Figure 9:** Schematic representation of a Waters Synapt G2-S. This IM-MS instrument utilizes a travelling wave ion mobility (TWIMS) drift cell to separate ions according to their mass, charge, size, and shape. Illustration provided by Waters Corporation.

Triwave): trap, IMS, and transfer cell. The trap cell focuses incoming ions and pulses them into the IMS cell as ion packages. In the IMS cell the actual separation takes place as described for the TWIMS mechanism before. The transfer cell helps to maintain ion mobility separation until the ions reach the time-of-flight analyser where they are detected. The trap and transfer cells are filled with argon at a pressure of  $1.5 \times 10^{-2}$  mbar and can additionally be used as fragmentation cells *via* collision-induced dissociation (CID). This setup allows the measurement of analytes with a high  $m/z$ -resolving power and sensitivity, which benefits the detection of very low concentrated samples. Furthermore, in contrast to front-end IMS instruments, CID fragmentation of  $m/z$ -selected precursors can be performed before and after IMS separation.

For the studies described later in this thesis, two versions of the Synapt G2 were used. In the original version, both instruments contained a TWIMS drift cells to separate ions according to their mobility. As described before, TWIMS does not allow to determine absolute CCS values due to the non-homogeneous electric field and requires careful calibration with a suitable standard. of known CCS. In 2015, one of the instruments was modified and the original TWIMS cell was replaced by linear drift tube in the same dimensions.<sup>126</sup> The replacement enables direct measurements of CCS values, but comes at

the cost of reduced IMS resolution. While the original TWIMS cell had a maximum resolution of  $\Delta\Omega/\Omega(N2) \approx 40$ , the DTIMS cell of the same length is only able to separate isomers with a resolution of  $\Delta\Omega/\Omega(N2) \approx 20-25$ . Data obtained on the DTIMS version of the instrument is labelled in the thesis as <sup>DT</sup>CCS to indicate absolute CCS values, while estimated values are labelled as <sup>TW</sup>CCS.

### 2.3.3 *Examples of Ion Mobility Separations in Glycan Analysis\**

One of the main advantages of ion mobility mass spectrometry (IM-MS) for glycan analysis is its universal separation power. Unlike LC separations, which are very sensitive to the stationary phase, IM-MS depends on the much more universal interaction principles of the investigated ions with the drift gas. Due to their distinct atomic composition, different molecular classes can exhibit a different mobility behaviour, especially when a polarizable gas such as nitrogen is used. This property can be used to significantly reduce the spectral complexity of acquired data <sup>127</sup>. It was recently demonstrated that whole molecular classes can be easily distinguished based on their trend lines in a plot of CCSs against  $m/z$ . For example, carbohydrates exhibit on average shorter drift times compared to lipids and peptides of the same  $m/z$ , allowing a rapid identification of each class <sup>119</sup>. Multiply charged ions generally exhibit a higher mobility than singly charged ions with the same  $m/z$ , resulting in individual signal groups. Selectively extracted data from complex spectra enables significantly reduced signal-to-noise ratios and thus allows for improved molecular identification of signals. HARVEY ET AL. used this approach to extract N-glycan profiles from crude incubation mixtures without further chemical clean-up <sup>128</sup>. It enabled the differentiation and analysis of distinct species within one measurement, therefore significantly decreasing the sample consumption. However, IM-MS is not

\* This sub-chapter is based on the publication "Glycan Analysis by Ion Mobility-Mass Spectrometry and Gas-Phase Spectroscopy" by C. Manz and K. Pagel, published in *Curr. Opin. Chem. Biol.* **2018**, 42, 16-24. Figures and content adapted with permission. Copyright 2017 Elsevier Ltd. <https://doi.org/10.1016/j.cbpa.2017.10.021>

limited to a coarse separation of molecular classes but can also be used to distinguish minor structural differences between isomers.

Recently, it was demonstrated that IM-MS can be used to distinguish small glycans as well as various glycopeptide isomers<sup>129</sup>. Fundamental work on the capabilities of IM-MS for glycan separation was done by HOFMANN ET AL., who investigated a set of six isomeric trisaccharides, which differed in their composition, connectivity, or configuration<sup>21</sup>. A comparison of the CCSs of the intact deprotonated trisaccharides showed significant differences for configurational isomers (alpha vs. beta glycosidic bonds) as well as for connectivity isomers (1,4 vs. 1,3 glycosidic linkages), whereas compositional isomers could not be distinguished. The study revealed the fundamental ability of IM-MS to separate many glycan isomers in the gas phase. The results allow the conclusion that IM-MS-based methods have the potential to serve as powerful analysing tool for glycans. Essential for structural identification is the combination of mass and mobility information within a multidimensional dataset and the comparison of obtained data with known, authentic standards. Unlike retention times in LC,  $m/z$  and CCSs are highly reproducible values when measured under controlled conditions. However, the assignment of drift peaks/CCSs to specific structural motifs can be complex due to the possibility of multiple ion conformations. In some cases, conformers can increase the number of drift peaks although the number of individual analytes remains the same, which complicates the analysis of the measured data<sup>130</sup>. The identification confidence can be increased by comparing obtained CCSs with reference values of comprehensive databases<sup>131-133</sup> or theoretical values. CCSs can be calculated theoretically by various methods<sup>134-136</sup>, however, finding structural candidates for theoretical calculations is not an easy task due to various effects such as solvation interaction, charge localisation and especially due to the enormous structural flexibility of glycans as briefly described in the introduction.

The separation capability of IM-MS is mainly dependent on the resolution of the used instrument, which is often defined by the length of the applied IMS cell<sup>137</sup>. Increasing resolution therefore requires instrumental modification, which often is not feasible. Alternatively, IM separation can often be improved when adding sodium or other metal ions to an analyte. It is known that metal adducts can influence the conformation of

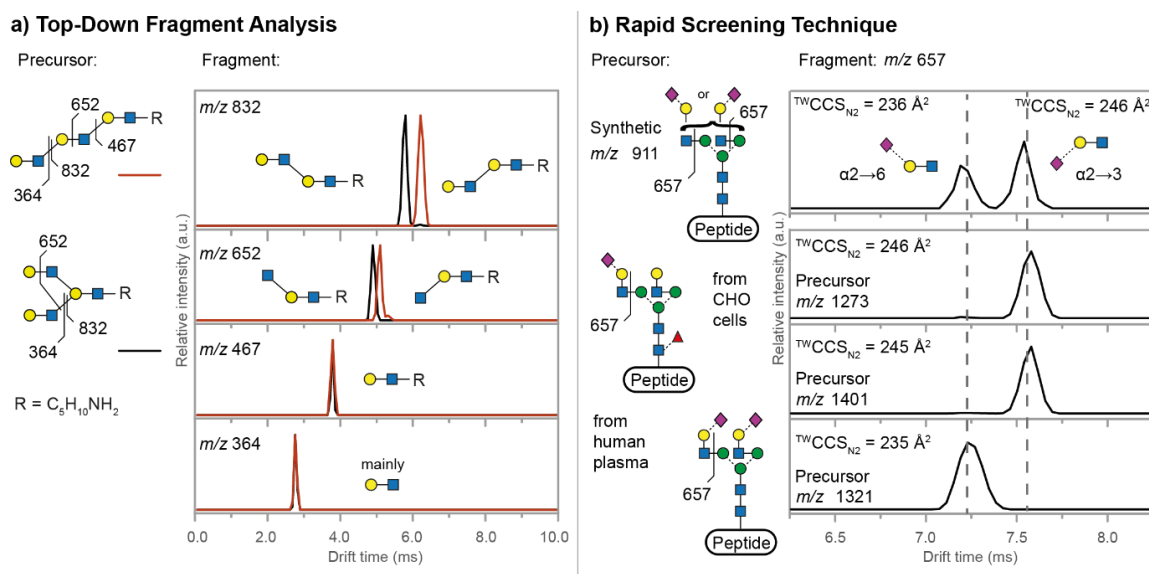


**Figure 10:** Application of IM-MS for structural analysis of complex carbohydrates. a) Top-down fragment analysis of two isomeric hexasaccharides. The fragmentation pattern is indicated for the two precursor structures and shown as respective fragment ATDs (Adapted with permission from Nature Publishing Group: Nature, copyright 2015.). b) The fragmentation of glycopeptide precursors leads to the generation of characteristic trisaccharide fragments ( $m/z$  657), which can be used to rapidly identify the sialylation pattern (upper panel). This is shown exemplarily for tryptic digests of  $\alpha$ 1-antitrypsin generated in Chinese hamster ovary (CHO) cell lines or extracted from human plasma (lower panels). (Adapted with permission from the Royal Society of Chemistry, copyright 2016.)

carbohydrate ions<sup>138</sup>. Experiments investigating oligosaccharides adducted with group I metal ions showed a general trend of increasing drift times of adducted species proportional to the size of the metal ion. However, many metal adducts showed an isomer-specific drift time dependency, demonstrating the potential utility of metal/carbohydrate interaction for improving the separation capability of glycans in IM-MS<sup>139, 140</sup>.

Due to the decreasing impact of small structural differences on the overall shape, IM-MS separation becomes less efficient for larger glycans. This often complicates the differentiation of large intact ions. However, the fragmentation of intact precursors can lead to diagnostic fragments with distinct CCSs, from which information on the structure of the precursor can be deduced<sup>141</sup>. Collision-induced dissociation (CID) experiments on the Man3-GlcNAc2 pentasaccharide core of *N*-glycans and fragments thereof showed the reproducibility of this approach<sup>142</sup>. Regardless of the nature of the precursor, similar

arrival time distributions (ATDs) and CCSs were obtained for mono- and disaccharide fragments of similar structure <sup>142</sup>. One application of this approach was shown for the differentiation of isomeric Lewis and blood group epitopes. <sup>19</sup> Fragment trisaccharides of larger glycans showed characteristic ATDs when compared to drift times of intact trisaccharides and enabled the assignment of the underlying fucosylation pattern. This procedure can also be used as top-down fragment analysis, as demonstrated by HOFMANN ET AL (**Figure 10**) <sup>21</sup>. Two isomeric hexasaccharides, which either exhibited a branched or a linear alignment of identical building blocks, were investigated (**Figure 10a**, precursor structures). As intact precursors, both oligosaccharides showed identical ATDs and CCSs. From the resulting di- to pentasaccharide fragments, however, it was possible to obtain detailed information on the structure and branching of the precursor ion (**Figure 10a**, fragment spectra of n=2-4 fragments). The analysis of fragment CCSs can therefore be more informative than analysing intact precursor ions <sup>143</sup> and has great potential to be used for the quality control and sequencing of larger, more complex glycans.

Fragment CCSs cannot only be used to piece together the structure of larger oligosaccharides, but also have immense potential to be used for the rapid screening of characteristic features in glycans and other glycoconjugates. In many cases, the assignment of certain structural motifs such as fucosylation and sialylation is sufficient for diagnostics or batch monitoring. The occurrence of specific glycan epitopes is for example associated with several human diseases and a rapid diagnostic screening tool for these epitope features is therefore highly desired <sup>144</sup>.

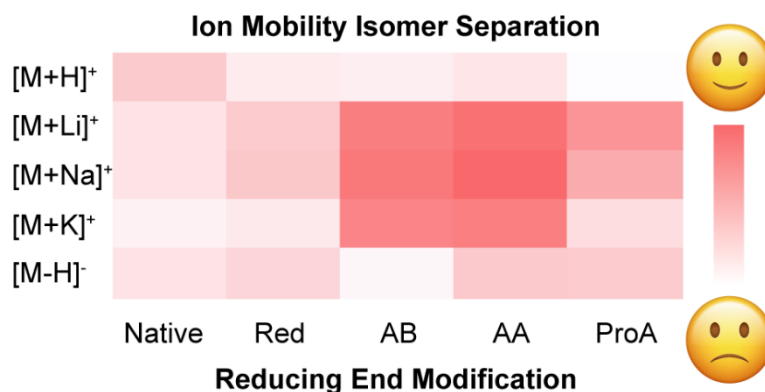
Recently, differences in sialic acid linkages were identified by analysing trisaccharide fragments derived from glycopeptide precursor ions (**Figure 10b**) <sup>20, 145</sup>. The fragments derived from synthetic as well as biological glycopeptide precursor ions and exclusively contained either  $\alpha$ 2,3 or  $\alpha$ 2,6 linked N-acetylneuraminic acid (NeuAc) (**Figure 10b**, precursor structures). CID experiments of the glycopeptides resulted in the generation of diagnostic trisaccharide fragments, which showed characteristic drift times depending on the regiochemistry of the NeuAc moiety (**Figure 10b**, fragment spectra). The results of these studies show that a rapid identification and unambiguous assignment of glycan motifs can be performed independent of the nature and origin of the investigated sample.

In addition, the method is fast and does not require derivatisation, therefore demonstrating the potential of IM-MS as a high-throughput method to screen larger glycans and glycoconjugates for specific biomarkers.

## 2.4 Combination of Liquid Chromatography and Ion Mobility-Mass Spectrometry

Numerous experiments have illustrated the outstanding potential of IM-MS for the analysis of stereo- and regioisomers of complex glycans and glycoconjugates. It was demonstrated how mobility information can be used to reduce spectral complexity and how diagnostic features in glycan structures can be used for rapid identification. There are very few other methods that can provide a comparably extensive analysis of compositional, regio- as well as stereochemical information of glycans on such short time scales with similar low sample consumption. However, IMS alone only provides information on the overall shape of the investigated ions; the separation power for extremely similar structural isomers such as compositional isomers is clearly limited. Therefore, the coupling of IM-MS to orthogonal techniques, most notably chromatographic methods, represents a promising approach to obtain more detailed information on the overall glycan structure. Although IM-MS in general is highly compatible to liquid chromatography (LC) with respect to time scale and orthogonality,<sup>146</sup> very few studies have addressed the direct hyphenation of both techniques for routine glycan analysis so far.<sup>63, 147</sup> It is largely unknown how the commonly applied reducing end modifications used for LC-MS affect the ion mobility separation of isomeric ions or how to adapt established LC-MS workflows to enable a meaningful integration of IMS in general. Current studies focus on technical aspects of glycan separation *via* IMS, while the implementation of ion mobility separations into well-established workflows to analyse real-world samples have been neglected. However, the solution of analytical problems arising in the field of glycomics requires robust methods that step beyond proof-of-principle studies.

### 3 Separation of Isomeric Glycans by Ion Mobility Spectrometry – the Impact of Fluorescent Labelling\*



#### 3.1 Introduction

As described in **Chapter 2**, glycans exhibit very complex structures due to the isomeric character of its building blocks and a common way to tackle this challenge is LC in combination with spectroscopic and/or spectrometric detection. However, as glycans naturally do not contain chromophores or fluorophores, it is often necessary to derivatize them with reducing end labels to facilitate a sufficient detection and enable quantification.<sup>148</sup> Although derivatizations are fundamental for LC-MS analysis, IMS does not require any chemical modifications and studies on glycans have almost exclusively been performed on native structures. Fluorescence labels, however, can substantially alter the three-dimensional gas-phase structure of glycans, which makes a prediction of the mobility behaviour and therefore the impact on the separation of isomeric glycans difficult

\* This chapter is based on the work “Separation of Isomeric Glycans by Ion Mobility Spectrometry – the Impact of Fluorescent Labelling” by C. Manz, M. Grabarics., F. Hoberg, M. Pugini, A. Stuckmann, W.B. Struwe, and K. Pagel, published in *Analyst* **2019**, 144, 5292-5298. Figures and content adapted with permission. Copyright 2017 The Royal Society of Chemistry. <https://doi.org/10.1039/C9AN00937J>

if not impossible. To close this gap, we present a systematic analysis using a set of isomeric glycans derivatized with different common glycan fluorophores as well as native and reduced species. Our data indicate that labelling can significantly affect the ability to separate individual glycan isomers *via* IM-MS. Depending on the label, this can diminish or improve selectivity, and therefore, labels should be specifically selected for a given glycan analysis.

## 3.2 Experimental Details

### 3.2.1 Sample Preparation

All labelling reagents and solvents were purchased from Sigma Aldrich (St Louis, USA) and used without further purification. Synthetically derived Lewis oligosaccharides were purchased from Dextra Laboratories Ltd (Reading, UK). Prior to analysis, the Lewis antigens were diluted to 1 mM stock solution in HPLC grade water. The stock solution was divided into 10  $\mu$ L (10 nmol) aliquots and freeze dried. Dried Lewis antigens were labelled with 2-aminobenzoic acid (2-AA), 2-aminobenzamide (2-AB), 4-amino-N-[2-(diethylamino)ethyl]benzamide (procainamide, ProA) *via* reductive amination.<sup>58</sup> Removal of excess label was performed using paper chromatography.<sup>149</sup> Alditols were synthesised *via* reduction with sodium borohydride.<sup>150</sup> The reduced, as well as 2-AB, 2-AA and ProA labelled glycans were further purified using HyperSep Hypercarb SPE cartridges (Thermo Fisher Scientific, Waltham, Massachusetts, US) according to manufacturer's instructions. Afterwards, the purified glycans were freeze dried and redissolved in HPLC grade water to yield a  $\sim$  100  $\mu$ M stock solution.

### 3.2.2 Ion Mobility-Mass Spectrometry

Linear drift tube (DT) IM-MS measurements were performed on a modified Synapt G2-S HDMS instrument (Waters Corporation, Manchester, UK), described in detail elsewhere.<sup>126</sup> Measurements were performed in positive and negative ion mode with platinum/palladium (Pt/Pd, 80/20) coated borosilicate capillaries prepared in-house. Prior

to measurements, each sample was diluted from stock solution with methanol: water (1:1) to result in a final concentration of 10  $\mu$ M. Salt solutions were generated by adding a 10 mg/mL aqueous stock solution of KCl/ LiCl/ NaCl to the labelled glycan solution to result in a of 1:5 ratio (salt:glycan).

For nano-electrospray ionization (nano-ESI) typically 5  $\mu$ L of sample were loaded to a capillary and electrosprayed by applying a capillary voltage of 0.6-1.1 kV. Typical parameters in positive ion mode were: 60 V sampling cone voltage, 1 V source offset voltage, 30°C source temperature, 0 V trap CE (MS) up to 30 V trap CE (MSMS), 2 V transfer CE, 3 mL/min trap gas flow. Ion mobility parameters were: 2.2 Torr helium IMS gas, 27-30°C IMS temperature, 5.0 V trap DC entrance voltage, 5.0 V trap DC bias voltage, -10.0 V trap DC voltage, 2.0 V trap DC exit voltage, -25.0 V IMS DC entrance voltage, 50-180 V helium cell DC voltage, -40.0 V helium exit voltage, 50-150 V IMS bias voltage, 0 V IMS DC exit voltage, 5.0 V transfer DC entrance voltage, 15.0 V transfer DC exit voltage, 150 m/s trap wave velocity, 1.0 V trap wave height voltage, 200 m/s transfer wave velocity, 5.0 V transfer wave height voltage.

In negative ion mode typical parameters were: 90 V sampling cone voltage, 10 V source offset voltage, 30°C source temperature, 0 V trap CE (MS) up to 30 V trap CE (MSMS), 2 V transfer CE, 3 mL/min trap gas flow. Ion mobility parameters were: 2.2 Torr helium IMS gas, 27-30°C IMS temperature, 1.0 V trap DC entrance voltage, 2.0 V trap DC bias voltage, -1.0 V trap DC voltage, 1.5 V trap DC exit voltage, -25.0 V IMS DC entrance voltage, 50-150 V helium cell DC voltage, -40.0 V helium exit voltage, 50-150 V IMS bias voltage, 0 V IMS DC exit voltage, 5.0 V transfer DC entrance voltage, 15.0 V transfer DC exit voltage, 200 m/s trap wave velocity, 10.0 V trap wave height voltage, 250 m/s transfer wave velocity, 3.0 V transfer wave height voltage. The resulting drift times were converted to rotationally-averaged collision cross-sections (CCS) using the Mason-Schamp equation.<sup>110</sup>

### 3.3 Results and Discussion

#### 3.3.1 ABO and Lewis Blood Group System

A common and widely studied set of isomeric glycans are the epitopes of two different blood group systems: the Lewis antigens (Le) and the ABO blood group system (H antigen, commonly referred to as BG H). These structures are typically found as features on larger glycoconjugates such as *N*- and *O*-linked glycans or on human milk oligosaccharides (HMO).<sup>151</sup> The two main types of Lewis antigens are the tetrasaccharide motifs LeY and LeB, which feature a common monosaccharide composition and are displayed in **Figure 11**. Type 1 antigens (LeB series) consist of galactose (Gal)  $\beta$ -(1 $\rightarrow$ 3) linked to *N*-acetylglucosamine (GlcNAc) core, whereas type 2 antigens (LeY-series) contain a  $\beta$ -(1 $\rightarrow$ 4) linked core. Both antigens are functionalized by two differently attached fucose (Fuc) units. The loss of one fucose unit leads to the regioisomeric trisaccharides LeX and BG H<sup>2</sup> (LeY-series) or LeA and BG H<sup>1</sup> (LeB-series). In larger glycan structures, epitopes are formed by terminal fucosylation. Each of the resulting epitopes has specific

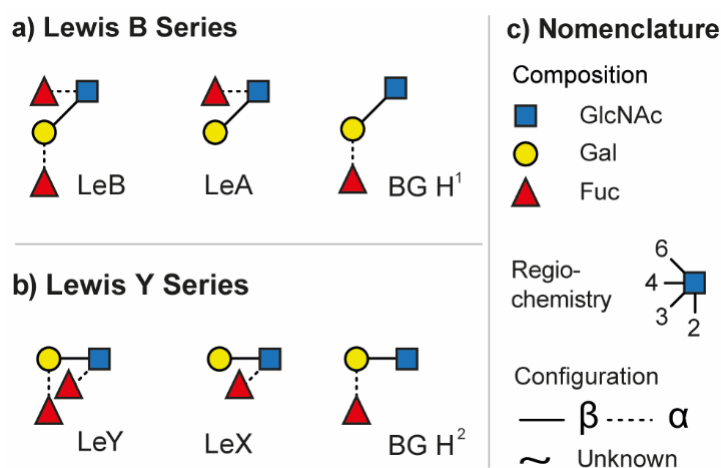


**Figure 11:** The investigated set of isomeric blood group epitopes. A) Tetrasaccharide Lewis B (LeB) and the corresponding trisaccharide fragments/motifs Lewis A (LeA) and blood group H1 (BG H1). B) Tetrasaccharide Lewis Y (LeY) and the corresponding trisaccharide fragments/ motifs Lewis X (LeX) and blood group H2 (BG H2). C) Glycan structures are depicted using the SNFG nomenclature.

functional properties and alteration is often associated with pathological processes, including cancer progression and atherosclerosis.<sup>152, 153</sup> Recently, we investigated these isomeric tri- and tetrasaccharides in an underivatized form using IM-MS and showed that fragment CCS can be used as fingerprints to systematically differentiate between the epitopes.<sup>19</sup> The intact

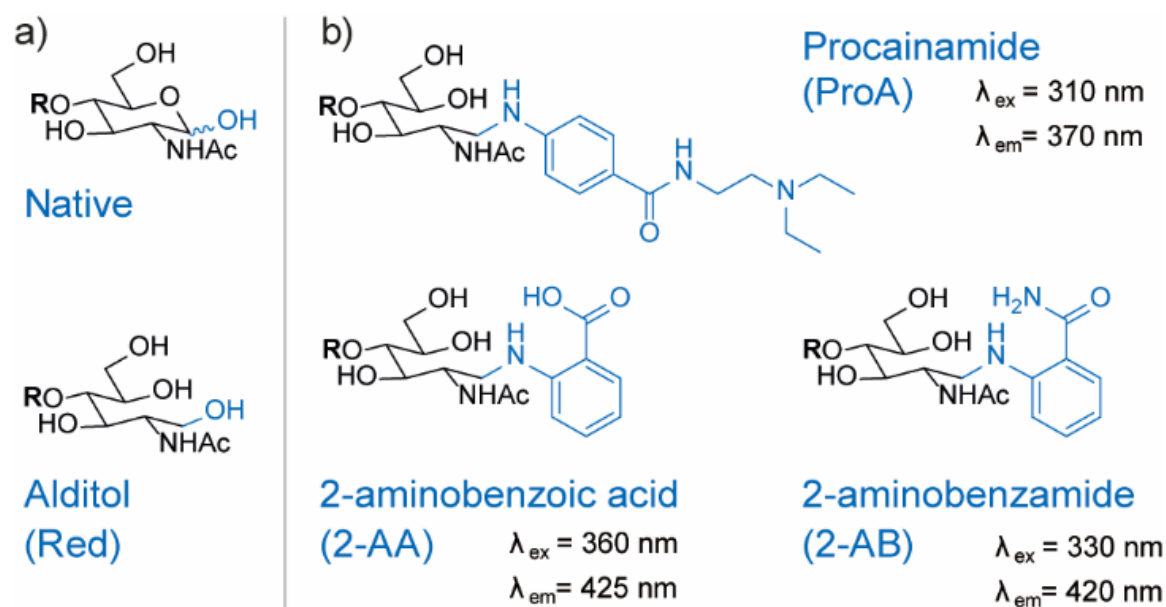


**Figure 12:** Reducing end modifications investigated in this study. A) Native glycan and the reduced alditol structure without chromophore at reducing end. B) Glycan derivatization with chromophore such as procainamide (ProA), 2-aminobenzoic acid (2-AA) and 2-aminobenzamide (2-AB) is a common strategy to increase sensitivity and enable quantification. For some labels there are additional benefits such as an improved ionization efficiency in ESI or an improved selectivity in HPLC.

tetrasaccharide precursors exhibit very similar drift times and CCS, which makes them hard to distinguish using IMS. However, fragmentation of the tetrasaccharide precursors with collision induced dissociation (CID) yields trisaccharide fragments that can be used to identify specific terminal fucose motifs. Some of those isomeric fragments such as LeX and BG H<sup>2</sup> can be readily distinguished by IMS, while LeA and BG H<sup>1</sup> are difficult to differentiate in underivatized form. In the present study, we focus on the IMS separation of derivatized forms of these epitopes.

### 3.3.2 Labelling of Glycans

Common glycan derivatization strategies, not only for the ABO and Lewis system, include permethylation, reduction, and various reducing end modifications *via* reductive amination.<sup>58</sup> Reducing end modifications have been studied extensively, namely the influence of fluorescent labels on retention in various chromatographic modes<sup>60, 154, 155</sup>, ionization efficiency in electrospray ionization (ESI)<sup>11</sup>, fragmentation patterns in MS<sup>56, 156</sup> and on rearrangement reactions of glycan ions<sup>97, 98</sup>. On the other hand, very little is known

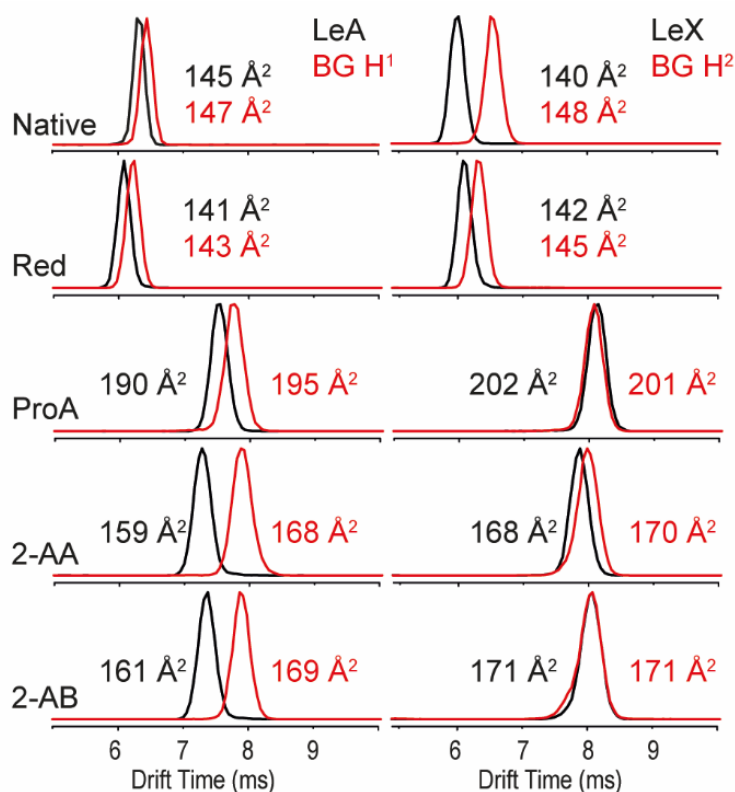


**Figure 13:** ATDs and  $DTCCS_{He}$  of the isomeric blood group epitopes LeA vs BG H1 (left panel) and LeX vs BG H2 (right panel) as sodium adducts with helium as drift gas.

about their influence on ion mobility separations. In the present study, we focus on the four most common reducing end modifications to study their influence on IMS separation (**Figure 12**). Due to the high labelling efficiency of reductive amination and the stability of the resulting labelled glycans, the fluorophores 2-aminobenzoic acid (2-AA) and 2-aminobenzamide (2-AB) are currently the most used labels. They are readily available and known for their sensitivity in fluorescence detection. Procainamide (ProA) is a beneficial fluorophore used for coupling LC with MS because its tertiary amine moiety significantly enhances ionization efficiency in matrix-assisted laser desorption/ionization (MALDI) and ESI.<sup>157, 158</sup> Since all three labels have a hydrophobic character, they increase retention of the inherently polar glycans in reversed-phase separations. As only one label is incorporated per individual glycan, derivatization with 2-AA, 2-AB or ProA furthermore enables a simple quantification.<sup>159</sup> After reductive amination with fluorescent labels such as 2-AB, 2-AA or ProA, the reducing end monosaccharide will exhibit an open ring structure. To study the influence of this ring opening, we reduced glycans to open-ring alditols (Red) to compare them with the predominantly closed-ring native structures. The reduction of

glycans often precedes permethylation, but alditols themselves are also often used as standalone modification for various stationary phases.<sup>159</sup>

### 3.3.3 Ion Mobility Separation of Labelled Glycans

In order to address the impact of labelling on the CCS of glycans, the set of blood group antigens shown in **Figure 11** was subjected to reducing end modifications displayed in **Figure 12**. For all modified species, the drift times in helium drift gas were measured and CCSs calculated ( $^{DT}CCS_{He}$ ). Measured arrival time distributions (ATDs) of the two fucosylated trisaccharide isomer pairs LeX/BG H<sup>2</sup> and LeA/BG H<sup>1</sup> as sodiated species with different reducing end modifications are shown in **Figure 13**. All ATDs were measured under the very same instrumental conditions (such as pressure, drift voltages and drift gas).

As native glycans, LeA and BG H<sup>1</sup> show minor isomer separation compared to LeX and BG H<sup>2</sup>, which are almost baseline separated. Compared to the native closed-ring structure, the ring opening during reduction to alditols does not seem to have a significant impact on the separation of LeA and BG H<sup>1</sup>. In contrast, the drift-time difference of LeX and BG H<sup>2</sup> decreases significantly after reduction. This effect is further amplified after introduction of the chromophore labels ProA, 2-AA and 2-AB. 2-AA and 2-AB labelled glycans show the largest isomer separation for the LeA and BG H<sup>1</sup> isomers, while LeX and BG H<sup>2</sup> are basically indistinguishable.

Similarly, all native and derivatized isomers were measured as alkali metal adducts, which are known to significantly alter isomer separation in IMS.<sup>138</sup> Negatively charged adducts such as chloride and nitrate complexes predominantly lead to the formation of deprotonated ions, which are therefore the only ions with negative polarity studied here.<sup>160, 161</sup> In **Table 1**, the CCSs of protonated and deprotonated glycans, as well as for three commonly observed typical alkali adducts (Li<sup>+</sup>, Na<sup>+</sup>, K<sup>+</sup>) measured in helium ( $^{DT}CCS_{He}$ ) are shown. The upper part of **Table 1** shows the CCSs of all derivatives and metal adducts of the LeB series, while the lower part shows the CCSs of all modifications of the LeY series. The exact masses of all labelled glycans are shown in **Table 2**.

**Table 1:** Comprehensive overview over all CCSs measured in helium for native and derivatized glycans.

<sup>DT</sup> CCS <sub>He</sub> (Å <sup>2</sup> )	Type	Native	Red	2-AB	2-AA	ProA
LeB	[M+H] <sup>+</sup>	167	167	189	189	209
	[M+Li] <sup>+</sup>	165	159	179	178	209
	[M+Na] <sup>+</sup>	166	160	180	178	210
	[M+K] <sup>+</sup>	166	164	182	180	214
	[M-H] <sup>-</sup>	165	161	184	179	218
LeA	[M+H] <sup>+</sup>	144	144	168	167	183
	[M+Li] <sup>+</sup>	143	138	159	158	188
	[M+Na] <sup>+</sup>	145	141	161	159	190
	[M+K] <sup>+</sup>	145	146	163	163	194
	[M-H] <sup>-</sup>	143	141	162	160	190
BG H <sup>1</sup>	[M+H] <sup>+</sup>	144	144	170	168	188
	[M+Li] <sup>+</sup>	146	142	167	167	195
	[M+Na] <sup>+</sup>	147	143	169	168	195
	[M+K] <sup>+</sup>	145	146	169	170	193
	[M-H] <sup>-</sup>	143	143	163	157	192
LeY	[M+H] <sup>+</sup>	171	169	190	191	209
	[M+Li] <sup>+</sup>	163	163	190	190	219
	[M+Na] <sup>+</sup>	164	164	192	191	218
	[M+K] <sup>+</sup>	165	166	192	191	217
	[M-H] <sup>-</sup>	167	164	185	183	213
LeX	[M+H] <sup>+</sup>	144	145	169	170	188
	[M+Li] <sup>+</sup>	138	141	169	165	202
	[M+Na] <sup>+</sup>	140	142	171	168	202
	[M+K] <sup>+</sup>	141	144	171	169	198
	[M-H] <sup>-</sup>	146	141	161	159	189
BG H <sup>2</sup>	[M+H] <sup>+</sup>	144	145	172	166	185
	[M+Li] <sup>+</sup>	148	145	170	169	201
	[M+Na] <sup>+</sup>	148	146	171	170	201
	[M+K] <sup>+</sup>	149	148	172	172	197
	[M-H] <sup>-</sup>	144	139	163	155	190

Generally, there is a clear trend of increasing CCS from the native glycans up to the ProA-labelled glycans. The CCSs for all species is growing proportionally to the size of the added fluorescent label, and is therefore correlated to the increase in molecular mass.<sup>138</sup> A similar trend is observed with the addition of alkali metals, which generally lead to larger

**Table 2:** Masses of the measured antigens as native and derivatized species.

Glycan	Modification	[M+H] <sup>+</sup>	[M+Na] <sup>+</sup>	[M+K] <sup>+</sup>	[M+Li] <sup>+</sup>	[M-H] <sup>-</sup>
Trisaccharides	Native	530.49	552.49	568.49	536.49	528.49
	Red	532.49	554.49	570.49	538.49	530.49
	2-AA	651.49	673.49	689.49	657.49	649.49
	2-AB	650.49	672.49	688.49	656.49	648.49
	ProA	749.49	771.49	787.49	755.49	747.49
Tetrasaccharides	Native	676.63	698.63	714.63	682.63	674.63
	Red	678.63	700.63	716.63	684.63	676.63
	2-AA	797.63	819.63	835.63	803.63	795.63
	2-AB	796.63	818.63	834.63	802.63	794.63
	ProA	895.63	917.63	933.63	901.63	893.63

CCSs in the order of  $H^+ < Li^+ < Na^+ < K^+$ . Deprotonated species on the other hand behave similar to their protonated counterparts. However, there are some exceptions to this behaviour. Especially alditols (Red) seem to have their largest CCS when protonated or adducted with potassium, while sodiated and lithiated species show significantly smaller CCSs. Another example are glycans labelled with 2-AA, whose protonated species show larger CCSs than metal adducted species, which indicates a compaction of the gas-phase structure with the addition of small alkali metal ions. This behaviour is a result of the structure of the oligosaccharide-metal complex, which is dictated by the solvation of the metal cation.

### 3.3.4 Comparison of Isomeric Labelled Glycan Isomers

As shown above, the CCSs of each species strongly depends on the modification of the reducing end and the type of adduct. The type of label will therefore also affect the ability to separate isomers. Based on the CCS for each individual species it is difficult to rank the quality of each individual separation. A highly useful index for evaluating this performance is the *peak-to-peak resolution* ( $R_s$ ). It serves as a quantitative measure of the extent to which a pair of peaks is separated. The definition of  $R_s$  – universally accepted in

column chromatography, ion mobility spectrometry, *etc.* – is given by the following equation:

$$R_s = \frac{t_2 - t_1}{2\sigma_2 + 2\sigma_1} \quad (2)$$

Here,  $2\sigma$  is the temporal peak width measured between the two inflection points of a peak of Gaussian profile and  $t$  the drift time. In case of separating isomers of the same charge state by linear drift tube ion mobility spectrometry (DTIMS), **Equation 2** can be rewritten in the following form:

$$R_s = \frac{\sqrt{N}}{4} \frac{|\Delta CCS|}{\overline{CCS}} = \frac{\overline{R}_p}{\sqrt{2/\ln 2}} \frac{|\Delta CCS|}{\overline{CCS}} \quad (3)$$

In **Equation 3**,  $\overline{N}$  and  $\overline{R}_p$  are the average *plate number* and average *resolving power*, respectively (the latter one should not be confused with peak-to-peak resolution). The relation between the two figures of merit is given by definition as  $\overline{R}_p = \sqrt{\overline{N}/8\ln 2}$ , the origin of the constant in the formula being the difference between the standard deviation and the full-width-at-half-maximum (FWHM) of Gaussian distributions. The fraction  $|\Delta CCS|/\overline{CCS}$  is the relative difference between the collision cross sections of the ions that are to be separated, *i.e.*, it is a measure of selectivity. In following, we used this term to describe the difference in CCS between the tetrasaccharide isomer pair LeY/LeB as well as the trisaccharide isomer pairs LeX/BG H<sup>2</sup> and LeA/BG H<sup>1</sup> and visualize this difference as heat map in **Table 3**.

The upper part of **Table 3** shows the isomer separation for the tetrasaccharides LeY/LeB. Here two general trends are observed: 1) isomer separation is increased when a fluorescent label is introduced and 2) isomer separation is improved upon adduct formation with alkali metal adducts. There are, however, significant differences between each individual modification. While native tetrasaccharides only show up to 2.4% CCS difference, 2-AA and 2-AB labelled species separate much better with a difference of up to 6.9% for sodium adducts. ProA-labelled isomers, on the other hand are separated as lithiated species with a difference of 4.9%. Thus, specific labels can increase isomer separation, which in some cases makes them beneficial for IMS separation.

**Table 3:** CCS differences of the three derivatized fucose-containing isomer pairs LeY/LeB, LeX/BG H2 and LeA/BG H1 displayed as heat map.

LeB/LeY	Native	Red	2-AB	2-AA	ProA
[M+H] <sup>+</sup>	2,4	0,8	0,7	1,1	0,0
[M+Li] <sup>+</sup>	1,2	2,3	5,9	6,5	4,9
[M+Na] <sup>+</sup>	1,2	2,5	6,2	6,9	3,8
[M+K] <sup>+</sup>	0,6	1,0	5,6	5,9	1,5
[M-H] <sup>-</sup>	1,2	1,8	0,4	2,4	2,3
LeA/BG H <sup>1</sup>	Native	Red	2-AB	2-AA	ProA
[M+H] <sup>+</sup>	0,0	0,1	1,5	0,2	2,8
[M+Li] <sup>+</sup>	2,1	3,5	4,7	5,1	3,8
[M+Na] <sup>+</sup>	1,4	1,5	4,9	5,5	2,5
[M+K] <sup>+</sup>	0,0	0,4	3,6	3,9	0,3
[M-H] <sup>-</sup>	0,0	1,1	0,7	1,4	1,1
LeX/BG H <sup>2</sup>	Native	Red	2-AB	2-AA	ProA
[M+H] <sup>+</sup>	0,0	0,2	2,1	2,1	1,6
[M+Li] <sup>+</sup>	7,0	3,0	1,0	1,9	0,6
[M+Na] <sup>+</sup>	5,6	2,5	0,1	1,5	0,5
[M+K] <sup>+</sup>	5,5	2,5	0,8	1,4	0,3
[M-H] <sup>-</sup>	1,4	1,3	0,9	2,3	0,3
$\Delta$ CCS/ CCS(%)	0	1	3	5	7

A very similar behaviour of improved separation is observed for the LeB submotifs LeA vs. BG H<sup>1</sup>. Native structures of these isomers do practically not separate in IMS independent of the charge carrier; only lithiated and sodiated species do show minor differences up to 2.1%. In contrast, a functionalization with fluorescent labels yields considerably different CCSs, which differ up to 5.5%.

However, as shown for the LeY submotifs LeX vs. BG H<sup>2</sup>, the above-mentioned trends cannot be generalized and may in some cases even be reversed. Here, the native,

underivatized from of the glycan can be separated best with 7% CCS difference for lithium adducts. Upon modification of the reducing end, the quality of the separation suffers drastically. With up to 3% difference alditol structures may be resolvable on some instruments, while 2-AA, 2-AB and ProA labelled ions cannot be distinguished (<2%). Remarkably, although the trend is reversed for the trisaccharide isomer pairs LeA / BG H<sup>1</sup> and LeX vs. BG H<sup>2</sup>, the average CCS difference is similar at ~2%. For the tetrasaccharides, the CCS difference is even larger with almost 3%.

To evaluate which CCS difference is sufficient to identify two isomeric species in a mixture, the resolving power from **Equation 3** must be considered. Besides showing the most important factors that influence and, ultimately, determine  $R_s$  in DTIMS, **Equation 3** also provides a means to calculate the required resolving power ( $R_p$ ) to achieve a specified peak-to-peak resolution for a given pair of ions. If the relative CCS difference of two ions is 2%, a resolving power of 64 (corresponding to a plate number of 22,500) is required to distinguish them (*i.e.*, separation with a peak-to-peak resolution of  $R_s = 0.75$ ). To achieve baseline resolution for the same two peaks ( $R_s = 1.5$ ), the resolving power must be substantially higher, approximately 127 (corresponding to a plate number of 90 000). This is already achievable with state-of-the-art custom-built and commercial instruments and shows that IMS can be readily applied for isomer separations, as shown in this study for fucose-containing isomers.

### 3.3.5 *The Impact of Labelling on Fucose Migration*

The isomer pairs LeA/BG H<sup>1</sup> and LeX/BG H<sup>2</sup> are known to undergo fucose migration as protonated ions. Fucose migration is a gas-phase rearrangement reaction during which fucose residues relocate within a glycan during a MS experiment. As a result, sequence information can get lost in tandem MS experiments, which can lead to erroneous structural assignments.<sup>162</sup> Traditionally, fucose migration was always closely related to a fragmentation *via* CID.<sup>97</sup> However, more recent studies using cold-ion IR spectroscopy showed that fucose migration reactions have a rather low activation barrier and can therefore also occur without dissociation.<sup>96, 98</sup> In this context, the type of adduct as well as the position of the charge was shown to be crucial.<sup>160</sup> Metal adducts generally do not show

fucose migration; protonated species on the other hand can rearrange when the proton is mobile and located at a certain position within the glycan.<sup>98</sup>

The results of the isomer pairs LeA/BG H<sup>1</sup> and LeX/BG H<sup>2</sup> obtained here fully agree with those of previous reports. LeA/BG H<sup>1</sup> as well as LeX/BG H<sup>2</sup> yield very similar CCSs as protonated ions and the ATDs are overlapping perfectly, which indicates migration into a similar structure. A similar behaviour can be hypothesized for protonated reduced glycans, which show very similar CCSs that are well within the error of the measurement (relative standard deviation (RSD) of 0.5%).<sup>116</sup> However, based on the present data a clear conclusion cannot be drawn. In strong contrast, most of the metal adducts differ substantially in CCS, which clearly contradicts a rearrangement reaction. Labelling with 2-AA, 2-AB and ProA not only changes the UV and fluorescence activity of the glycan, but also introduces apparent basic sites, which reduces or inhibits proton mobility. As a result, different structures leading to distinct CCSs are retained. Fluorescence labelling can therefore not only help to increase isomer separation in IMS as shown above but can also inhibit fucose migration in protonated glycan ions.

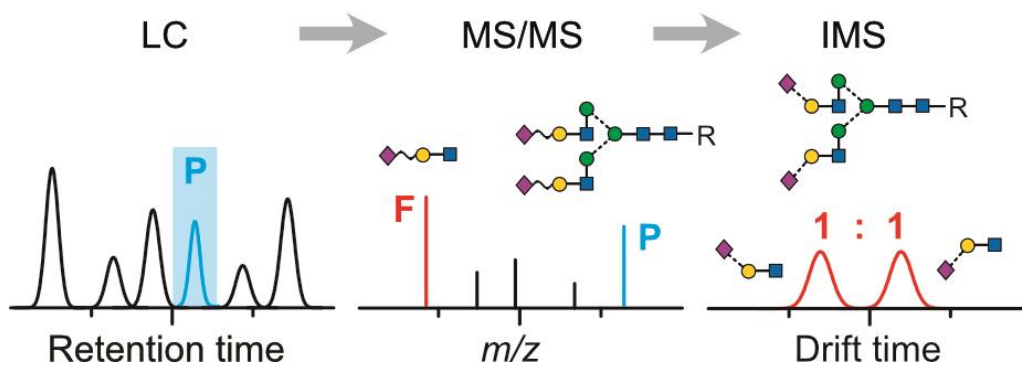
### 3.4 Conclusion

Here we systematically evaluate the impact of reducing end modifications on the CCS and isomer separation of glycans. A set of Lewis and ABO blood group isomers was derivatized using labels established in LC. Their <sup>DT</sup>CCS<sub>SHe</sub> were measured in positive and negative ion polarity. Furthermore, the influence of alkali metal salt adduction was evaluated. Our results show that fluorescent labels can significantly influence the gas-phase structure of glycans. As a result, reducing end modifications can considerably improve, but in some cases also diminish the quality of a given isomer separation. Based on the limited set of investigated glycans, no general trends to increase selectivity was observable. Therefore, more glycans have to be analysed in order to predict, which reducing-end modification is required to optimize a particular isomer separation.

Seen from a broader perspective, the presented data show the great potential of an LC-IM-MS coupling for glycomics. Both methods have previously shown their individual

strengths and weaknesses in glycan analysis. LC can resolve and quantify certain isomers and retention indices (i.e. glucose units<sup>163</sup>) can be used for the structural identification of known components. IM-MS on the other hand is more sensitive and can also resolve isomers with an amphiphilic character such as synthetic glycans or glycolipids, which due to their mixed polarity can often not be separated by LC.<sup>21</sup> In addition, fragmentation and subsequent IMS analysis enables the rapid identification of unknown components based on database CCSs of small fragments.<sup>19, 20, 164</sup> Regarding time scale, LC and IM-MS are furthermore highly complementary and data can be obtained simultaneously on a high-throughput scale.<sup>86, 165</sup> A combination of LC and IM-MS is therefore highly synergistic and more than the sum of its parts. When combined with suitable software tools to annotate tandem MS spectra and calculate glucose units<sup>84</sup> and CCSs<sup>166</sup>, LC-IM-MS has the potential to serve as the future core technology in glycomics.

## 4 Determination of Sialic Acid and Fucose Isomers from Released N-glycans Using Ion Mobility Spectrometry<sup>†</sup>



### 4.1 Introduction

An interesting field for the application of LC-IM-MS lies in diagnostic research to study the impact of glycosylation on different glycoconjugates and particularly on glycoproteins. Glycosylation is very sensitive to the environment of the protein and changes are therefore often directly associated to diseases.<sup>1, 5</sup> In the case of *N*-linked glycans for example, pathologic changes can translate into altered levels of sialylation<sup>167</sup> or fucosylation.<sup>168</sup>

The sialylation pattern is described by the type and linkage of sialic acid, which is a generic term for a family of more than fifty different acidic monosaccharides and is used

<sup>†</sup> This chapter is based on the work "Determination of Sialic Acid and Fucose Isomers from Released N-glycans Using Ion Mobility Spectrometry" by C. Manz, M. Mancera-Artu, A. Zappe, E. Hanozin, L. Polewski, E. Giménez, V. Sanz-Nebot and K. Pagel, submitted to *Analytical Chemistry* 2022.

This is a pre-peer-review, pre-copyedit version of an article published in *Analytical Chemistry*. The final authenticated version is available online at: <https://doi.org/10.1021/acs.analchem.2c00783>

synonymously in humans for its most prominent member, *N*-acetylneuraminic acid (Neu5Ac). Neu5Ac is usually found at the non-reducing end of branched *N*-glycans as terminal monosaccharide residue connected to a galactose *via*  $\alpha$ 2,3- or  $\alpha$ 2,6-linkages. Due to its exposed location, sialic acids often participate as recognition sites in biological processes including cancerogenesis.<sup>169</sup> As the up- or downregulation of each linkage isomer can correlate to different types of cancer<sup>41, 170, 171</sup>, it is important to monitor the sialic acid linkage type and the glycan structure in general.

The detailed analysis of sialylated glycans is a particularly challenging task, especially when isomers must be identified. Today, the gold standard method for glycan analysis relies on LC-MS and involves the enzymatic release of the glycans from a glycoprotein and derivatization with a fluorescence tag. While LC-MS is able to separate and identify most of the common *N*-glycan structures, a detailed assignment of  $\alpha$ 2,3- or  $\alpha$ 2,6-linkage isomers is still laborious and tedious due to their very similar MS/MS fragmentation patterns.<sup>172, 173</sup> In addition to conventional LC-MS, sequential digestion with several exoglycosidases can be applied to identify the regiochemistry of the sialic acid linkage.<sup>82, 174</sup> This however, also leads to significant increase in costs and analysis time. Recently, linkage-specific derivatization of  $\alpha$ 2,3- and  $\alpha$ 2,6- isomers in combination with matrix-assisted laser desorption/ionization-MS (MALDI-MS) emerged as a promising alternative to the slower LC-MS and enzyme based approaches.<sup>39, 66</sup> Using this approach, the linkage types can be directly identified by a mass difference, however, the sample preparation is complex and not yet applicable in routine work.

As alternative to common MS-based approaches, ion mobility spectrometry (IMS) recently emerged as a promising tool in the field of glycomics.<sup>15, 16, 21</sup> Although IMS is only able to partially resolve intact sialylated glycans<sup>175, 176</sup>,  $\alpha$ 2,3- and  $\alpha$ 2,6- sialic acid linkages can be unambiguously identified using a fragment-based approach.<sup>20, 145</sup> Furthermore, and in contrast to MALDI-MS, IMS can be easily implemented in existing LC-MS workflows and is fully compatible with commonly applied fluorescent labels.<sup>177</sup>

In this study, we assessed the potential of IM-MS to assign sialic acid linkage isomers on the level of released complex *N*-glycans. For this purpose, we selected human alpha-1-acid

glycoprotein (hAGP) as model due to its large *N*-glycan microheterogeneity and its potential as biomarker in pancreatic cancer and other diseases. In addition, characterization of the sialic acid linkage type of hAGP *N*-glycans has been previously addressed by several LC-MS approaches<sup>82, 173</sup> which allows a thorough validation of our results. Our data indicate that a direct injection IM-MS approach can identify the general sialic acid distribution of hAGP without prior derivatization. It allows the quantification of sialic acid linkage isomers individually for each isomeric class and is highly suitable for a rapid screening of glycoproteins. Subsequently, we used hydrophilic interaction liquid chromatography (HILIC) directly coupled to IM-MS to simultaneously analyse the glycan composition and sialylation pattern of complex *N*-glycans released from hAGP. The combination of both techniques proved to be a powerful tool for the characterization of *N*-glycans. It can fully resolve all sialic acid linkage isomers for each glycan individually, while being fully compatible with existing workflows for *N*-glycan analysis.

## 4.2 Experimental Details

### 4.2.1 Chemicals

All chemicals and reagents were at least analytical reagent grade and used without further purification. Rapid™ PNGase F and Rapid™ PNGase F Buffer were supplied by New England Biolabs (Ipswich, USA). Human alpha-1-acid glycoprotein (hAGP, ≥95%), Discovery Glycan solid phase extraction (SPE) tubes, TFA (≥99%), procainamide hydrochloride (≥98%) and both trisaccharide standards 6'/3'-Sialyl-N-acetylactosamine were purchased from Sigma-Aldrich (St Louis, USA). The fucosylated standard 3'-Sialyl-Lewis X were supplied by Biosynth Carbosynth (UK). Hypercarb SPE tubes were purchased from Thermo Fisher Scientific (Waltham, USA). Ammonium formate (>99%) was obtained from VWR International (Radnor, USA). All solvents (acetonitrile, methanol, water) were LC-MS grade and purchased from Sigma-Aldrich (St Louis, USA).

#### 4.2.2 *Sample Preparation for Native Glycans*

10  $\mu\text{L}$  of glycoprotein stock solution (10 mg/mL in water) was mixed with 10  $\mu\text{L}$  water and 4  $\mu\text{L}$  Rapid<sup>TM</sup> PNGase F Buffer and denatured at 95°C for 10 min. After cooling to room temperature, 1  $\mu\text{L}$  of Rapid<sup>TM</sup> PNGase F was added to the mixture and incubated at 50°C for 10 min. Afterwards, the released glycans were enriched with Hypercarb SPE tubes according to vendor's instruction, dried *via* SpeedVac (Thermo Fisher Scientific, Waltham, USA) and suspended in 50  $\mu\text{L}$  water: methanol: formic acid (1:1:0.1 v/v/v) prior to direct injection IM-MS analysis.

#### 4.2.3 *Sample Preparation for Labelled Glycans*

10  $\mu\text{L}$  of glycoprotein stock solution (10 mg/mL in water) was mixed with 10  $\mu\text{L}$  water and 4  $\mu\text{L}$  Rapid<sup>TM</sup> PNGase F Buffer and denatured at 95°C for 10 min. After cooling to room temperature, 1  $\mu\text{L}$  of Rapid<sup>TM</sup> PNGase F was added to the mixture and incubated at 50°C for 10 min. Afterwards, the released glycans were labelled with procainamide according to established protocols.<sup>177, 178</sup> The labelled glycans were purified with the Discovery Glycan SPE tubes according to vendor's instruction, dried *via* SpeedVac (Thermo Fisher Scientific, Waltham, USA) and further suspended in 50  $\mu\text{L}$  water before storing them in the HPLC autosampler at 4°C.

#### 4.2.4 *Offline IM-MS Experiments*

Travelling wave (TW) IM-MS measurements were performed on a Synapt G2-S HDMS instrument (Waters Corporation, Manchester, UK), described in detail elsewhere.<sup>111</sup> Direct infusion measurements with released native glycans were performed in positive ion mode using platinum/palladium (Pt/Pd, 80/20) coated borosilicate capillaries prepared in-house. For nano electrospray ionization (nESI), typically 5  $\mu\text{L}$  of sample were loaded to a capillary and electrosprayed by applying a capillary voltage of 0.6-1.1 kV.

#### 4.2.5 *Online HILIC-IM-MS Experiments*

Released and procainamide-labelled glycans were separated by a glycan BEH amide column (150 mm x 2.1 mm, 130A, 1.7  $\mu$ m, Waters, Milford, USA) before ESI ionization. Solvent A was 50 mM ammonium formate adjusted to pH 4.4, and solvent B was acetonitrile. The column temperature was set to 65°C and samples were analysed at a flow rate of 0.4 mL/min using a linear gradient of 75-54 % B from 0-35 min. The injection volume was 4-5  $\mu$ L. The separated glycans were then ionized online with a capillary voltage of 2.2-2.5 kV.

Typical MS parameters in resolution mode (for offline and online measurements) for positive ion polarity were: 30 V sampling cone voltage, 1 V source offset voltage, 120°C source temperature, 0 V trap CE (MS) up to 30 V trap CE (MS/MS), 2 V transfer CE, 3 mL/min trap gas flow. Ion mobility parameters were: 5.0 V trap DC entrance voltage, 5.0 V trap DC bias voltage, -10.0 V trap DC voltage, 2.0 V trap DC exit voltage, -25.0 V IMS DC entrance voltage, 50-180 V helium cell DC voltage, -40.0 V helium exit voltage, 50-150 V IMS bias voltage, 0 V IMS DC exit voltage, 5.0 V transfer DC entrance voltage, 15.0 V transfer DC exit voltage, 150 m/s trap wave velocity, 1.0 V trap wave height voltage, 200 m/s transfer wave velocity, 5.0 V transfer wave height voltage.

Data were acquired with MassLynx v4.1 and processed with Driftscope version 2.8 software (Waters, Manchester, UK), and OriginPro 8.5 (OriginLab Corporation, Northampton).

### 4.3 **Results and Discussion**

#### 4.3.1 *Direct Injection IM-MS Analysis of Released Glycans*

As the separation power of IMS is often insufficient to fully separate larger glycan structures, intact precursors are usually cleaved into smaller fragments to deduce their overall structure from specific motifs. Such a characteristic fragment for the differentiation of sialic acid isomers *via* IM-MS was recently established on the level of glycopeptides. The proteolytic digestion of glycoproteins derived from Chinese hamster ovary cells

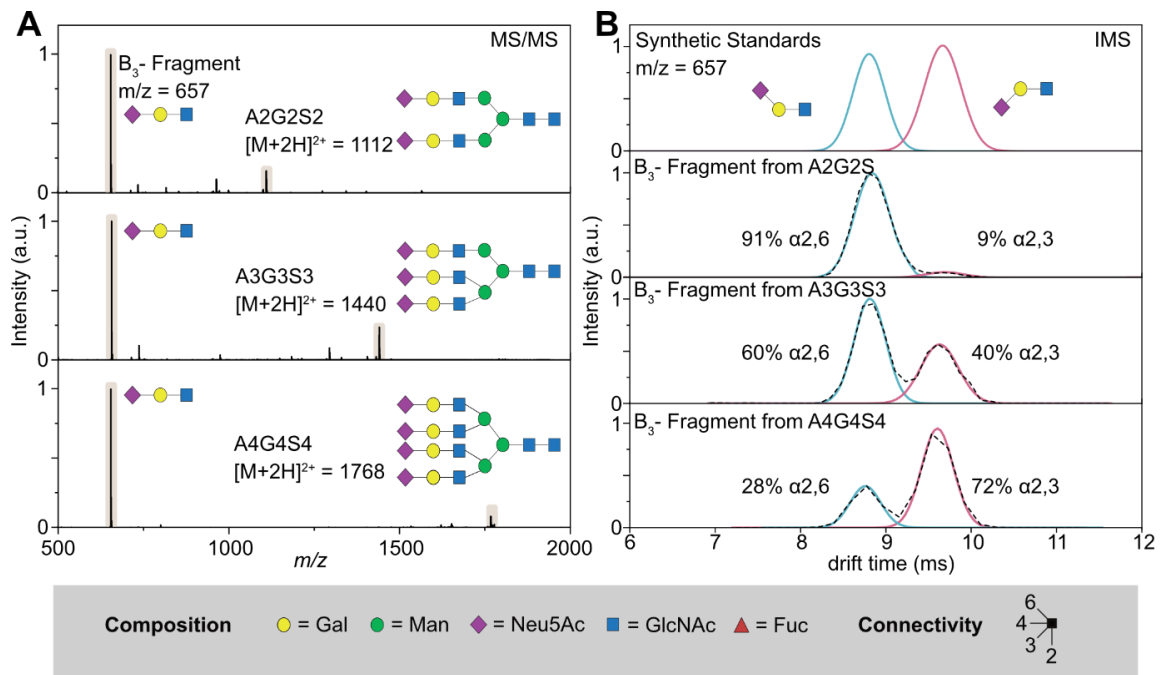


**Figure 14:** Differentiation of N-acetylneuraminic acid (Neu5Ac) linkage isomers using CID fragmentation and subsequent IM-MS analysis in positive ion mode. (a) MS/MS spectra of sialylated N-glycans A2G2S2 (top panel), A3G3S3 (middle panel) and A4G4S4 (bottom panel). Upon CID activation each sialylated precursor exhibits a characteristic B<sub>3</sub> trisaccharide fragment ( $m/z$  657). (b) Mobilogram of two synthetic trisaccharide standards which contain a terminal  $\alpha$ 2,6-linked sialic acid (blue trace) or a terminal  $\alpha$ 2,3-linked sialic acid (red trace). They can be used as reference to identify the isoforms of the B<sub>3</sub> fragments cleaved from the sialylated glycan precursors. The black dotted line is the original ATD while the blue and red traces represent the gaussian fits to indicate  $\alpha$ 2,6- and  $\alpha$ 2,3-linked sialic acid isomers. Glycans are represented using the SNFG nomenclature which depicts monosaccharides as coloured symbols. The here crucial regiochemistry is defined by the angle of the glycosidic bond.

(CHO) and human plasma resulted in N-glycopeptides, which were subsequently analysed in a fragment-based IM-MS approach.<sup>20, 145</sup> The fragmentation of sialylated glycopeptides *via* collision-induced dissociation (CID) generates a characteristic B<sub>3</sub> trisaccharide fragment which contains a terminal  $\alpha$ 2,6- or  $\alpha$ 2,3-linked Neu5Ac. Both trisaccharide fragments exhibit almost baseline separated IMS features and can therefore be used to qualitatively differentiate sialic acid isomers on the level of glycopeptides.

The above-mentioned approach, however, was never applied for isomer separation on the level of released glycans. Therefore, we established the direction injection approach for complex N-glycan samples with the released glycans of hAGP as references. hAGP is an acute phase protein (APP) found in human plasma and displays a high N-glycan content

(45 %, w/w). The *N*-glycans of hAGP are relatively large (up to tetraantennary) and heavily sialylated, with both  $\alpha$ 2,6- and  $\alpha$ 2,3-linked Neu5Ac isomers.<sup>173, 179</sup> APPs in general are prone to contain potential biomarkers as they show changes on the protein and glycosylation level when confronted with inflammatory processes.<sup>180, 181</sup> In the case of hAGP, altered glycosylation was observed for several cancer types in which specific sialylated epitopes are formed.<sup>182</sup> To release the glycans from the glycoprotein, hAGP was treated with PNGase F and the free glycans were enriched *via* PGC SPE. Subsequent direct injection MS analysis of the released glycans in positive ion mode reveals multiple highly sialylated glycan structures (see **Figure S-4** in the appendix). The fragmentation of these sialylated glycans *via* CID generates highly abundant B<sub>3</sub> fragment ions ( $m/z = 657$ ) which is exemplarily shown for the glycan species A2G2S2, A3G3S3 and A4G4S4 of hAGP in **Figure 14**. They represent typical complex *N*-glycans with multiple sialic acids which are usually very demanding to distinguish by MS and MS/MS alone. The resulting MS/MS spectra reveal several fragment ions; in all cases the characteristic B<sub>3</sub> fragment ( $m/z = 657$ ) was the dominant and most intense signal (**Figure 14A**). The mobilograms of the B<sub>3</sub> fragments reveal two almost baseline separated features at ~8.7 ms and ~9.5 ms (**Figure 14B**). The structural assignment of both arrival time distributions (ATDs) can be accomplished by comparison with two synthetic trisaccharide standards (**Figure 14B**, top panel). 6'-sialyl-*N*-acetyllactosamine (blue trace) and 3'-sialyl-*N*-acetyllactosamine (red trace) share the same structure as the characteristic B<sub>3</sub> fragment ( $m/z = 657$ ) cleaved from sialylated *N*-glycans.<sup>20, 145</sup>

The ATDs clearly reveal that the ratio of sialic acid isomers is highly dependent on the size of the glycan and the degree of branching (**Figure 14B**). While biantennary species almost exclusively contain  $\alpha$ 2,6-linked sialic acid (~91%  $\alpha$ 2,6 : 9%  $\alpha$ 2,3), a more balanced ratio of both isomers (~60%:40%) is observed for the triantennary species. The tetraantennary structure, on the other hand, exhibits a reversed trend with a higher content of  $\alpha$ 2,3-linked

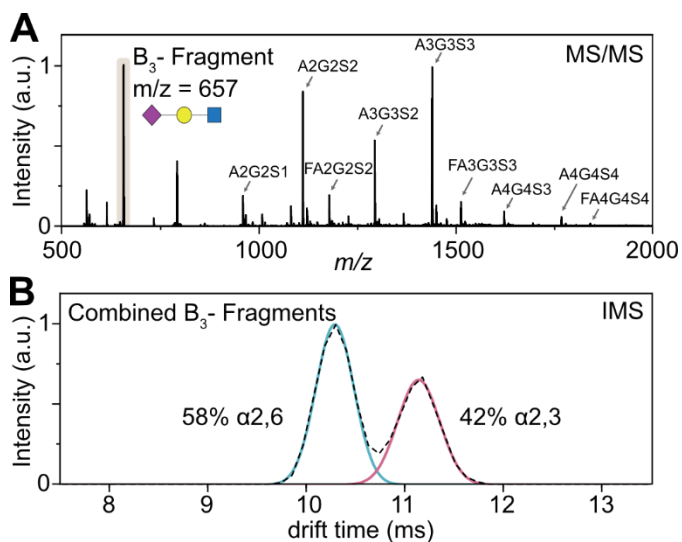


**Figure 15:** Non-targeted IM-MS analysis of released glycans from hAGP. (a) MS of native glycans shows nine complex-type, sialylated species. Without prior quadrupole isolation, CID activation leads to the fragmentation of all ionized glycans. The resulting B<sub>3</sub> fragment is resulting from all sialylated glycans. (b) The ATD of the B<sub>3</sub> fragment represents the averaged drift time of α<sub>2,6</sub>- and α<sub>2,3</sub>-linked sialic acids for all sialylated glycans and can be used to estimate the overall sialic acid ratio.

sialic acid (~28%:72%). Similar trends were reported based on LC-IM-MS data obtained from glycopeptides.<sup>145</sup> Therefore our results suggest that sialic acid isomers can be described qualitatively and quantitatively on the level of non-derivatized, native glycans in a direct injection IM-MS approach even for large glycan structures containing multiple sialic acids. Although acidic glycans are usually analysed in negative ion mode (due to the negative charge of sialic acids), this approach can only be performed in positive ion mode.

Both ion polarities were assessed by direct injection and isomer separation was only observed in positive mode. Furthermore, only protonated precursors are amenable to the presented IMS analysis as metal adducted species (e.g., sodium adducts) do not allow to distinguish the characteristic B<sub>3</sub> fragment *via* IMS. The direct injection analysis of the complex *N*-glycans released from hAGP shows that the IM-MS workflow is suitable to distinguish sialic acid isomers qualitatively on the level of released glycans.

In addition to the targeted approach described for individual glycans, we assessed the possibility to quantify the sialylation by IMS in a non-targeted approach. For this we induced fragmentation of all precursor ions without prior mass selection in the quadrupole, which results in the combined ATD from all released *N*-glycans (**Figure 15**). The overall ratio of sialic acid linkage isomers released from hAGP shows a balanced ratio of 58% α<sub>2,6</sub>- vs. 42% α<sub>2,3</sub>-linked sialic acids. This ratio matches values obtained in earlier

IMS experiments on glycopeptides.<sup>145</sup> This underlines the quantitative character of the presented fragment-based IMS approach on the level of released glycans.

Taken together, the results show the enormous potential of direct infusion nESI as a high throughput approach to recognize changes in the sialic acid isomer ratio without prior derivatization steps. IMS can quantitatively detect minor isomeric components with relative concentrations as low as 1%.<sup>21</sup> The method described here is therefore well suited to quantitatively describe the ratio of  $\alpha$ 2,6- and  $\alpha$ 2,3-linked Neu5Ac isomers without chromatographic separation. In comparison to the corresponding glycopeptide workflows<sup>20, 145, 183</sup>, it is more straightforward to identify sialic acid isomers on the level of released glycans. Sialic acid isomers of complex *N*-glycans (like hAGP) can be identified and quantified separately for individual *N*-glycan classes as bi-, tri- and tetraantennary glycans. In the case of glycopeptides, this is much more challenging as not only the microheterogeneity of the glycans (i.e., multiple possible isomers on one glycosylation site), but also the macroheterogeneity of the glycopeptides (i.e., multiple possible glycosylation sites) needs to be considered. The presented approach is therefore a major advancement for screening purposes in clinical biomarker research where general statements about sialic acid linkage isomers are required to identify pathological changes.

#### 4.3.2 HILIC-MS Characterisation of *N*-Glycans Released from hAGP

When hyphenated to liquid chromatography, the above-described method should in principle be able to provide glycan-resolved sialylation data. To evaluate this, we implemented the developed IMS technique into the existing gold standard HILIC-MS *N*-glycan analysis workflow. Accordingly, the sample preparation for hAGP was modified to match typical HILIC-FLD and HILIC-MS workflows: the *N*-glycans were cleaved from the glycoprotein *via* PNGase F digestion and directly labelled at the free reducing end with procainamide. As the LC-MS and the LC-IM-MS workflow are not dependent on the utilized fluorescent dye, this method is generally applicable to any available reducing end modification. Subsequently, the labelled glycans were purified using HILIC SPE and analysed by HILIC-ESI-MS. More than 20 individual glycan species were identified based on their retention time, mass, and literature data<sup>82</sup> (see **Table S-2** in the appendix).

According to the elution order of the identified glycans, the chromatogram can be divided into three areas, corresponding to bi-, tri- and tetraantennary glycans, respectively. Biantennary glycans elute first (<~20 minutes), followed by triantennary (from 20 to 26 minutes) and tetraantennary species (> ~26 minutes). Although HILIC can separate multiple glycan isomers, it struggles to confidently identify all structural components. Especially the orientation of the terminal sialic acid building blocks can often only be identified on the basis of glucose units (GU).<sup>163</sup> GU values serve as reference standards to calibrate relative retention times of each eluting species, which can further be compared with database information.<sup>131</sup> However, with growing complexity of glycans the LC resolving power can reach its limit and database assignments may be inconclusive. Especially, unknown samples are challenging to characterize solely based on LC-MS data and GU databases. Therefore, additional experiments are usually required to confidently assign all structural elements.

#### 4.3.3 *Quantitative Assignment of Sialic Acid Isomers based on LC-IM-MS*

The incorporation of IMS into the described standard HILIC-MS workflow is straightforward and does not require changes to the general routine. The workflow in a data dependent acquisition with IMS is shown in **Figure 16** for the doubly sialylated biantennary species (A2G2S2). This glycan structure shows two well-separated peaks in the HILIC chromatogram (**Figure 16A**) but exhibits identical MS/MS spectra in positive ion mode (**Figure 16B**) as both species correspond to isomeric structures. To investigate if these isomers differ in the orientation of the terminal sialic acid residues, the mobilograms of the B<sub>3</sub> fragments obtained from both precursors were studied. As can be observed, they significantly differ from each other (**Figure 16C**). The fragment generated from peak 1 shows two features in the mobilogram with similar peak areas (48%:52%) while the fragment of peak 2 only shows a single feature in the mobilogram (100%). In contrast to the direct injection experiments shown before, the upstream separation of isomers achieved by HILIC in combination with the IMS peak areas and drift times enables a quantitative assessment of sialic acid isomer proportions. In the case of A2G2S2, only three possible sialic acid ratios are possible (2x  $\alpha$ 2,6; 2x  $\alpha$ 2,3; or a 1:1 mix of both). The

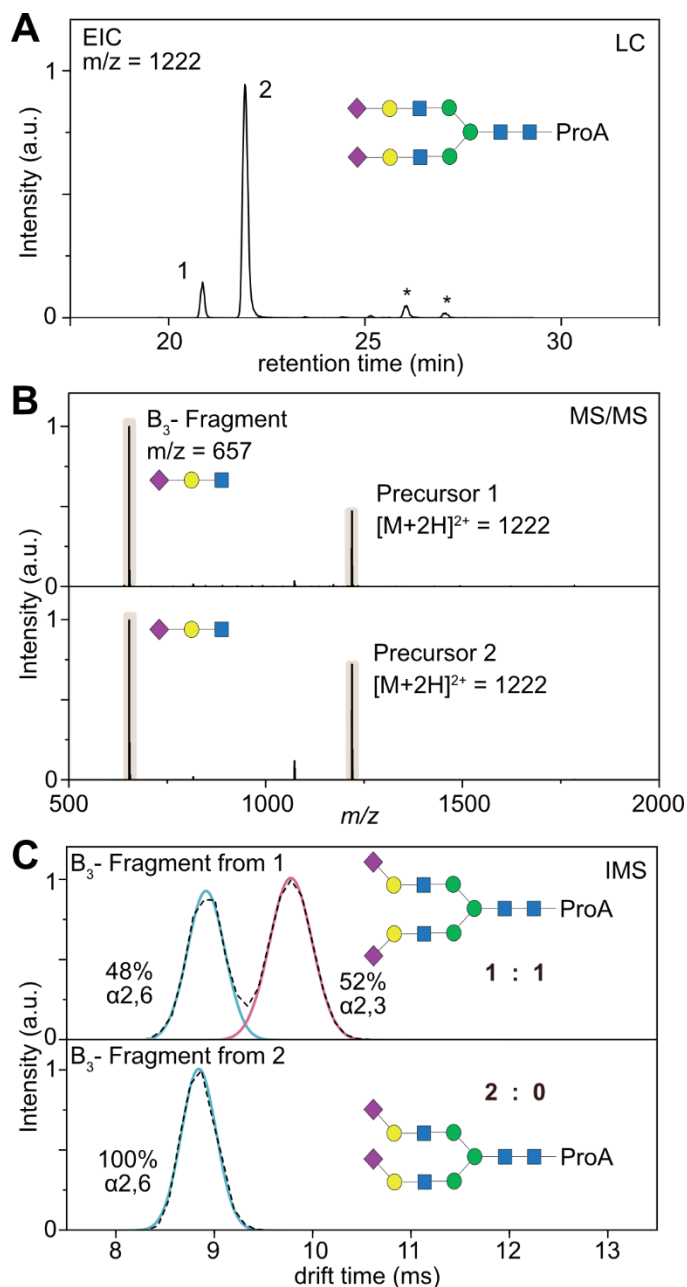


**Figure 16:** HILIC-CID-IM-MS feature mapping of released glycans of hAGP. (a) Extracted ion chromatogram (EIC) of a doubly sialylated biantennary glycan ( $m/z = 1222$ ) in positive ion mode. Minor peaks marked with an asterisk are fragment ions generated from larger glycans. (b) MS/MS spectra of the precursor ions 1 and 2, which are almost identical and show the dominant  $B_3$  trisaccharide fragment. (c) Mobilograms of the  $B_3$  fragment generated from precursor ions 1 and 2 respectively. Comparison with the synthetic standards (red and blue overlay) allows to identify the sialic acid isoforms and to deduce the general structure of the glycans 1 and 2.

proportions derived from IMS separation allow a confident and simple structural assignment of both LC peaks. While the glycan corresponding to LC peak 1 contains a mixture of one  $\alpha 2,6$ - and one  $\alpha 2,3$ -linked sialic acid, the glycan corresponding to LC peak 2

exclusively contains  $\alpha 2,6$ -linked sialic acids located at both terminal positions of the biantennary structure. This structural assignment shows that the retention time of a glycan correlates with the type of sialic acid linkage. The higher the content of  $\alpha 2,6$ -linked isomers, the later the glycan species will elute, which is in good agreement with reported HILIC data.<sup>173</sup> The structural assignments is confirmed by previous assignments of hAGP *N*-glycans using exoglycosidase digestions<sup>82</sup> and MS/MS<sup>173</sup> demonstrating the reliability of the established LC-IM-MS method. Although the total number and proportion of sialic acid isomers can be identified based on the presented data, no information on the relative position of the sialic acids on the individual antennae is obtained. For an application in

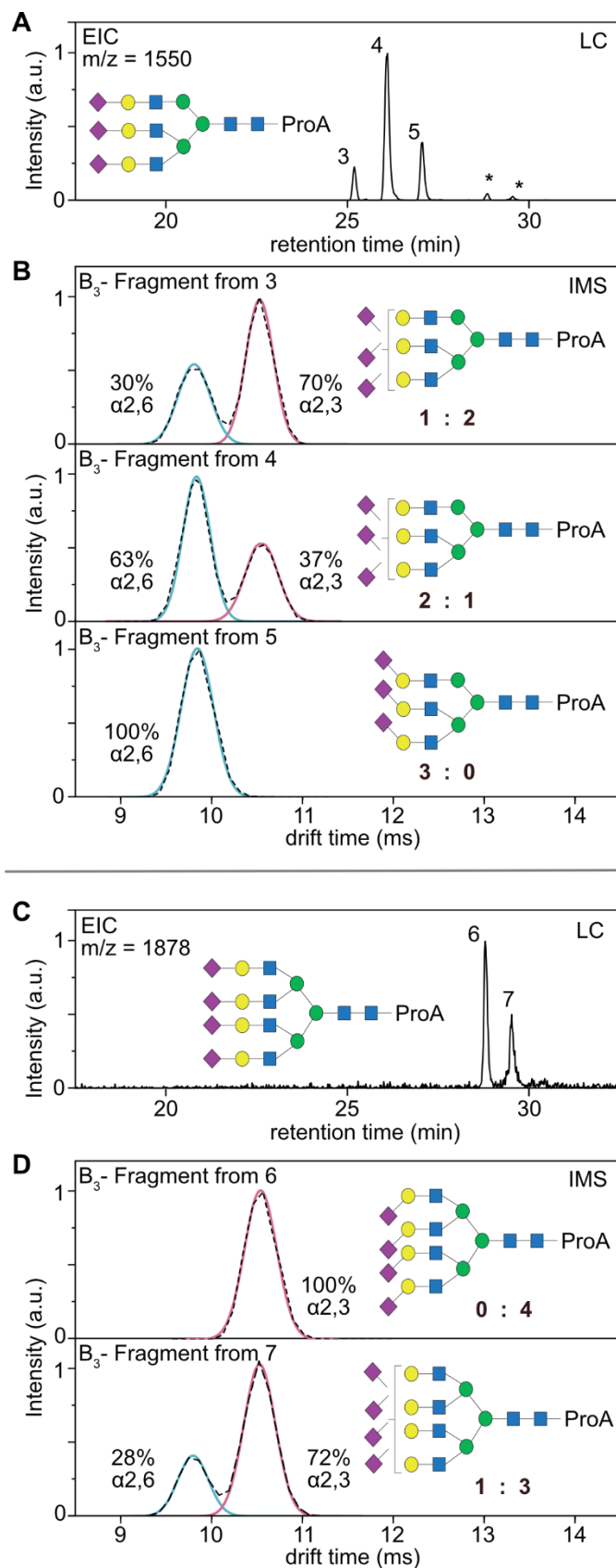


**Figure 17:** HILIC-IM-MS analysis of large, sialylated glycans. (a) Extracted ion chromatogram (EIC) of a triply sialylated triantennary glycan ( $m/z = 1550$ ) of hAGP in positive ion mode. Minor peaks marked with an asterisk are fragment ions generated from larger glycans. (b) Mobilograms of the  $B_3$  fragment generated from precursor ions 3, 4 and 5 respectively. (c) Extracted ion chromatogram (EIC) of a quadruply sialylated tetraantennary glycan ( $m/z = 1878$ ) of hAGP in positive ion mode. (d) Mobilograms of the  $B_3$  fragment generated from precursor ions 6 and 7 respectively. Comparison with the synthetic standards (red and blue overlay) allows to identify the sialic acid isoforms and to deduce the general structure of the glycans species.

diagnostics, however, these details are usually not important. Instead, a general quantitative and qualitative assignment is more crucial to monitor pathological changes.

Similarly to the biantennary glycans, the LC-IM-MS workflow can also be applied to larger sialylated structures. Figure 4 shows the analysis of the fully sialylated tri- and tetraantennary glycans released from hAGP. The

EIC of  $m/z = 1550$  corresponds to a triply sialylated, triantennary glycan and shows three distinct LC peaks (Figure 17A). As shown in Figure 17B, the mobilogram of the  $B_3$

fragment generated from LC peak 3 reveals a peak area ratio of 1:2 (30% vs 70%), which indicates that the three antennae contain in total one  $\alpha$ 2,6- and two  $\alpha$ 2,3-linked sialic acids. The fragment of LC peak 4 has a ratio of 2:1 (63% vs 37%), which indicates the presence of two  $\alpha$ 2,6-linked sialic acids and one  $\alpha$ 2,3-linked sialic acid. The latest eluting LC peak 5 exclusively contains  $\alpha$ 2,6-linked sialic acid. The quadruply sialylated tetraantennary species show two signals in the chromatogram (LC peaks 6 and 7, **Figure 17C**). The ATD reveals that isomer 6 exclusively contains  $\alpha$ 2,3-linked sialic acid, while isomer 7 shows a 1:3 ratio of  $\alpha$ 2,6:  $\alpha$ 2,3-linked sialic acid (**Figure 17D**). These quantitative sialic acid assignments are in good agreement with the general ratios obtained by the direct injection approach (**Figure 14**). After chromatographic separation, however, only integer ratios of sialic acid isomers are possible which significantly simplifies the detailed assignment of larger glycan structures. A comprehensive list of all identified glycans from hAGP and their respective sialic acid composition is shown in the supporting information (see **Table S-2** and **Table S-3**).

Taken together, the presented results show the universal applicability of the approach to all sialylated *N*-glycans independent of their size and structure. In addition to the diagnostic nature of the B<sub>3</sub> fragment to distinguish  $\alpha$ 2,6- and  $\alpha$ 2,3-linked sialic acid isomers, the workflow can be used to derive quantitative information based on the relative IMS peak area of the two isomers and thereby benefits the general structural assignment of sialylated glycans.

#### 4.3.4 Assignment of Fucosylated Complex *N*-glycans

Another important structural motif of *N*-glycosylation is the type and level of fucosylation. Similar to the sialylation pattern, fucosylation can be used as potential biomarker for cancer and therefore represents a particular important target for diagnostics applications. Fucosylation of complex glycans frequently occurs as core fucosylation linked *via*  $\alpha$ 1,6 to the *N*-acetyl-glucosamine at the reducing end. However, it can also be present as antenna fucosylation which mainly occurs *via*  $\alpha$ 1,3-linkage at the antenna *N*-acetylhexosamine but can occasionally be linked to galactose residues to form typical blood group antigens.<sup>19, 177</sup> For diagnostic purposes, the primary concern is to distinguish

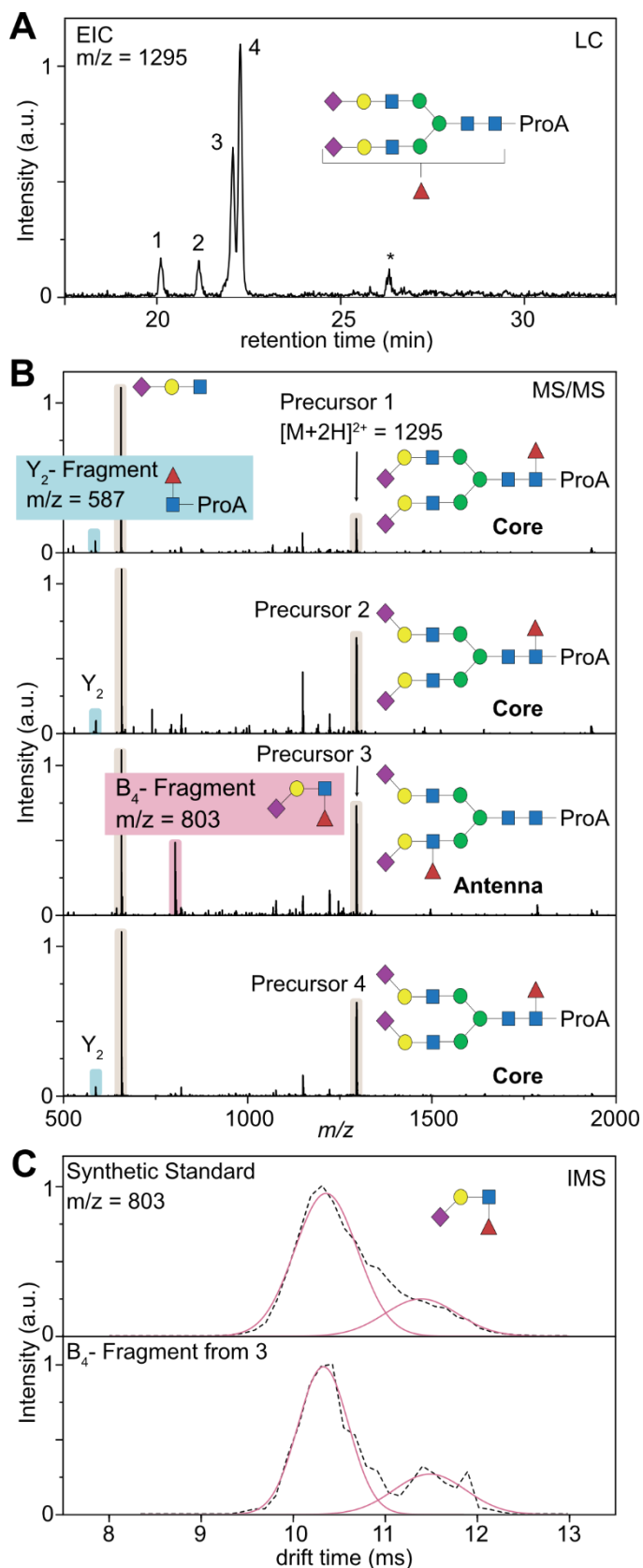


**Figure 18:** Determination of fucosylation pattern based on HILIC-IM-MS. (a) Extracted ion chromatogram (EIC) of a doubly sialylated biantennary glycan with one fucose attached ( $m/z = 1295$ ). Minor peaks marked with an asterisk are fragment ions generated from larger glycans. (b) MS/MS spectra of the precursor ions 1 to 4 which are almost identical and show the dominant B3 trisaccharide fragment. One major difference stem from either Y<sub>2</sub> fragmentation (highlighted in blue) or B<sub>4</sub> fragmentation (highlighted in red). (c) Mobilograms of the B<sub>4</sub> fragment generated from precursor ion 3. Comparison with a synthetic standard (3'-Sialyl-Lewis-X) allows to identify the fucose isoforms and confirm the native state of the fucosylation.

between core and antenna fucosylation while the secondary concern is related to the actual fucosylation motif (blood group antigens).

In our HILIC-IM-MS studies, we identified three fucosylated species, namely FA2G2S2, FA3G3S3 and FA4G4S4. For the smallest observed fucosylated species FA2G2S2 we observe four distinct isomers for the mass of  $m/z = 1295$  which represents the biantennary

glycan with two sialic acids and one fucose attached (**Figure 18A**). The identification of sialic acid linkage isomers is based on the ATD of the B<sub>3</sub> fragment for each separated

species and reveals that precursor 1 has a 0:2 ratio, precursor 2 and 3 have a 1:1 ratio and precursor 4 has a 2:0 ratio (see **Table S-3** in the appendix). The trend in elution order is similar to that of non-fucosylated glycans and is highly dependent on the type of sialic acid attached. For isomer 2 and 3, however, we can observe two baseline separated peaks in the chromatogram although both species contain a 1:1 ratio of  $\alpha$ 2,6- and  $\alpha$ 2,3-linked sialic acid isomers. Therefore, we can assume that differences in the retention times stem from a different fucosylation pattern (core *vs.* antenna). A tentative identification of core or antennary fucosylation can be achieved by the analysis of the MS/MS data (**Figure 18B**). Isomers 1,2 and 4 share a very similar fragmentation pattern and a common  $Y_2$  fragment ( $m/z = 587$ ) which corresponds to [GlcNAc + Fucose + Procainamide + H]<sup>+</sup>. It was shown previously that this fragment is characteristic for core fucosylation.<sup>184</sup> Although fucose monosaccharides tend to migrate along the oligosaccharide backbone during mass spectrometry analysis<sup>96, 97</sup>, core fucose is strongly bound to the sugar core<sup>185</sup> and migration reactions are further inhibited by an immobilization of the charge at the procainamide label<sup>98</sup>. Therefore, this specific fragment is a strong indicator for core fucosylation. On the other hand, there is a clearly recognisable difference in the MS/MS spectra for isomer 3.

Instead of a  $Y_2$  fragment indicating core fucosylation, isomer 3 shows an intense fragment signal at  $m/z = 803$ . This signal corresponds to a terminal  $B_4$  fragment [Neu5Ac + Gal + GlcNAc + Fuc + H]<sup>+</sup>. Although this fragment is indicative for antennary fucosylation, antennary fucosylation is very labile and requires low activation energies for migration reactions to occur.<sup>97, 185</sup> In this case IMS can support the discrimination between native antennary fucosylation and non-native, migrated structures. Recent studies showed that natively fucosylated structures yield reproduceable ATDs which can be compared to suitable standards, while rearranged structures exhibit multiple features in the ATD.<sup>99</sup> This can be explained by the fucose migration mechanism as the rearrangement might only occur to certain functional groups (such as N-Acetylation on Neu5Ac and GlcNAc) and therefore creates distinguishable isomeric structures.

A typical antenna fucosylation for sialylated species is the Sialyl Lewis X ( $\alpha$ 1,3-linked fucose) epitope.<sup>186</sup> We therefore compared the ATD of the occurring terminal  $B_4$  fragment [Neu5Ac + Gal + GlcNAc + Fuc + H]<sup>+</sup> with a commercially available standard of Sialyl

Lewis X (**Figure 18C**). Both ATDs show one distinct feature at ~10.5 ms and additionally have a small shoulder on the right side at 11.6 ms which is in good agreement with literature ATDs<sup>99</sup>. Migrated structures, for example migration reactions resulting from other epitope structures or from the core position, exhibit significantly different ATDs and can therefore be readily distinguished from native  $\alpha$ 1,3-linked structures.<sup>99</sup> The perfect match of both standard and sample ATD supports the assignment as native antenna fucosylation and more specifically as native Sialyl Lewis X epitopes. This observation agrees with recent experiments conducted with sequential enzymatic reactions utilizing fucosidase digestions.<sup>82</sup>

Both larger fucosylated structures observed in this study (FA3G3S3 and FA4G4S4) were examined in the same way to identify both the sialic acid and the fucosylation pattern. The characterisation of the sialic acid linkage isomer ratio was performed on basis of the generated B<sub>3</sub> fragment and allowed for unambiguous assignment of all sialylated isomers (see **Table S-2** and **Table S-3** in the appendix). We further checked the fragmentation pattern of all fucosylated species for either Y<sub>2</sub> or B<sub>4</sub> fragmentation to indicate core or antenna fucosylation (see **Figure S-4** and **Figure S-5** in the appendix). All tri- and tetraantennary species with one fucose showed exclusively B<sub>4</sub> fragments which is indicative for antenna fucosylation. Additionally, we compared the ATD of all B<sub>4</sub> fragments to check for native Sialyl Lewis X epitopes or migrated structures. As all ATDs showed good agreement with the ATD from Sialyl Lewis X, we assume that the triantennary and tetraantennary glycans of hAGP exclusively contain native antenna fucosylation and more specifically Sialyl Lewis X epitopes.

This example shows that LC-IM-MS is not only able to clearly distinguish core and antenna fucosylation, but the sialylation and fucosylation pattern in general. Furthermore, this workflow can be applied within a single LC run without further modification of established LC-MS workflows. Alternative approaches such as enzymatic digestions require multiple LC runs and additional experimental effort for sample processing. Furthermore, enzymatic approaches often have problems with the analysis of larger glycans such as tri- and tetraantennary species as their digestion leads to multiple overlapping species due to the sheer number of possible isomers. This is especially

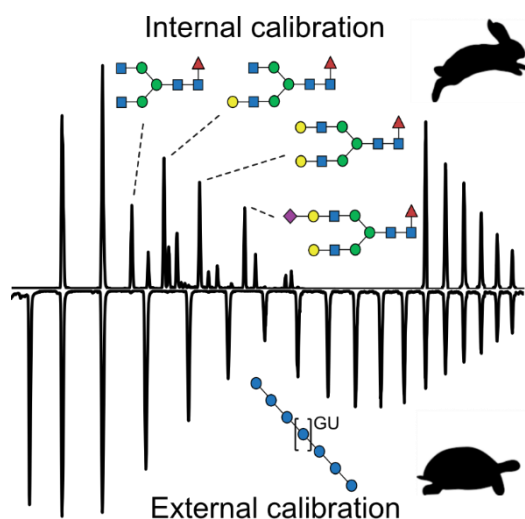
difficult for structural motifs that contain both sialic acid and fucose at the same time as they can mutually inhibit enzymatic digestion of each other.<sup>82</sup> The proposed LC-IM-MS approach does not show this limitation and can be easily applied to very large glycans. With suitable glycan standards and instrumental conditions, it could be possible to study all kinds of fucosylation motifs including blood group antigens for an extensive *N*- and even *O*-glycan analysis.

## 4.4 Conclusion

In conclusion, IMS has the potential to fill the informational gap in *N*-glycan analysis left by LC-MS. It enables the analyst to unambiguously identify characteristic structural motifs such as the sialic acid and fucose pattern in both a qualitative and a quantitative way. The regiochemistry of terminal sialic acid linkages can be identified based on B<sub>3</sub>-type fragments that are cleaved from the corresponding *N*-glycan before the IMS separation and further quantified based on their respective peak areas in the mobilogram. While in direct injection approaches this allows to derive a general  $\alpha$ 2,6- and  $\alpha$ 2,3 ratio, LC separation in combination with IM-MS allows to deduce more accurate *N*-glycan structures. Here, this workflow was applied to characterize the sialic acid of the released glycans from hAGP for highly sialylated biantennary, triantennary and tetraantennary glycans. Furthermore, it is possible to distinguish core and antennary fucosylation based on the LC-MS/MS data in conjunction with IMS data. The presented approach adequately complements existing LC-MS workflows and allows to obtain information on structural motifs without the need for further sample preparation and instrument modification. Given the already broad distribution of commercial IM-MS instruments, the proposed fragment-based approach can be readily implemented and applied in many laboratories. As IMS identification works independently from the LC dimension, the approach is not limited to HILIC methods and can be used with PGC, C18 or even capillary electrophoresis. Furthermore, the strategy does not require special sample preparation and can therefore be easily implemented into existing methods.

Very few other methods are able to identify a comparable level of structural information within the time frame of a single LC run. LC-IM-MS therefore has the potential to serve as a universally applicable analysis tool for future *N*-glycan analysis. In principle, the method should also be applicable for *O*-glycan analysis. It was for example shown that IMS of characteristic terminal fragments can also be used to identify the fucosylated structural motifs of glycans<sup>19</sup> and further experiments are required to test if this approach is also compatible with existing LC-MS workflows.

## 5 Dextran as Universal Calibrant for N-Glycan Analysis by Liquid Chromatography Coupled to Ion Mobility-Mass Spectrometry<sup>‡</sup>



### 5.1 Introduction

The analysis of released glycans is often based on liquid chromatography (LC) in combination with fluorescence (FLD) or mass spectrometry (MS) detection.<sup>12, 154</sup> Although MS-based sequencing is generally a powerful approach for the analysis of biomolecules, it is often brought to its limit by the broad variety of same-mass glycan isomers. LC separation therefore takes a crucial role in the routine analysis of N-glycans. The combination of retention time and  $m/z$  can be stored in databases and is essential for the identification of unknown samples.<sup>133</sup> However, retention times are highly dependent on

<sup>‡</sup> This chapter is based on the work “Dextran as Universal Calibrant for N-Glycan Analysis by Liquid Chromatography Coupled to Ion Mobility-Mass Spectrometry” by C. Manz, M. Götze, C. Frank, A. Zappe, and K. Pagel, submitted to *Analytical and Bioanalytical Chemistry* **2022**.

This is a pre-peer-review, pre-copyedit version of an article published in *Analytical and Bioanalytical Chemistry*. The final authenticated version is available online at: <https://doi.org/10.1007/s00216-022-04133-0>

instrumental parameters and can therefore not be directly used in databases. For this reason, an external calibration with a standard glucose homopolymer – usually referred to as dextran ladder – is indispensable to convert retention times into robust, comparable values, the so-called glucose units (GU).<sup>84,86</sup> For larger sets of samples, multiple calibration runs in regular intervals are necessary to achieve accurate GU values. In ideal case, each sample run is accompanied by a second dextran ladder run to maximize identification confidence. This calibration procedure significantly increases the measurement time and prevents a higher throughput in LC-FLD and LC-MS workflows. New developments for creating relative retention times are therefore necessary to increase the speed of N-glycan analysis.

Here, we present a dextran ladder with a reduced number of oligosaccharides as internal calibration standard to reduce absolute measurement time. By minimizing the number of dextran oligosaccharides, the calibrant can be spiked directly into the sample without generating overlapping signals. This allows the qualitative and quantitative analysis of N-glycans in a single LC run. We demonstrate the use of the minimized dextran ladder for GU calibration in HILIC chromatography with the released glycans of human immunoglobulin (hIgG) as reference. Furthermore, we illustrate the use of the minimized dextran ladder for the estimation of collision cross-section (CCS) values from travelling wave (TW) ion mobility-mass spectrometry (IM-MS) experiments.

## 5.2 Experimental Details

### 5.2.1 Chemicals

All chemicals and reagents were at least analytical reagent grade and used without further purification. Rapid™ PNGase F and Rapid™ PNGase F Buffer were supplied by New England Biolabs (Ipswich, USA). Immunoglobulin from human serum (hIgG, ≥95%), Human alpha-1-acid glycoprotein (hAGP, ≥95%), Dextran Mw5000, dextran Mw1000, Discovery Glycan solid phase extraction (SPE) tubes and procainamide hydrochloride (≥98%) were purchased from Sigma-Aldrich (St Louis, USA). Ammonium formate (>99%)

was obtained from VWR International (Radnor, USA). All solvents (acetonitrile, water) were LC-MS grade and purchased from Sigma-Aldrich (St Louis, USA).

### 5.2.2 *Sample Preparation for Labelled Glycans*

10  $\mu\text{L}$  of glycoprotein stock solution (10 mg/mL in water) was mixed with 6  $\mu\text{L}$  water and 4  $\mu\text{L}$  Rapid™ PNGase F Buffer and denatured at 95°C for 10 min. After cooling to room temperature, 1  $\mu\text{L}$  of Rapid™ PNGase F was added to the mixture and incubated at 50°C for 10 min. To create the dextran calibration ladder, a 1:1 mix of dextran 5000 and dextran 1000 was solved in 20  $\mu\text{L}$  water. Afterwards, both the released glycans and the dextran mix were labelled with procainamide according to established protocols.<sup>177, 178</sup> The labelled glycans were purified with the Discovery Glycan SPE tubes according to vendor's instruction, dried *via* SpeedVac (Thermo Fisher Scientific, Waltham, USA) and further suspended in 50  $\mu\text{L}$  water before storing them in the HPLC autosampler at 4°C.

### 5.2.3 *Offline IM-MS Experiments*

Drift tube (DT) IM-MS measurements were performed on a modified Synapt G2-S HDMS instrument (Waters Corporation, Manchester, UK), described in detail elsewhere.<sup>126</sup> Direct infusion measurements were performed in positive ion mode using platinum/palladium (Pt/Pd, 80/20) coated borosilicate capillaries prepared in-house. For nano electrospray ionization (nESI), typically 5  $\mu\text{L}$  of sample were loaded to a capillary and electrosprayed by applying a capillary voltage of 0.6-1.1 kV.

### 5.2.4 *Online HILIC-IM-MS Experiments*

Procainamide-labelled glycans were separated by a glycan BEH amide column (150 mm x 2.1 mm, 130A, 1.7  $\mu\text{m}$ , Waters, Milford, USA) before ESI ionization. Solvent A was 50 mM ammonium formate adjusted to pH 4.4, and solvent B was acetonitrile. The column temperature was set to 65°C and samples were analysed at a flow rate of 0.4 mL/min using a linear gradient of 75-48 % B from 0-40 min. The injection volume was 4-5  $\mu\text{L}$ . The separated glycans were then ionized online with a capillary voltage of 2.2-2.5 kV.

Typical MS parameters in resolution mode (offline and online measurements) for positive ion polarity were: 30 V sampling cone voltage, 1 V source offset voltage, 120°C source temperature, 0 V trap CE (MS) up to 30 V trap CE (MS/MS), 2 V transfer CE, 3 mL/min trap gas flow. Ion mobility parameters were: 5.0 V trap DC entrance voltage, 5.0 V trap DC bias voltage, -10.0 V trap DC voltage, 2.0 V trap DC exit voltage, -25.0 V IMS DC entrance voltage, 50–180 V helium cell DC voltage, -40.0 V helium exit voltage, 50-150 V IMS bias voltage, 0 V IMS DC exit voltage, 5.0 V transfer DC entrance voltage, 15.0 V transfer DC exit voltage, 150 m/s trap wave velocity, 1.0 V trap wave height voltage, 200 m/s transfer wave velocity, 5.0 V transfer wave height voltage. Data were acquired with MassLynx v4.1 and processed with Driftscope version 2.8 software (Waters, Manchester, UK), and OriginPro 8.5 (OriginLab Corporation, Northampton).

### 5.2.5 CCS Determination

Absolute  $^{DT}CCS_{N_2}$  were determined *via* Stepped-Field method described elsewhere.<sup>115, 116</sup> In short, each sample was measured at eight different drift voltages with increasing axial potential across the drift tube. For each ion, the corresponding arrival time distribution (ATD) is recorded and extracted by fitting a gaussian distribution to the raw data. The extrapolation of the reversed axial potential against ATD gives an intercept that is equivalent to the dead time required to transport the ions from the end of the drift tube to the detector. Subtracting the dead time from the observed ATD results in the corrected drift time of each ion to actually traverse the drift cell. This corrected drift time can be used to calculate the mobility of the ion which can be inserted into the Mason-Schamp equation to determine CCS values.

Estimated  $^{TW}CCS_{N_2}$  were obtained by measuring a calibrant (procainamide-labelled dextran) at a fixed travelling wave (TW) height and speed.<sup>115</sup> The drift times were extracted by fitting the ATDs of the ions with a Gaussian distribution and plotted in a logarithmic scale against the corresponding absolute CCS values obtained before. A linear regression can then be used as a calibration curve to estimate CCS. Further details about the calibration procedure can be found in the Supporting Information.

## 5.3 Results and Discussion

### 5.3.1 External GU calibration

The retention behaviour of *N*-glycans in HILIC mode can slightly change over extended periods of time due to external conditions such as the column age, alterations in solvent mixture or system temperature.<sup>187, 188</sup> Although minor drifts are normal, they can impede structural identifications which are based on accurate retention times. External calibration with a homopolymeric glucose standard (dextran ladder) allows the conversion of retention times into more robust glucose units which can help to minimize this problem. Dextran calibration in HILIC applications is usually performed by plotting a polynomial curve of the respective dextran oligosaccharide retention time against log(GU) (**Figure 19**). The polynomial equation of this curve can then be used to calibrate the retention time of unknown samples. The resulting GU values are universally comparable and can therefore be used as references in suitable databases<sup>83, 84, 86</sup>. This is inevitable to simplify structural assignments of unknown glycans.

To reach maximum calibration precision, it is necessary to accompany sample runs in regular terms with calibration runs (ideally for each sample) which can double the total measurement time. Coinjection of the calibration standard directly within the sample run is one way to circumvent this increase in measurement time.<sup>24, 69</sup> Although very simple to perform, direct spiking of the complete dextran ladder into the sample leads to overlapping sample and calibrant peaks. LC-MS based experiments can circumvent this by separating calibrant and sample signals based on exact masses. However, overlapping signals interfere with spectroscopic detection methods such as fluorescence or UV detection, which in turn complicates quantification. As fluorescence detection represents the gold standard for glycan analysis, coinjection of calibrant and sample seems impractical without modifications. For applications involving capillary electrophoresis, Guttman et al. circumvent the problem of overlapping peaks by reducing the absolute number of spiked oligosaccharides.<sup>85</sup> Based on only three data points, they generate a virtual calibration ladder to determine GU values for CE, empirically. For HILIC

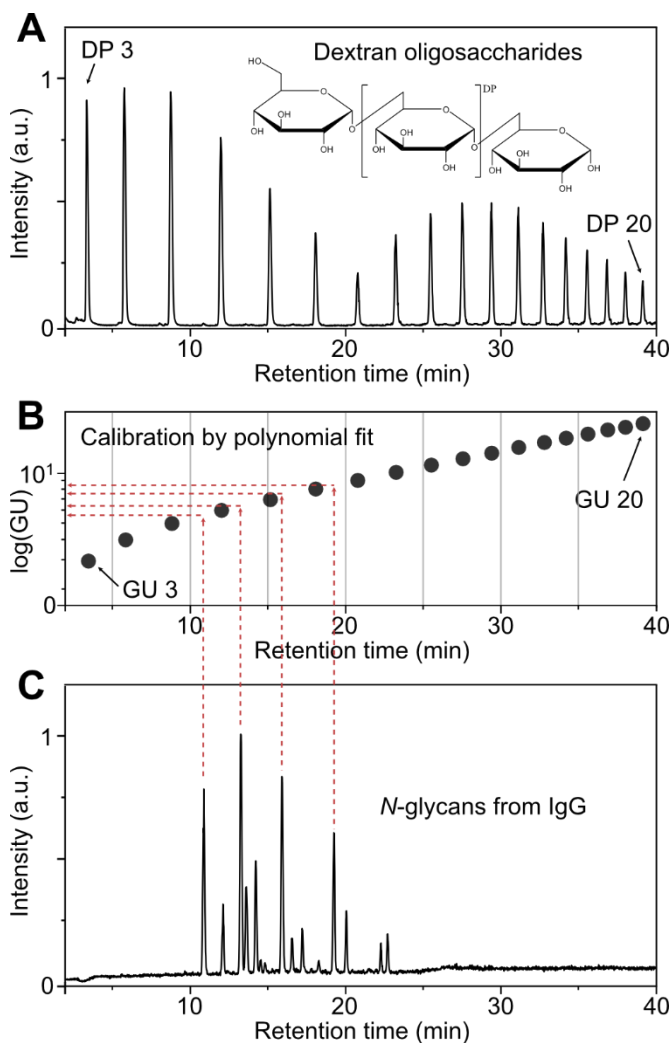


**Figure 19:** Typical workflow for external GU calibration shown for the released glycans of human IgG. (a) Chromatogram of procainamide-labelled dextran oligomers in HILIC mode with corresponding DP (degree of polymerisation) assignment. (b) Plotting GU retention times against log(GU) results in a polynomial shape which can be fitted with a fifth-order equation. (c) Chromatogram of glycans released from human IgG. The resulting polynomial fit of part B can be used for external calibration of unknown samples as indicated by the red-dotted line.

applications, however, no comparable approach for internal calibration was reported although the potential time savings for HPLC runs (hours) would be much larger compared to short CE runs (seconds to minutes).

### 5.3.2 Internal GU calibration

To adapt the dextran ladder for internal calibration in HILIC applications, we have to consider three major points: 1) Typical gradient times in HILIC *N*-glycan analysis are up to 40 minutes and result in a total run time of 60 minutes per sample (including washing and re-equilibration steps).<sup>61</sup> To avoid extension of the original measurement time, only dextran oligosaccharide peaks observed in this gradient window can be considered. The chromatogram of the dextran ladder shows 20 peaks in this time frame. The dextran mono- and disaccharides (GU 1 and 2) usually elute with the injection peak, together with excess label and salts. In the intended internal calibration these signals therefore must be excluded and only the GU data points from 3 to 20 can be considered (fig. 1A+B).

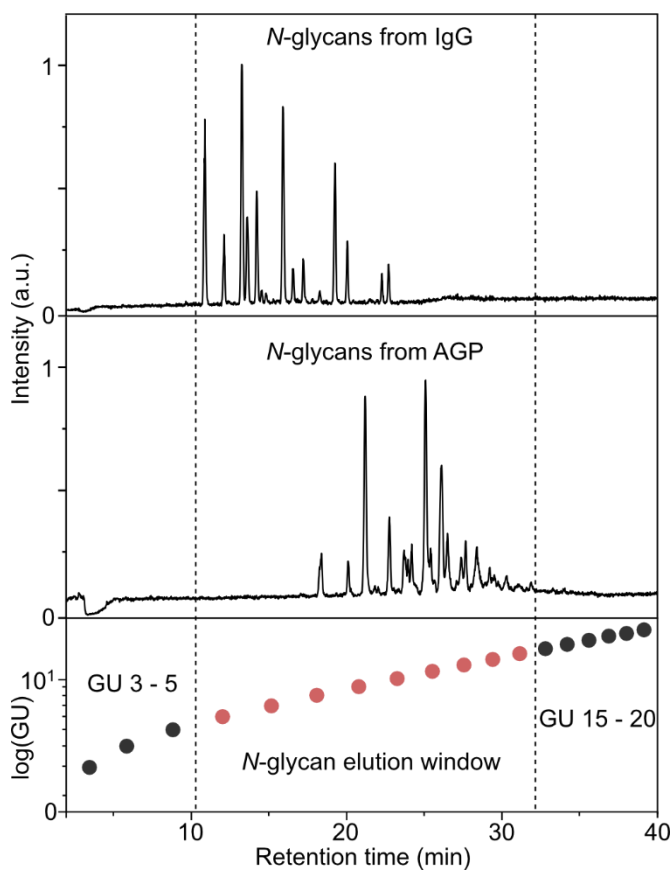


**Figure 20:** Determination of N-glycan elution window for HILIC HPLC. HILIC chromatograms of released glycans of IgG (top panel) and AGP (middle panel). Smallest N-glycans from IgG start to elute at ~10 minutes and largest glycans from AGP stop to elute at ~32 minutes (indicated by dashed lines). GU data points inside the N-glycan elution window cannot be used for internal calibration and therefore are marked in red. Internal calibration can make use of GU 3 to 5 and GU 15 to 20.

2) The calibrant signals should not overlap with sample signals to allow qualification and relative quantification *via* spectroscopic

detection (e.g., fluorescence or UV). Similar to the CE approach reported by Guttman et al.,<sup>85</sup> this makes it necessary to reduce the number of spiked dextran oligosaccharides to omit an elution window in the HILIC chromatogram (**Figure 20**). The spiked dextran peaks only should occur before and after the elution window in which the actual sample elutes from the column. To determine the elution window for the applied gradient, the released N-glycans of human IgG and human AGP are used as reference points. Human IgG glycosylation mainly consists of complex biantennary N-glycans with a high degree of fucosylation but low levels of sialylation.<sup>48</sup> It can therefore serve as lower limit for the N-glycan elution window. As example for larger glycan structures human AGP can be applied as it mostly contains fully sialylated bi-, tri- and tetraantennary N-glycan structures.<sup>182</sup> With these two sets of samples, it is possible to estimate the elution window for a vast majority of N-glycans.

**Figure 20** shows the HILIC separation of the N-glycans from IgG and AGP with the corresponding external GU calibration. The chromatograms reveal that the smallest N-glycans from human IgG start to elute after GU 5 while the largest N-glycans from AGP

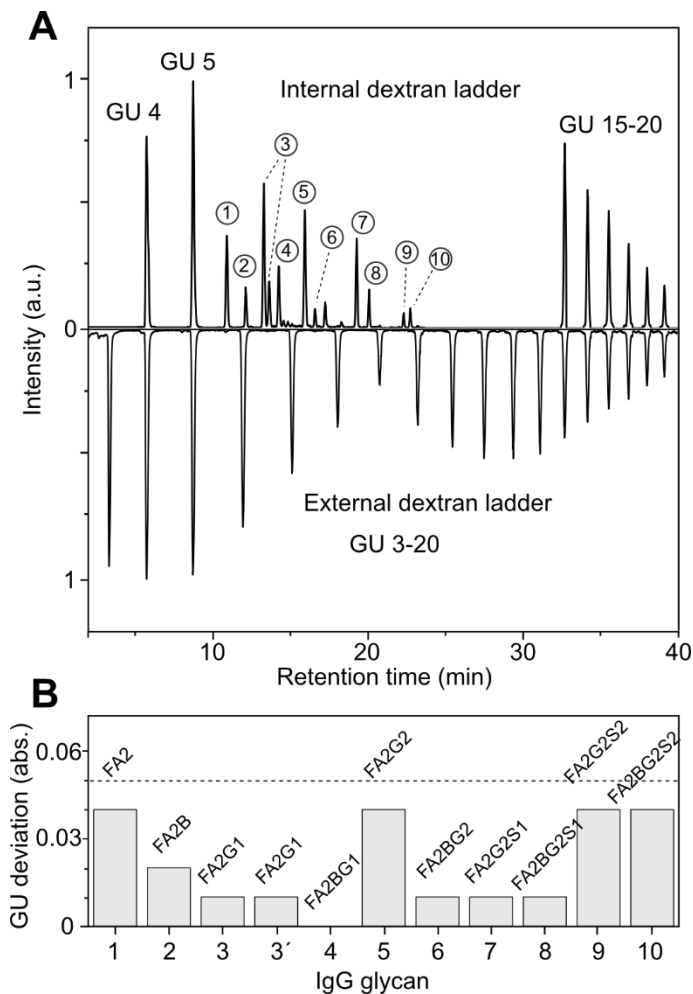


**Figure 21:** Evaluation of the internal GU calibration on the example of human IgG. (a) Mirror plot of HILIC chromatograms of released N-glycans from IgG spiked with the minimized dextran ladder compared to the complete external dextran ladder. The numbers in circles indicate the identified N-glycan species from IgG. (b) Bar graph of GU deviation (in absolute numbers) between internal and external calibration. The dashed line indicates the Gu tolerance typically applied in Gu database searches.

are eluted before GU 15. This means, that typical N-glycans are released from the columns within an elution window of ~10 to ~32 minutes or between GU values 5 and 15, respectively. To avoid

overlapping signals of sample and calibrant, it is therefore necessary to omit the GU values between 6 and 14. An internal dextran calibration should hence only rely on the GU values 3 to 5 and 15 to 20.

3) The most important part is the quality of the calibration. The internal dextran calibration needs to be as accurate as the routinely used external calibration. For this purpose, different combinations of dextran oligosaccharides of GU 3 to 5 and 15 to 20 were evaluated (see **Figure S-6** in the appendix). Although the absolute number of data points is reduced (especially in the N-glycan elution window), the polynomial fit must compensate for this to resemble the actual GU values. The combination of GU 4+5 and GU 15 to 20 resulted in the most accurate polynomial fit and nicely resembles the external calibration (see **Table S-7** in the appendix). This combination of data points is therefore utilized as internal dextran ladder for the following experiments.

To generate the minimized set of standards, all relevant dextran oligosaccharides were fractionated and then a small aliquot was spiked into the released glycans of human IgG. **Figure 21** shows the HILIC chromatogram with internal dextran calibration. As intended, there is a clear separation of sample (from minutes ~10 to ~25) and calibrant signals. This allows the simple discrimination of signals from human IgG and leads to the identification of 11 *N*-glycans (marked with a number). The comparison with the external calibration (mirror plot, **Figure 21A**) shows that multiple IgG signals overlap with the dextran ladder and would therefore be difficult to quantify based on optical detection methods. Both, the internal and the external dextran ladder are used to calculate the GU units of the 11 IgG peaks and the resulting values are compared in **Figure 21B**. Although the minimized dextran ladder uses nine data points less than the full set of standards, the differences between both calibration strategies are surprisingly small (see **Table S-8** in the appendix). The highest deviation is 0.04 GU, while most other species show deviations below 0.01 GU. Databases usually apply a GU tolerance of 0.05 to 0.2<sup>84, 189</sup> which is easily accessible with the internal calibration as indicated by the dashed line in **Figure 21B**. As the GU values for procainamide-labelled *N*-glycans of human IgG can be found in the glycostore database<sup>83</sup>, we further compared the results of the internal and external dextran calibration with GU values of the database (see **Table S-9** in the appendix). The GU datasets of both, internal and external, calibrations are in good agreement with the database entries and exhibit average deviations below 1.5%. With these results, we can conclude that the spiked dextran ladder produces an accurate calibration on equal grounds with the external dextran ladder. Spiking of the calibrant into the sample can be easily applied to a large number of samples and can therefore help to speed up the time-consuming calibration procedure.

### 5.3.3 CCS calibration

Besides the widespread LC methods, IMS emerged as promising orthogonal tool to improve glycan characterization.<sup>15, 16</sup> IMS can separate glycan isomers based on their drift times in the gas phase to identify specific glycan motifs.<sup>19-21</sup> The generated drift time behaves similar to retention times of LC applications and represents an instrument-

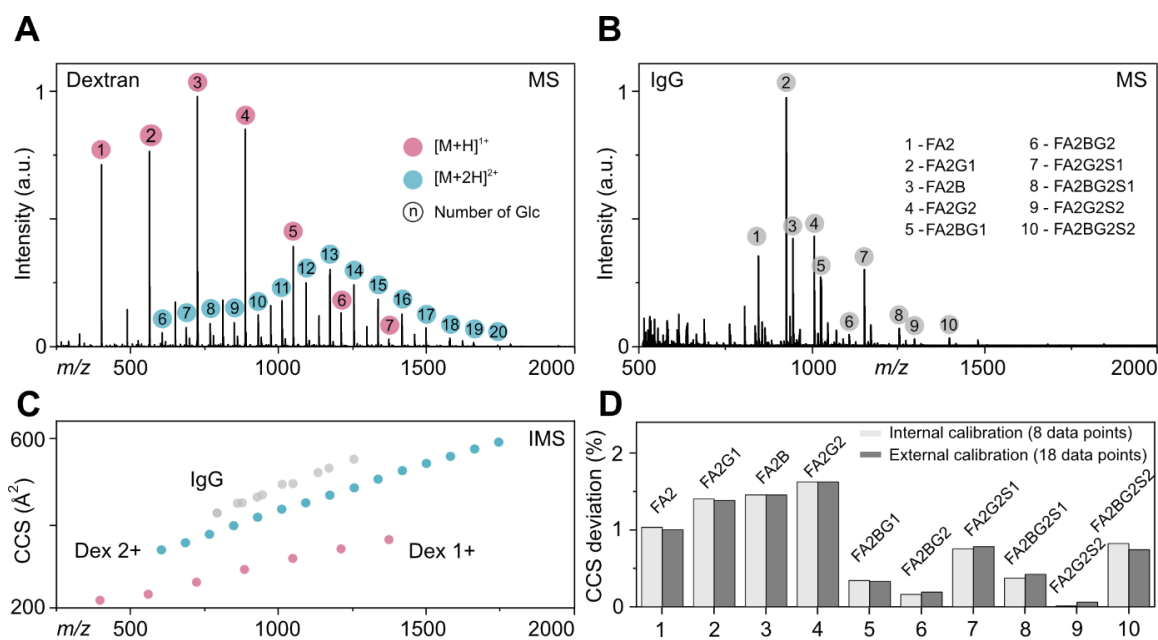


**Figure 22:** CCS calculation with internal and external dextran ladder. (a) MS spectrum of procainamide-labelled dextran ladder. Singly charged species are notated with a red circle while doubly charged species are highlighted in blue. (b) MS spectrum of procainamide-labelled N-glycans of human IgG. (c) CCS plot of absolute DTCCSN2 values of dextran and IgG. (d) Bar plot of CCS deviation for internal and external calibration in comparison to absolute CCS values.

dependent parameter. This means that drift times are affected by external conditions and therefore hard to compare between different instruments (or in databases). This can be avoided by converting the drift times into collision cross-sections (CCSs) which describe a molecular property of the ion and are independent of instrumental parameters.<sup>190</sup> For linear drift cells (DTIMS) drift times can be directly converted mathematically using the Mason-Schamp Equation.<sup>110</sup> Most of the state-of-the-art IMS instruments, however, utilize non-homogeneous electric fields which preclude the determination of absolute CCSs (e.g. TWIMS, TIMS).<sup>12</sup> To enable the estimation of CCSs, these IMS instruments require careful calibration with a suitable standard. The calibrant should ideally be of the same biomolecular class and in the same  $m/z$  range as the actual sample. For CCS calibration of glycans, dextran is regularly used as external standard as it is well-characterized and readily available.<sup>19, 115</sup> The IMS calibration process requires absolute <sup>DT</sup>CCS values as reference. We therefore measured the IM-MS data for the procainamide-labelled glycans of dextran and IgG on a modified Synapt G2 instrument equipped with a linear drift cell (**Figure 22**). The resulting mass spectrum of dextran shows oligomers starting from

monomers up to 20-mers with charge states ranging from 1+ to 2+ (**Figure 22A**). This covers basically all types of *N*-glycans as the typical *m/z* range starts from biantennary glycans (*m/z* 500-1000 with charge states 1+) and goes up to fully sialylated tetraantennary glycans (*m/z* up to 4000 with charge states 2+/3+). The mass range for the released glycans of human IgG are presented in **Figure 22B** and shows doubly charged species ranging from *m/z* ~750 to 1250. For all these species, we determined absolute <sup>DT</sup>CCS<sub>N2</sub> (**Figure 22C**). The singly charged oligosaccharides of dextran cover a CCS range from ~200 to ~400 Å<sup>2</sup>, while the doubly charged dextran oligomers cover a bigger span of ~300 to ~600 Å<sup>2</sup>. The glycans of IgG are inside this limit and range from ~400 to ~550 Å<sup>2</sup>. As dextran covers the complete mass and CCS range, it is suitable as calibrant for IgG. With this information, we estimated the <sup>TW</sup>CCS<sub>N2</sub> of IgG glycans calibrated by either internal calibration with eight data points in total (GU 4+5 and 15-20) or *via* external calibration with a complete set of 17 data points (for a comprehensive table of all calculated CCS values, see table **Table S-10** and **Table S-11**). To evaluate the estimated <sup>TW</sup>CCS<sub>N2</sub>, we compared both datasets (external and internal calibration) to the calculated absolute <sup>DT</sup>CCS<sub>N2</sub> values from IgG (**Figure 22D**). The CCS deviation for each glycan is shown as bar plot to visualize the negligible differences between internal and external calibration (<0.1%). Both datasets follow a similar trend with decreasing CCS deviation for increasing *m/z*-ratio. The error is highest for the smallest glycans (FA2 to FA2G2) with 1 to 1.5% and decreases for the largest glycans to well below 1%. The average CCS deviation over all glycans is <0.8% and therefore in the order of the general calibration error reported for CCS estimations.<sup>116, 191</sup> Similarly to the GU calibration discussed above, CCS calibration with a reduced number of dextran oligosaccharides does not reduce the accuracy of the calibration. The internal calibration therefore results in very similar GU and CCS values compared to the external calibration but has a significant advantage with respect to throughput.

## 5.4 Conclusion

In this study we established an internal calibration approach for the analysis of released *N*-glycans *via* LC in conjunction with FLD and/or IM-MS. For the internal calibration, we reduced the number of dextran oligomers to spike the dextran ladder directly into the

sample. It was found that only 8 dextran oligosaccharides are necessary for accurate calibration. When used for GU calibration, the minimized dextran ladder can be clearly discriminated from sample signals in the HILIC chromatogram and therefore does not disturb quantification *via* optical detection. Although the absolute number of data points for calibration is reduced, the minimized dextran ladder exhibits negligibly deviations from the external GU calibration and allows for accurate determination of GU glucose units. The situation is similar for CCS calibration. The reduced number of dextran oligosaccharides did not lead to a loss in calibration accuracy and only minor differences to the external calibration are observed. Furthermore, the GU and CCS datasets generally exhibit very low error margins and therefore are readily compatible to established databases such as Glycostore or GlycoMob.<sup>83, 164</sup>

For the internal calibration, dextran proved to be a universal standard for the analysis of *N*-glycans. It is readily available, cheap, and well-characterized. Once the dextran oligosaccharides are fractionated, the direct spiking of calibrant into the sample significantly reduces the measurement time as there is no need for additional LC or CCS calibration runs. It further requires minimal adaptations in data acquisition and processing as the general calibration procedures does not change. It can therefore directly replace external calibration to save time and increase the throughput for *N*-glycan analysis.

## 6 Summary and Future Perspective

In this thesis, it was investigated if IMS can be hyphenated to classical LC-MS workflows to create a novel and powerful technique for the structural elucidation of complex *N*-glycans. For this purpose, three major aspects were studied: How does the sample preparation employed for LC-MS affect the IMS separation? How can IMS be effectively integrated into LC-MS to improve glycan analysis? And how can data acquisition and processing be unified to avoid unnecessary calibration steps?

A major part of sample preparation for *N*-glycan analysis relies on the modification of the original glycan structure and in particular on the addition of a fluorescence label at the reducing end. These labels can substantially alter the three-dimensional gas-phase structure of glycans, which makes a prediction of the mobility behaviour difficult if not impossible. We addressed this problem by the systematic study of a set of six isomeric fucose-containing blood group antigens that are derivatized with the most common fluorescent tags using IMS. The quality of the separation is evaluated by comparing the CCS values of all species in positive and negative ion mode as well as with adduct ions. The comparison reveals that isomer separation of the tri- and tetrasaccharides strongly depends on the type of label and the ion polarity. In some cases, the derivatization with a fluorescent label significantly enhances the peak-to-peak resolution and enables a better separation compared to native glycans. However, there seems to be no clear bias for a specific type of fluorescent label based on IMS separation. The selection of the type of reducing end label should therefore be based on the influence that a label has on the LC and MS dimension rather than on the IMS dimension.

Previously, it was shown that glycans at the size of tri- to pentasaccharides exhibit the greatest potential for IMS separation as larger glycans tend to be less resolved.<sup>21</sup> The integration of IMS into typical LC-MS *N*-glycan workflows is therefore especially effective for the analysis of characteristic glycan motifs that are cleaved from a *m/z*-selected precursor in the gas phase. In particular, we focused on the characterisation of sialylated and fucosylated *N*-glycans which pose an enormous challenge to conventional LC-MS.

The exact assignment of  $\alpha$ 2,3- and  $\alpha$ 2,6-linked sialic acid isomers usually require time-consuming and expensive enzymatic digestions or sample derivatization. We demonstrated here that IMS can identify sialic acid and fucose isomers and proved the applicability of HILIC-IM-MS by analysing the released glycans from human AGP. HILIC separated the crude mixture of highly sialylated multi-antennary glycans, MS provided information on glycan composition, and IMS was used to distinguish and quantify  $\alpha$ 2,6- and  $\alpha$ 2,3-linked sialic acid isomers based on characteristic fragments. We fully unravelled the isomeric structure of even highly sialylated glycans up to tetraantennary species without changing the sample preparation and within a single LC run. In addition, the analysis of fucosylated fragments *via* IMS allowed for an effective distinction of core *vs* antenna fucosylation and in some cases even a detailed assignment of the specific fucose epitope.

One reason for the limited use of LC-IM-MS for glycan analysis is the lack of robust calibration routines that readily integrate into existing LC workflows. While LC relies on a dextran ladder to process retention times into GU values, IMS utilizes a variety of different calibration standards to calculate CCS values from drift times. Furthermore, both calibration approaches are based on the measurement of external standards that unnecessarily prolongs the overall measurement time. Both problems were circumvented by establishing dextran as universal calibration standard for both, LC and IMS, for the analysis of *N*-glycans. In particular, we focus on the direct spiking of the standard into the analyte solution to obtain an accurate GU and CCS calibration in a single measurement, without the need of external calibration. Technically, this is achieved using a dextran ladder with a reduced number of oligosaccharides to avoid overlap with the analyte signal. Although this internal calibration is performed with much less data points than a conventional external calibration, similar and sometimes even more accurate GU and CCS values are obtained. The minimized dextran ladder shows only minor deviations of well below 1% and can be applied without modifications in sample preparation or data processing. This enables a faster, more accurate analysis for both LC and IMS without loss in calibration accuracy or informational content.

The above findings present significant progress in the field of *N*-glycan analysis, but they also leave some space for improvements. Future developments will evolve around instrumental improvements and in particular around the separation power of IMS instruments. In this thesis, a DTIMS with a peak-to-peak resolution of  $\Delta\Omega/\Omega \approx 20$  and a TWIMS instrument with  $\Delta\Omega/\Omega \approx 40$  were used for the separation of complex *N*-glycans. This basically limited all measurements to the separation of smaller glycan motifs, while modern instruments employ a much higher resolution and thus potentially allow for the effective separation of intact *N*-glycans. Although fragment ions often provide a sufficient level of detail to backtrack the overall structure of the precursor, it is not straightforward to generate the same fragments on all mass spectrometers. Ion polarity, adducts, type of activation and even the structure of the glycan itself play a huge role in the formation of specific fragments.<sup>93-95</sup> Contrary, the generation of precursor ions with a defined number of charges is generally much easier on common MS instruments. There are the first examples of state-of-the-art IMS instruments with resolutions  $\Delta\Omega/\Omega > 200$ <sup>192-194</sup>, that can separate intact glycan compounds. It was shown that sialylated as well as fucosylated biantennary glycans can be distinguished based on IM-MS data of intact glycan structures alone without the need for additional fragmentation experiments. However, the application for very large glycans, such as tri- or tetraantennary glycans, still needs to be shown.

The analysis of intact glycans would also have a positive impact on the development of supporting bioinformatic tools. Despite the rapid development of powerful techniques for glycan analysis, the field of glycomics still lags behind the advances that have been made in genomics and proteomics. One major reason for that is the absence of computational tools to store and handle the growing quantity of glycomics data.<sup>195, 196</sup> There are very few software approaches available to annotate fragment spectra from complex *N*-glycan spectra as the fragment ions very often exhibit exactly the same masses. Without prior knowledge of the structure or the biosynthesis of the molecule, it is often impossible to manually characterize a molecule based on its fragmentation spectra and much less in an automatic way. Although IMS can support the assignment of some specific fragments (as shown for the characteristic B<sub>3</sub> fragment of sialylated glycans in **chapter 4**), the sheer

number of possible fragment ions makes it difficult to create a comprehensive CCS database for all of them. The combination of  $m/z$ , GU, and CCS for intact precursor ions, however, is much more tangible and could provide an alternative to the difficult interpretation of tandem MS data. Databases for  $m/z$  and GU values already exist, so CCS values can easily be added. *N*-glycan analysis soon will very likely profit from this powerful combinational dataset as it enables a straightforward analysis of almost all known *N*-glycans and glycoconjugates.

## References

- [1] Varki, A., Biological roles of glycans. *Glycobiology* **2017**, *27* (1), 3-49.
- [2] Reily, C.; Stewart, T. J.; Renfrow, M. B.; Novak, J., Glycosylation in health and disease. *Nat Rev Nephrol* **2019**, *15* (6), 346-366.
- [3] Costa, A. F.; Campos, D.; Reis, C. A.; Gomes, C., Targeting Glycosylation: A New Road for Cancer Drug Discovery. *Trends Cancer* **2020**, *6* (9), 757-766.
- [4] O'Flaherty, R.; Trbojevic-Akmacic, I.; Greville, G.; Rudd, P. M.; Lauc, G., The Sweet Spot for Biologics: Recent Advances in Characterization of Biotherapeutic Glycoproteins. *Expert Rev Proteomics* **2017**.
- [5] Pearce, O. M.; Laubli, H., Sialic acids in cancer biology and immunity. *Glycobiology* **2016**, *26* (2), 111-28.
- [6] Dwek, R. A., Glycobiology: Toward Understanding the Function of Sugars. *Chem. Rev.* **1996**, *96* (2), 683-720.
- [7] Bertozzi, C. R.; Rabuka, D., Structural Basis of Glycan Diversity. In *Essentials of Glycobiology*, 2nd ed.; Varki, A.; Cummings, R. D.; Esko, J. D.; Freeze, H. H.; Stanley, P.; Bertozzi, C. R.; Hart, G. W.; Etzler, M. E., Eds. Cold Spring Harbor (NY), 2009.
- [8] Duus, J. Ø.; Gotfredsen, C. H.; Bock, K., Carbohydrate Structural Determination by NMR Spectroscopy: Modern Methods and Limitations†. *Chem. Rev.* **2000**, *100* (12), 4589-4614.
- [9] Lu, G.; Crieffeld, C. L.; Gattu, S.; Veltri, L. M.; Holland, L. A., Capillary Electrophoresis Separations of Glycans. *Chem. Rev.* **2018**, *118* (17), 7867-7885.
- [10] Melmer, M.; Stangler, T.; Premstaller, A.; Lindner, W., Comparison of hydrophilic-interaction, reversed-phase and porous graphitic carbon chromatography for glycan analysis. *J. Chromatogr. A* **2011**, *1218* (1), 118-123.
- [11] Reusch, D.; Habberger, M.; Falck, D.; Peter, B.; Maier, B.; Gassner, J.; Hook, M.; Wagner, K.; Bonnington, L.; Bulau, P.; Wuhler, M., Comparison of methods for the analysis of therapeutic immunoglobulin G Fc-glycosylation profiles-Part 2: Mass spectrometric methods. *MAbs* **2015**, *7* (4), 732-742.
- [12] Grabarics, M.; Lettow, M.; Kirschbaum, C.; Greis, K.; Manz, C.; Pagel, K., Mass Spectrometry-Based Techniques to Elucidate the Sugar Code. *Chem. Rev.* **2021**.
- [13] Cataldi, T. R. I.; Campa, C.; Angelotti, M.; Bufo, S. A., Isocratic separations of closely-related mono- and disaccharides by high-performance anion-exchange chromatography with pulsed amperometric detection using dilute alkaline spiked with barium acetate. *J. Chromatogr. A* **1999**, *855* (2), 539-550.
- [14] Abd Hamid, U. M.; Royle, L.; Saldova, R.; Radcliffe, C. M.; Harvey, D. J.; Storr, S. J.; Pardo, M.; Antrobus, R.; Chapman, C. J.; Zitzmann, N.; Robertson, J. F.; Dwek, R. A.; Rudd, P. M., A strategy to reveal potential glycan markers from serum

- glycoproteins associated with breast cancer progression. *Glycobiology* **2008**, *18* (12), 1105-1118.
- [15] Hofmann, J.; Pagel, K., Glycan Analysis by Ion Mobility-Mass Spectrometry. *Angew. Chem. Int. Ed. Engl.* **2017**, *56* (29), 8342-8349.
- [16] Manz, C.; Pagel, K., Glycan analysis by ion mobility-mass spectrometry and gas-phase spectroscopy. *Curr. Opin. Chem. Biol.* **2018**, *42*, 16-24.
- [17] Collins, D. C.; Lee, M. L., Developments in ion mobility spectrometry-mass spectrometry. *Anal Bioanal Chem* **2002**, *372* (1), 66-73.
- [18] Cumeras, R.; Figueras, E.; Davis, C. E.; Baumbach, J. I.; Gracia, I., Review on ion mobility spectrometry. Part 1: current instrumentation. *Analyst* **2015**, *140* (5), 1376-1390.
- [19] Hofmann, J.; Stuckmann, A.; Crispin, M.; Harvey, D. J.; Pagel, K.; Struwe, W. B., Identification of Lewis and Blood Group Carbohydrate Epitopes by Ion Mobility-Tandem-Mass Spectrometry Fingerprinting. *Anal. Chem.* **2017**, *89* (4), 2318-2325.
- [20] Hinneburg, H.; Hofmann, J.; Struwe, W. B.; Thader, A.; Altmann, F.; Varon Silva, D.; Seeberger, P. H.; Pagel, K.; Kolarich, D., Distinguishing N-acetylneuraminic acid linkage isomers on glycopeptides by ion mobility-mass spectrometry. *Chem. Commun.* **2016**, *52* (23), 4381-4384.
- [21] Hofmann, J.; Hahm, H. S.; Seeberger, P. H.; Pagel, K., Identification of carbohydrate anomers using ion mobility-mass spectrometry. *Nature* **2015**, *526* (7572), 241-244.
- [22] Karlsson, N. G.; Schulz, B. L.; Packer, N. H., Structural determination of neutral O-linked oligosaccharide alditols by negative ion LC-electrospray-MSn. *J. Am. Soc. Mass. Spectrom.* **2004**, *15* (5), 659-672.
- [23] Prien, J. M.; Prater, B. D.; Cockrill, S. L., A multi-method approach toward de novo glycan characterization: a Man-5 case study. *Glycobiology* **2010**, *20* (5), 629-647.
- [24] Pabst, M.; Bondili, J. S.; Stadlmann, J.; Mach, L.; Altmann, F., Mass + retention time = structure: a strategy for the analysis of N-glycans by carbon LC-ESI-MS and its application to fibrin N-glycans. *Anal. Chem.* **2007**, *79* (13), 5051-5057.
- [25] Guile, G. R.; Rudd, P. M.; Wing, D. R.; Prime, S. B.; Dwek, R. A., A rapid high-resolution high-performance liquid chromatographic method for separating glycan mixtures and analyzing oligosaccharide profiles. *Anal. Biochem.* **1996**, *240* (2), 210-226.
- [26] Broussard, A. C.; Boyce, M., Life is sweet: the cell biology of glycoconjugates. *Mol Biol Cell* **2019**, *30* (5), 525-529.
- [27] Moremen, K. W.; Tiemeyer, M.; Nairn, A. V., Vertebrate protein glycosylation: diversity, synthesis and function. *Nat Rev Mol Cell Biol* **2012**, *13* (7), 448-462.
- [28] Lauc, G.; Kristic, J.; Zoldos, V., Glycans - the third revolution in evolution. *Front. Genet.* **2014**, *5*, 145.

- [29] Juaristi, E.; Cuevas, G., *The anomeric effect*. CRC Press: Boca Raton and London, 1995.
- [30] Secrist, J. A., 3rd, Nucleoside and nucleotide nomenclature. *Curr Protoc Nucleic Acid Chem* **2001**, Appendix 1, Appendix 1D.
- [31] Nomenclature and symbolism for amino acids and peptides (Recommendations 1983). *Pure Appl. Chem.* **1984**, 56 (5), 595-624.
- [32] Neelamegham, S.; Aoki-Kinoshita, K.; Bolton, E.; Frank, M.; Lisacek, F.; Lutteke, T.; O'Boyle, N.; Packer, N. H.; Stanley, P.; Toukach, P.; Varki, A.; Woods, R. J.; Group, S. D., Updates to the Symbol Nomenclature for Glycans guidelines. *Glycobiology* **2019**, 29 (9), 620-624.
- [33] Varki, A.; Cummings, R. D.; Aebi, M.; Packer, N. H.; Seeberger, P. H.; Esko, J. D.; Stanley, P.; Hart, G.; Darvill, A.; Kinoshita, T.; Prestegard, J. J.; Schnaar, R. L.; Freeze, H. H.; Marth, J. D.; Bertozzi, C. R.; Etzler, M. E.; Frank, M.; Vliegenthart, J. F.; Lutteke, T.; Perez, S.; Bolton, E.; Rudd, P.; Paulson, J.; Kanehisa, M.; Toukach, P.; Aoki-Kinoshita, K. F.; Dell, A.; Narimatsu, H.; York, W.; Taniguchi, N.; Kornfeld, S., Symbol Nomenclature for Graphical Representations of Glycans. *Glycobiology* **2015**, 25 (12), 1323-1324.
- [34] Marino, K.; Bones, J.; Kattla, J. J.; Rudd, P. M., A systematic approach to protein glycosylation analysis: a path through the maze. *Nat Chem Biol* **2010**, 6 (10), 713-23.
- [35] Liu, Y. C.; Yen, H. Y.; Chen, C. Y.; Chen, C. H.; Cheng, P. F.; Juan, Y. H.; Chen, C. H.; Khoo, K. H.; Yu, C. J.; Yang, P. C.; Hsu, T. L.; Wong, C. H., Sialylation and fucosylation of epidermal growth factor receptor suppress its dimerization and activation in lung cancer cells. *Proc Natl Acad Sci U S A* **2011**, 108 (28), 11332-7.
- [36] Giron, L. B.; Tanes, C. E.; Schleimann, M. H.; Engen, P. A.; Mattei, L. M.; Anzurez, A.; Damra, M.; Zhang, H.; Bittinger, K.; Bushman, F.; Kossenkov, A.; Denton, P. W.; Tateno, H.; Keshavarzian, A.; Landay, A. L.; Abdel-Mohsen, M., Sialylation and fucosylation modulate inflammasome-activating eIF2 Signaling and microbial translocation during HIV infection. *Mucosal Immunol* **2020**, 13 (5), 753-766.
- [37] Schauer, R., Sialic acids as regulators of molecular and cellular interactions. *Curr Opin Struct Biol* **2009**, 19 (5), 507-14.
- [38] Varki, A.; Gagneux, P., Multifarious roles of sialic acids in immunity. *Ann N Y Acad Sci* **2012**, 1253, 16-36.
- [39] de Haan, N.; Yang, S.; Cipollo, J.; Wuhrer, M., Glycomics studies using sialic acid derivatization and mass spectrometry. *Nature Reviews Chemistry* **2020**, 4 (5), 229-242.
- [40] Carlin, A. F.; Uchiyama, S.; Chang, Y. C.; Lewis, A. L.; Nizet, V.; Varki, A., Molecular mimicry of host sialylated glycans allows a bacterial pathogen to engage neutrophil Siglec-9 and dampen the innate immune response. *Blood* **2009**, 113 (14), 3333-6.

- [41] Alley, W. R., Jr.; Novotny, M. V., Glycomic analysis of sialic acid linkages in glycans derived from blood serum glycoproteins. *J Proteome Res* **2010**, *9* (6), 3062-72.
- [42] Pereira, N. A.; Chan, K. F.; Lin, P. C.; Song, Z., The "less-is-more" in therapeutic antibodies: Afucosylated anti-cancer antibodies with enhanced antibody-dependent cellular cytotoxicity. *MAbs* **2018**, *10* (5), 693-711.
- [43] Chung, S.; Quarmby, V.; Gao, X.; Ying, Y.; Lin, L.; Reed, C.; Fong, C.; Lau, W.; Qiu, Z. J.; Shen, A.; Vanderlaan, M.; Song, A., Quantitative evaluation of fucose reducing effects in a humanized antibody on Fcγ receptor binding and antibody-dependent cell-mediated cytotoxicity activities. *MAbs* **2012**, *4* (3), 326-40.
- [44] Pearce, O. M. T., Cancer glycan epitopes: biosynthesis, structure and function. *Glycobiology* **2018**, *28* (9), 670-696.
- [45] Blanas, A.; Sahasrabudhe, N. M.; Rodriguez, E.; van Kooyk, Y.; van Vliet, S. J., Fucosylated Antigens in Cancer: An Alliance toward Tumor Progression, Metastasis, and Resistance to Chemotherapy. *Front Oncol* **2018**, *8*, 39.
- [46] Ma, Z.; Yang, H.; Peng, L.; Kuhn, C.; Chelariu-Raicu, A.; Mahner, S.; Jeschke, U.; von Schonfeldt, V., Expression of the Carbohydrate Lewis Antigen, Sialyl Lewis A, Sialyl Lewis X, Lewis X, and Lewis Y in the Placental Villi of Patients With Unexplained Miscarriages. *Front Immunol* **2021**, *12*, 679424.
- [47] de Haan, N.; Falck, D.; Wuhrer, M., Monitoring of immunoglobulin N- and O-glycosylation in health and disease. *Glycobiology* **2020**, *30* (4), 226-240.
- [48] Cymer, F.; Beck, H.; Rohde, A.; Reusch, D., Therapeutic monoclonal antibody N-glycosylation - Structure, function and therapeutic potential. *Biologicals* **2018**, *52*, 1-11.
- [49] Bhatia, S.; Dimde, M.; Haag, R., Multivalent glycoconjugates as vaccines and potential drug candidates. *Med. Chem. Commun.* **2014**, *5* (7), 862-878.
- [50] Zhang, L.; Luo, S.; Zhang, B., Glycan analysis of therapeutic glycoproteins. *MAbs* **2016**, *8* (2), 205-15.
- [51] Duivelshof, B. L.; Denorme, S.; Sandra, K.; Liu, X.; Beck, A.; Lauber, M. A.; Guillarme, D.; D'Atri, V., Quantitative N-Glycan Profiling of Therapeutic Monoclonal Antibodies Performed by Middle-Up Level HILIC-HRMS Analysis. *Pharmaceutics* **2021**, *13* (11).
- [52] Vilaj, M.; Lauc, G.; Trbojevic-Akmacic, I., Evaluation of different PNGase F enzymes in immunoglobulin G and total plasma N-glycans analysis. *Glycobiology* **2021**, *31* (1), 2-7.
- [53] Wilkinson, H.; Saldova, R., Current Methods for the Characterization of O-Glycans. *J Proteome Res* **2020**, *19* (10), 3890-3905.
- [54] Gutierrez Reyes, C. D.; Jiang, P.; Donohoo, K.; Atashi, M.; Mechref, Y. S., Glycomics and glycoproteomics: Approaches to address isomeric separation of glycans and glycopeptides. *J. Sep. Sci.* **2021**, *44* (1), 403-425.

- [55] Walker, S. H.; Lilley, L. M.; Enamorado, M. F.; Comins, D. L.; Muddiman, D. C., Hydrophobic derivatization of N-linked glycans for increased ion abundance in electrospray ionization mass spectrometry. *J. Am. Soc. Mass. Spectrom.* **2011**, *22* (8), 1309-17.
- [56] Zhou, S.; Veillon, L.; Dong, X.; Huang, Y.; Mechref, Y., Direct comparison of derivatization strategies for LC-MS/MS analysis of N-glycans. *Analyst* **2017**, *142* (23), 4446-4455.
- [57] Mechref, Y.; Hu, Y.; Desantos-Garcia, J. L.; Hussein, A.; Tang, H., Quantitative glycomics strategies. *Mol Cell Proteomics* **2013**, *12* (4), 874-84.
- [58] Pabst, M.; Kolarich, D.; Poltl, G.; Dalik, T.; Lubec, G.; Hofinger, A.; Altmann, F., Comparison of fluorescent labels for oligosaccharides and introduction of a new postlabeling purification method. *Anal. Biochem.* **2009**, *384* (2), 263-273.
- [59] Kozak, R. P.; Tortosa, C. B.; Fernandes, D. L.; Spencer, D. I., Comparison of procainamide and 2-aminobenzamide labeling for profiling and identification of glycans by liquid chromatography with fluorescence detection coupled to electrospray ionization-mass spectrometry. *Anal. Biochem.* **2015**, *486*, 38-40.
- [60] Keser, T.; Pavic, T.; Lauc, G.; Gornik, O., Comparison of 2-Aminobenzamide, Procainamide and RapiFluor-MS as Derivatizing Agents for High-Throughput HILIC-UPLC-FLR-MS N-glycan Analysis. *Front Chem* **2018**, *6*, 324.
- [61] Lauber, M. A.; Yu, Y. Q.; Brousmiche, D. W.; Hua, Z.; Koza, S. M.; Magnelli, P.; Guthrie, E.; Taron, C. H.; Fountain, K. J., Rapid Preparation of Released N-Glycans for HILIC Analysis Using a Labeling Reagent that Facilitates Sensitive Fluorescence and ESI-MS Detection. *Anal. Chem.* **2015**, *87* (10), 5401-5409.
- [62] Krenkova, J.; Dusa, F.; Cmelik, R., Comparison of oligosaccharide labeling employing reductive amination and hydrazone formation chemistries. *Electrophoresis* **2020**, *41* (9), 684-690.
- [63] Butler, K. E.; Kalmar, J. G.; Muddiman, D. C.; Baker, E. S., Utilizing liquid chromatography, ion mobility spectrometry, and mass spectrometry to assess INLIGHT derivatized N-linked glycans in biological samples. *Anal Bioanal Chem* **2022**, *414* (1), 623-637.
- [64] Ciucanu, I.; Kerek, F., A simple and rapid method for the permethylation of carbohydrates. *Carbohydr. Res.* **1984**, *131* (2), 209-217.
- [65] Zhou, S.; Wooding, K. M.; Mechref, Y., Analysis of Permethyated Glycan by Liquid Chromatography (LC) and Mass Spectrometry (MS). *Methods Mol Biol* **2017**, *1503*, 83-96.
- [66] Nishikaze, T., Sialic acid derivatization for glycan analysis by mass spectrometry. *Proc Jpn Acad Ser B Phys Biol Sci* **2019**, *95* (9), 523-537.
- [67] Furukawa, J. I.; Hanamatsu, H.; Nishikaze, T.; Manya, H.; Miura, N.; Yagi, H.; Yokota, I.; Akasaka-Manya, K.; Endo, T.; Kanagawa, M.; Iwasaki, N.; Tanaka, K.,

- Lactone-Driven Ester-to-Amide Derivatization for Sialic Acid Linkage-Specific Alkylamidation. *Anal. Chem.* **2020**.
- [68] Nishikaze, T.; Tsumoto, H.; Sekiya, S.; Iwamoto, S.; Miura, Y.; Tanaka, K., Differentiation of Sialyl Linkage Isomers by One-Pot Sialic Acid Derivatization for Mass Spectrometry-Based Glycan Profiling. *Anal. Chem.* **2017**, *89* (4), 2353-2360.
- [69] Ashwood, C.; Pratt, B.; MacLean, B. X.; Gundry, R. L.; Packer, N. H., Standardization of PGC-LC-MS-based glycomics for sample specific glycotyping. *Analyst* **2019**, *144* (11), 3601-3612.
- [70] Bapiro, T. E.; Richards, F. M.; Jodrell, D. I., Understanding the Complexity of Porous Graphitic Carbon (PGC) Chromatography: Modulation of Mobile-Stationary Phase Interactions Overcomes Loss of Retention and Reduces Variability. *Anal. Chem.* **2016**, *88* (12), 6190-4.
- [71] Zhou, S.; Huang, Y.; Dong, X.; Peng, W.; Veillon, L.; Kitagawa, D. A. S.; Aquino, A. J. A.; Mechref, Y., Isomeric Separation of Permethylated Glycans by Porous Graphitic Carbon (PGC)-LC-MS/MS at High Temperatures. *Anal. Chem.* **2017**, *89* (12), 6590-6597.
- [72] Chen, C. H.; Lin, Y. P.; Ren, C. T.; Shivatare, S. S.; Lin, N. H.; Wu, C. Y.; Chen, C. H.; Lin, J. L., Enhancement of fucosylated N-glycan isomer separation with an ultrahigh column temperature in porous graphitic carbon liquid chromatography-mass spectrometry. *J. Chromatogr. A* **2020**, *1632*, 461610.
- [73] Ashwood, C.; Lin, C. H.; Thaysen-Andersen, M.; Packer, N. H., Discrimination of Isomers of Released N- and O-Glycans Using Diagnostic Product Ions in Negative Ion PGC-LC-ESI-MS/MS. *J. Am. Soc. Mass. Spectrom.* **2018**, *29* (6), 1194-1209.
- [74] Molnarova, K.; Kozlik, P., Comparison of Different HILIC Stationary Phases in the Separation of Hemopexin and Immunoglobulin G Glycopeptides and Their Isomers. *Molecules* **2020**, *25* (20).
- [75] Qing, G.; Yan, J.; He, X.; Li, X.; Liang, X., Recent advances in hydrophilic interaction liquid interaction chromatography materials for glycopeptide enrichment and glycan separation. *TrAC, Trends Anal. Chem.* **2020**, *124*.
- [76] Zaia, J., Capillary electrophoresis-mass spectrometry of carbohydrates. *Methods Mol Biol* **2013**, *984*, 13-25.
- [77] Schlecht, J.; Stolz, A.; Hofmann, A.; Gerstung, L.; Neususs, C., nanoCEasy: An Easy, Flexible, and Robust Nanoflow Sheath Liquid Capillary Electrophoresis-Mass Spectrometry Interface Based on 3D Printed Parts. *Anal. Chem.* **2021**, *93* (44), 14593-14598.
- [78] Zhang, Q.; Li, Z.; Song, X., Preparation of Complex Glycans From Natural Sources for Functional Study. *Front Chem* **2020**, *8*, 508.
- [79] Hahm, H. S.; Schlegel, M. K.; Hurevich, M.; Eller, S.; Schuhmacher, F.; Hofmann, J.; Pagel, K.; Seeberger, P. H., Automated glycan assembly using the Glyconeer 2.1 synthesizer. *Proc Natl Acad Sci U S A* **2017**, *114* (17), E3385-E3389.

- [80] Wang, Z.; Chinoy, Z. S.; Ambre, S. G.; Peng, W.; McBride, R.; de Vries, R. P.; Glushka, J.; Paulson, J. C.; Boons, G. J., A general strategy for the chemoenzymatic synthesis of asymmetrically branched N-glycans. *Science* **2013**, *341* (6144), 379-83.
- [81] Guberman, M.; Seeberger, P. H., Automated Glycan Assembly: A Perspective. *J. Am. Chem. Soc.* **2019**, *141* (14), 5581-5592.
- [82] Mancera-Arteu, M.; Gimenez, E.; Barbosa, J.; Sanz-Nebot, V., Identification and characterization of isomeric N-glycans of human alpha-acid-glycoprotein by stable isotope labelling and ZIC-HILIC-MS in combination with exoglycosidase digestion. *Anal. Chim. Acta* **2016**, *940*, 92-103.
- [83] Zhao, S.; Walsh, I.; Abrahams, J. L.; Royle, L.; Nguyen-Khuong, T.; Spencer, D.; Fernandes, D. L.; Packer, N. H.; Rudd, P. M.; Campbell, M. P., GlycoStore: a database of retention properties for glycan analysis. *Bioinformatics* **2018**, *34* (18), 3231-3232.
- [84] Radcliffe, C. M.; Royle, L.; Campbell, M. P.; Rudd, P. M.; Dwek, R. A., GlycoBase and autoGU: tools for HPLC-based glycan analysis. *Bioinformatics* **2008**, *24* (9), 1214-1216.
- [85] Jarvas, G.; Szigeti, M.; Chapman, J.; Guttman, A., Triple-Internal Standard Based Glycan Structural Assignment Method for Capillary Electrophoresis Analysis of Carbohydrates. *Anal. Chem.* **2016**, *88* (23), 11364-11367.
- [86] Royle, L.; Campbell, M. P.; Radcliffe, C. M.; White, D. M.; Harvey, D. J.; Abrahams, J. L.; Kim, Y. G.; Henry, G. W.; Shadick, N. A.; Weinblatt, M. E.; Lee, D. M.; Rudd, P. M.; Dwek, R. A., HPLC-based analysis of serum N-glycans on a 96-well plate platform with dedicated database software. *Anal. Biochem.* **2008**, *376* (1), 1-12.
- [87] Hillenkamp, F.; Karas, M.; Beavis, R. C.; Chait, B. T., Matrix-Assisted Laser Desorption/Ionization Mass Spectrometry of Biopolymers. *Anal. Chem.* **1991**, *63* (24), 1193A-1203A.
- [88] Fenn, J. B.; Mann, M.; Meng, C. K.; Wong, S. F.; Whitehouse, C. M., Electrospray ionization for mass spectrometry of large biomolecules. *Science* **1989**, *246* (4926), 64-71.
- [89] Heijs, B.; Potthoff, A.; Soltwisch, J.; Dreisewerd, K., MALDI-2 for the Enhanced Analysis of N-Linked Glycans by Mass Spectrometry Imaging. *Anal. Chem.* **2020**, *92* (20), 13904-13911.
- [90] Domon, B.; Costello, C. E., A systematic nomenclature for carbohydrate fragmentations in FAB-MS/MS spectra of glycoconjugates. *Glycoconjugate J.* **1988**, *5* (4), 397-409.
- [91] An, H. J.; Lebrilla, C. B., Structure elucidation of native N- and O-linked glycans by tandem mass spectrometry (tutorial). *Mass Spectrom. Rev.* **2011**, *30* (4), 560-78.
- [92] Harvey, D. J., Ionization and collision-induced fragmentation of N-linked and related carbohydrates using divalent cations. *J. Am. Soc. Mass. Spectrom.* **2001**, *12* (8), 926-937.

- [93] Harvey, D. J., Fragmentation of negative ions from carbohydrates: part 1. Use of nitrate and other anionic adducts for the production of negative ion electrospray spectra from N-linked carbohydrates. *J. Am. Soc. Mass. Spectrom.* **2005**, *16* (5), 622-630.
- [94] Harvey, D. J., Fragmentation of negative ions from carbohydrates: part 2. Fragmentation of high-mannose N-linked glycans. *J. Am. Soc. Mass. Spectrom.* **2005**, *16* (5), 631-646.
- [95] Harvey, D. J., Fragmentation of negative ions from carbohydrates: part 3. Fragmentation of hybrid and complex N-linked glycans. *J. Am. Soc. Mass. Spectrom.* **2005**, *16* (5), 647-659.
- [96] Mucha, E.; Lettow, M.; Marianski, M.; Thomas, D. A.; Struwe, W. B.; Harvey, D. J.; Meijer, G.; Seeberger, P. H.; von Helden, G.; Pagel, K., Fucose Migration in Intact Protonated Glycan Ions: A Universal Phenomenon in Mass Spectrometry. *Angew. Chem. Int. Ed. Engl.* **2018**, *57* (25), 7440-7443.
- [97] Wuhler, M.; Koeleman, C. A.; Hokke, C. H.; Deelder, A. M., Mass spectrometry of proton adducts of fucosylated N-glycans: fucose transfer between antennae gives rise to misleading fragments. *Rapid Commun. Mass Spectrom.* **2006**, *20* (11), 1747-1754.
- [98] Lettow, M.; Mucha, E.; Manz, C.; Thomas, D. A.; Marianski, M.; Meijer, G.; von Helden, G.; Pagel, K., The role of the mobile proton in fucose migration. *Anal Bioanal Chem* **2019**, *411* (19), 4637-4645.
- [99] Sastre Torano, J.; Gagarinov, I. A.; Vos, G. M.; Broszeit, F.; Srivastava, A. D.; Palmer, M.; Langridge, J. I.; Aizpurua-Olaizola, O.; Somovilla, V. J.; Boons, G. J., Ion-Mobility Spectrometry Can Assign Exact Fucosyl Positions in Glycans and Prevent Misinterpretation of Mass-Spectrometry Data After Gas-Phase Rearrangement. *Angew. Chem. Int. Ed. Engl.* **2019**, *58* (49), 17616-17620.
- [100] Hoffmann, W.; von Helden, G.; Pagel, K., Ion mobility-mass spectrometry and orthogonal gas-phase techniques to study amyloid formation and inhibition. *Curr Opin Struct Biol* **2017**, *46*, 7-15.
- [101] Roscioli, K. M.; Davis, E.; Siems, W. F.; Mariano, A.; Su, W.; Guharay, S. K.; Hill, H. H., Jr., Modular ion mobility spectrometer for explosives detection using corona ionization. *Anal. Chem.* **2011**, *83* (15), 5965-5971.
- [102] Ruzsanyi, V., Ion mobility spectrometry for pharmacokinetic studies--exemplary application. *J. Breath. Res.* **2013**, *7* (4), 046008.
- [103] Fenn, L. S.; Kliman, M.; Mahsut, A.; Zhao, S. R.; McLean, J. A., Characterizing ion mobility-mass spectrometry conformation space for the analysis of complex biological samples. *Anal Bioanal Chem* **2009**, *394* (1), 235-244.
- [104] Seo, J.; Hoffmann, W.; Warnke, S.; Bowers, M. T.; Pagel, K.; von Helden, G., Retention of Native Protein Structures in the Absence of Solvent: A Coupled Ion Mobility and Spectroscopic Study. *Angew. Chem. Int. Ed. Engl.* **2016**, *55* (45), 14173-14176.

- [105] Thalassinos, K.; Grabenauer, M.; Slade, S. E.; Hilton, G. R.; Bowers, M. T.; Scrivens, J. H., Characterization of phosphorylated peptides using traveling wave-based and drift cell ion mobility mass spectrometry. *Anal. Chem.* **2009**, *81* (1), 248-254.
- [106] Hernandez, D. R.; DeBord, J. D.; Ridgeway, M. E.; Kaplan, D. A.; Park, M. A.; Fernandez-Lima, F., Ion dynamics in a trapped ion mobility spectrometer(). *Analyst* **2014**, *139* (8), 1913-1921.
- [107] Struwe, W. B.; Benesch, J. L.; Harvey, D. J.; Pagel, K., Collision cross sections of high-mannose N-glycans in commonly observed adduct states - identification of gas-phase conformers unique to [M - H] ions. *Analyst* **2015**.
- [108] Gabelica, V.; Shvartsburg, A. A.; Afonso, C.; Barran, P.; Benesch, J. L. P.; Bleiholder, C.; Bowers, M. T.; Bilbao, A.; Bush, M. F.; Campbell, J. L.; Campuzano, I. D. G.; Causon, T.; Clowers, B. H.; Creaser, C. S.; De Pauw, E.; Far, J.; Fernandez-Lima, F.; Fjeldsted, J. C.; Giles, K.; Groessl, M.; Hogan, C. J., Jr.; Hann, S.; Kim, H. I.; Kurulugama, R. T.; May, J. C.; McLean, J. A.; Pagel, K.; Richardson, K.; Ridgeway, M. E.; Rosu, F.; Sobott, F.; Thalassinos, K.; Valentine, S. J.; Wyttenbach, T., Recommendations for reporting ion mobility Mass Spectrometry measurements. *Mass Spectrom. Rev.* **2019**, *38* (3), 291-320.
- [109] Mason, E. A.; Schamp, H. W., Mobility of gaseous ions in weak electric fields. *Ann. Phys.* **1958**, *4* (3), 233-270.
- [110] Revercomb, H. E.; Mason, E. A., Theory of plasma chromatography/gaseous electrophoresis. Review. *Anal. Chem.* **1975**, *47* (7), 970-983.
- [111] Pringle, S. D.; Giles, K.; Wildgoose, J. L.; Williams, J. P.; Slade, S. E.; Thalassinos, K.; Bateman, R. H.; Bowers, M. T.; Scrivens, J. H., An investigation of the mobility separation of some peptide and protein ions using a new hybrid quadrupole/travelling wave IMS/oa-ToF instrument. *Int. J. Mass spectrom.* **2007**, *261* (1), 1-12.
- [112] Giles, K.; Williams, J. P.; Campuzano, I., Enhancements in travelling wave ion mobility resolution. *Rapid Commun. Mass Spectrom.* **2011**, *25* (11), 1559-1566.
- [113] Richardson, K.; Langridge, D.; Giles, K., Fundamentals of travelling wave ion mobility revisited: I. Smoothly moving waves. *Int. J. Mass spectrom.* **2018**, *428*, 71-80.
- [114] Shvartsburg, A. A.; Smith, R. D., Fundamentals of traveling wave ion mobility spectrometry. *Anal. Chem.* **2008**, *80* (24), 9689-99.
- [115] Hofmann, J.; Struwe, W. B.; Scarff, C. A.; Scrivens, J. H.; Harvey, D. J.; Pagel, K., Estimating collision cross sections of negatively charged N-glycans using traveling wave ion mobility-mass spectrometry. *Anal. Chem.* **2014**, *86* (21), 10789-10795.
- [116] Stow, S. M.; Causon, T. J.; Zheng, X.; Kurulugama, R. T.; Mairinger, T.; May, J. C.; Rennie, E. E.; Baker, E. S.; Smith, R. D.; McLean, J. A.; Hann, S.; Fjeldsted, J. C., An Interlaboratory Evaluation of Drift Tube Ion Mobility-Mass Spectrometry Collision Cross Section Measurements. *Anal. Chem.* **2017**, *89* (17), 9048-9055.

- [117] Campuzano, I. D. G.; Giles, K., Historical, current and future developments of travelling wave ion mobility mass spectrometry: A personal perspective. *TrAC, Trends Anal. Chem.* **2019**, *120*.
- [118] Ujma, J.; Ropartz, D.; Giles, K.; Richardson, K.; Langridge, D.; Wildgoose, J.; Green, M.; Pringle, S., Cyclic Ion Mobility Mass Spectrometry Distinguishes Anomers and Open-Ring Forms of Pentasaccharides. *J. Am. Soc. Mass. Spectrom.* **2019**, *30* (6), 1028-1037.
- [119] May, J. C.; Goodwin, C. R.; Lareau, N. M.; Leaptrot, K. L.; Morris, C. B.; Kurulugama, R. T.; Mordehai, A.; Klein, C.; Barry, W.; Darland, E.; Overney, G.; Imatani, K.; Stafford, G. C.; Fjeldsted, J. C.; McLean, J. A., Conformational Ordering of Biomolecules in the Gas Phase: Nitrogen Collision Cross Sections Measured on a Prototype High Resolution Drift Tube Ion Mobility-Mass Spectrometer. *Anal. Chem.* **2014**, *86* (4), 2107-2116.
- [120] Kirk, A. T.; Bohnhorst, A.; Raddatz, C. R.; Allers, M.; Zimmermann, S., Ultra-high-resolution ion mobility spectrometry-current instrumentation, limitations, and future developments. *Anal Bioanal Chem* **2019**, *411* (24), 6229-6246.
- [121] Fernandez-Lima, F.; Kaplan, D. A.; Suetering, J.; Park, M. A., Gas-phase separation using a trapped ion mobility spectrometer. *Int J Ion Mobil Spectrom* **2011**, *14* (2-3).
- [122] Meier, F.; Beck, S.; Grassl, N.; Lubeck, M.; Park, M. A.; Raether, O.; Mann, M., Parallel Accumulation-Serial Fragmentation (PASEF): Multiplying Sequencing Speed and Sensitivity by Synchronized Scans in a Trapped Ion Mobility Device. *J Proteome Res* **2015**, *14* (12), 5378-87.
- [123] Michelmann, K.; Silveira, J. A.; Ridgeway, M. E.; Park, M. A., Fundamentals of trapped ion mobility spectrometry. *J. Am. Soc. Mass. Spectrom.* **2015**, *26* (1), 14-24.
- [124] Silveira, J. A.; Ridgeway, M. E.; Laukien, F. H.; Mann, M.; Park, M. A., Parallel accumulation for 100% duty cycle trapped ion mobility-mass spectrometry. *Int. J. Mass spectrom.* **2017**, *413*, 168-175.
- [125] Ridgeway, M. E.; Lubeck, M.; Jordens, J.; Mann, M.; Park, M. A., Trapped ion mobility spectrometry: A short review. *Int. J. Mass spectrom.* **2018**, *425*, 22-35.
- [126] Allen, S. J.; Giles, K.; Gilbert, T.; Bush, M. F., Ion mobility mass spectrometry of peptide, protein, and protein complex ions using a radio-frequency confining drift cell. *Analyst* **2016**, *141* (3), 884-891.
- [127] Li, H.; Bendiak, B.; Siems, W. F.; Gang, D. R.; Hill, H. H., Jr., Ion Mobility-Mass Correlation Trend Line Separation of Glycoprotein Digests without Deglycosylation. *Int J Ion Mobil Spectrom* **2013**, *16* (2), 105-115.
- [128] Harvey, D. J.; Sobott, F.; Crispin, M.; Wrobel, A.; Bonomelli, C.; Vasiljevic, S.; Scanlan, C. N.; Scarff, C. A.; Thalassinou, K.; Scrivens, J. H., Ion mobility mass spectrometry for extracting spectra of N-glycans directly from incubation mixtures following glycan release: application to glycans from engineered glycoforms of intact, folded HIV gp120. *J. Am. Soc. Mass. Spectrom.* **2011**, *22* (3), 568-581.

- [129] Gray, C. J.; Thomas, B.; Upton, R.; Migas, L. G.; Evers, C. E.; Barran, P. E.; Flitsch, S. L., Applications of ion mobility mass spectrometry for high throughput, high resolution glycan analysis. *Biochim. Biophys. Acta* **2016**, *1860* (8), 1688-1709.
- [130] Harvey, D. J.; Scarff, C. A.; Edgeworth, M.; Struwe, W. B.; Pagel, K.; Thalassinou, K.; Crispin, M.; Scrivens, J., Travelling-wave ion mobility and negative ion fragmentation of high-mannose N-glycans. *J. Mass Spectrom.* **2016**, *51* (3), 219-235.
- [131] Campbell, M. P.; Peterson, R.; Mariethoz, J.; Gasteiger, E.; Akune, Y.; Aoki-Kinoshita, K. F.; Lisacek, F.; Packer, N. H., UniCarbKB: building a knowledge platform for glycoproteomics. *Nucleic Acids Res.* **2014**, *42* (Database issue), D215-221.
- [132] Struwe, W. B.; Pagel, K.; Benesch, J. L.; Harvey, D. J.; Campbell, M. P., GlycoMob: an ion mobility-mass spectrometry collision cross section database for glycomics. *Glycoconj. J.* **2016**, *33* (3), 399-404.
- [133] Lisacek, F.; Mariethoz, J.; Alocchi, D.; Rudd, P. M.; Abrahams, J. L.; Campbell, M. P.; Packer, N. H.; Stahle, J.; Widmalm, G.; Mullen, E.; Adamczyk, B.; Rojas-Macias, M. A.; Jin, C.; Karlsson, N. G., Databases and Associated Tools for Glycomics and Glycoproteomics. *Methods Mol Biol* **2017**, *1503*, 235-264.
- [134] von Helden, G.; Hsu, M. T.; Gotts, N.; Bowers, M. T., Carbon cluster cations with up to 84 atoms: structures, formation mechanism, and reactivity. *The Journal of Physical Chemistry* **1993**, *97* (31), 8182-8192.
- [135] Mesleh, M. F.; Hunter, J. M.; Shvartsburg, A. A.; Schatz, G. C.; Jarrold, M. F., Structural Information from Ion Mobility Measurements: Effects of the Long-Range Potential. *The Journal of Physical Chemistry* **1996**, *100* (40), 16082-16086.
- [136] Shvartsburg, A. A.; Jarrold, M. F., An exact hard-spheres scattering model for the mobilities of polyatomic ions. *Chem. Phys. Lett.* **1996**, *261* (1-2), 86-91.
- [137] Deng, L.; Webb, I. K.; Garimella, S. V. B.; Hamid, A. M.; Zheng, X.; Norheim, R. V.; Prost, S. A.; Anderson, G. A.; Sandoval, J. A.; Baker, E. S.; Ibrahim, Y. M.; Smith, R. D., Serpentine Ultralong Path with Extended Routing (SUPER) High Resolution Traveling Wave Ion Mobility-MS using Structures for Lossless Ion Manipulations. *Anal. Chem.* **2017**, *89* (8), 4628-4634.
- [138] Huang, Y.; Dodds, E. D., Ion mobility studies of carbohydrates as group I adducts: isomer specific collisional cross section dependence on metal ion radius. *Anal. Chem.* **2013**, *85* (20), 9728-9735.
- [139] Gaye, M. M.; Nagy, G.; Clemmer, D. E.; Pohl, N. L., Multidimensional Analysis of 16 Glucose Isomers by Ion Mobility Spectrometry. *Anal. Chem.* **2016**, *88* (4), 2335-2344.
- [140] Huang, Y.; Dodds, E. D., Discrimination of Isomeric Carbohydrates as the Electron Transfer Products of Group II Cation Adducts by Ion Mobility Spectrometry and Tandem Mass Spectrometry. *Anal. Chem.* **2015**, *87* (11), 5664-5668.

- [141] Li, H.; Bendiak, B.; Siems, W. F.; Gang, D. R.; Hill, H. H., Jr., Ion mobility mass spectrometry analysis of isomeric disaccharide precursor, product and cluster ions. *Rapid Commun. Mass Spectrom.* **2013**, *27* (23), 2699-2709.
- [142] Both, P.; Green, A. P.; Gray, C. J.; Sardzik, R.; Voglmeir, J.; Fontana, C.; Austeri, M.; Rejzek, M.; Richardson, D.; Field, R. A.; Widmalm, G.; Flitsch, S. L.; Eyers, C. E., Discrimination of epimeric glycans and glycopeptides using IM-MS and its potential for carbohydrate sequencing. *Nat Chem* **2014**, *6* (1), 65-74.
- [143] Gaye, M. M.; Kurulugama, R.; Clemmer, D. E., Investigating carbohydrate isomers by IMS-CID-IMS-MS: precursor and fragment ion cross-sections. *Analyst* **2015**.
- [144] Takada, A.; Ohmori, K.; Yoneda, T.; Tsuyuoka, K.; Hasegawa, A.; Kiso, M.; Kannagi, R., Contribution of Carbohydrate Antigens Sialyl Lewis A and Sialyl Lewis X to Adhesion of Human Cancer Cells to Vascular Endothelium. *Cancer Research* **1993**, *53* (2), 354-361.
- [145] Guttman, M.; Lee, K. K., Site-Specific Mapping of Sialic Acid Linkage Isomers by Ion Mobility Spectrometry. *Anal. Chem.* **2016**, *88* (10), 5212-7.
- [146] Causon, T. J.; Hann, S., Theoretical evaluation of peak capacity improvements by use of liquid chromatography combined with drift tube ion mobility-mass spectrometry. *J. Chromatogr. A* **2015**, *1416*, 47-56.
- [147] Pallister, E. G.; Choo, M. S. F.; Walsh, I.; Tai, J. N.; Tay, S. J.; Yang, Y. S.; Ng, S. K.; Rudd, P. M.; Flitsch, S. L.; Nguyen-Khuong, T., Utility of Ion-Mobility Spectrometry for Deducing Branching of Multiply Charged Glycans and Glycopeptides in a High-Throughput Positive ion LC-FLR-IMS-MS Workflow. *Anal. Chem.* **2020**, *92* (23), 15323-15335.
- [148] Largy, E.; Cantais, F.; Van Vyncht, G.; Beck, A.; Delobel, A., Orthogonal liquid chromatography–mass spectrometry methods for the comprehensive characterization of therapeutic glycoproteins, from released glycans to intact protein level. *J. Chromatogr. A* **2017**, *1498*, 128-146.
- [149] Royle, L.; Dwek, R. A.; Rudd, P. M., Determining the structure of oligosaccharides N- and O-linked to glycoproteins. *Curr Protoc Protein Sci* **2006**, *43*, 12.6.01-12.6.45.
- [150] Altmann, F., Determination of amino sugars and amino acids in glycoconjugates using precolumn derivatization with o-phthalaldehyde. *Anal. Biochem.* **1992**, *204* (1), 215-219.
- [151] Mantovani, V.; Galeotti, F.; Maccari, F.; Volpi, N., Recent advances on separation and characterization of human milk oligosaccharides. *Electrophoresis* **2016**, *37* (11), 1514-1524.
- [152] Myers, R. B.; Srivastava, S.; Grizzle, W. E., Lewis Y antigen as detected by the monoclonal antibody BR96 is expressed strongly in prostatic adenocarcinoma. *J Urol* **1995**, *153* (5), 1572-4.

- [153] Pendu, J.; Marionneau, S.; Cailleau-Thomas, A.; Rocher, J.; Moullac-Vaidye, B.; Clément, M., ABH and Lewis histo-blood group antigens in cancer. *Apmis* **2001**, *109* (1), 9-26.
- [154] Veillon, L.; Huang, Y.; Peng, W.; Dong, X.; Cho, B. G.; Mechref, Y., Characterization of isomeric glycan structures by LC-MS/MS. *Electrophoresis* **2017**, *38* (17), 2100-2114.
- [155] Reusch, D.; Habegger, M.; Maier, B.; Maier, M.; Kloseck, R.; Zimmermann, B.; Hook, M.; Szabo, Z.; Tep, S.; Wegstein, J.; Alt, N.; Bulau, P.; Wuhrer, M., Comparison of methods for the analysis of therapeutic immunoglobulin G Fc-glycosylation profiles--part 1: separation-based methods. *MAbs* **2015**, *7* (1), 167-179.
- [156] Lattova, E.; Snovida, S.; Perreault, H.; Krokhin, O., Influence of the labeling group on ionization and fragmentation of carbohydrates in mass spectrometry. *J. Am. Soc. Mass. Spectrom.* **2005**, *16* (5), 683-696.
- [157] Harvey, D. J., Electrospray mass spectrometry and fragmentation of N-linked carbohydrates derivatized at the reducing terminus. *J. Am. Soc. Mass. Spectrom.* **2000**, *11* (10), 900-915.
- [158] Harvey, D. J., Analysis of carbohydrates and glycoconjugates by matrix-assisted laser desorption/ionization mass spectrometry: An update for 2011-2012. *Mass Spectrom. Rev.* **2017**, *36* (3), 255-422.
- [159] Ruhaak, L. R.; Zauner, G.; Huhn, C.; Bruggink, C.; Deelder, A. M.; Wuhrer, M., Glycan labeling strategies and their use in identification and quantification. *Anal Bioanal Chem* **2010**, *397* (8), 3457-3481.
- [160] Struwe, W. B.; Baldauf, C.; Hofmann, J.; Rudd, P. M.; Pagel, K., Ion mobility separation of deprotonated oligosaccharide isomers - evidence for gas-phase charge migration. *Chem. Commun.* **2016**, *52* (83), 12353-12356.
- [161] Struwe, W. B.; Benesch, J. L.; Harvey, D. J.; Pagel, K., Collision cross sections of high-mannose N-glycans in commonly observed adduct states--identification of gas-phase conformers unique to [M-H]<sup>-</sup> ions. *Analyst* **2015**, *140* (20), 6799-6803.
- [162] Vachet, R. W.; Bishop, B. M.; Erickson, B. W.; Glish, G. L., Novel Peptide Dissociation: Gas-Phase Intramolecular Rearrangement of Internal Amino Acid Residues. *J. Am. Chem. Soc.* **1997**, *119* (24), 5481-5488.
- [163] Royle, L.; Radcliffe, C. M.; Dwek, R. A.; Rudd, P. M., Detailed Structural Analysis of N-Glycans Released From Glycoproteins in SDS-PAGE Gel Bands Using HPLC Combined With Exoglycosidase Array Digestions. In *Glycobiology Protocols*, Brockhausen, I., Ed. Humana Press: Totowa, NJ, 2007; pp 125-143.
- [164] Struwe, W. B.; Pagel, K.; Benesch, J. L. P.; Harvey, D. J.; Campbell, M. P., GlycoMob: an ion mobility-mass spectrometry collision cross section database for glycomics. *Glycoconjugate J.* **2016**, *33* (3), 399-404.
- [165] Shubhakar, A.; Reiding, K. R.; Gardner, R. A.; Spencer, D. I.; Fernandes, D. L.; Wuhrer, M., High-Throughput Analysis and Automation for Glycomics Studies. *Chromatographia* **2015**, *78* (5-6), 321-333.

- [166] Marty, M. T.; Baldwin, A. J.; Marklund, E. G.; Hochberg, G. K.; Benesch, J. L.; Robinson, C. V., Bayesian deconvolution of mass and ion mobility spectra: from binary interactions to polydisperse ensembles. *Anal. Chem.* **2015**, *87* (8), 4370-4376.
- [167] Varki, A., Sialic acids in human health and disease. *Trends in molecular medicine* **2008**, *14* (8), 351-360.
- [168] Hashimoto, S.; Asao, T.; Takahashi, J.; Yagihashi, Y.; Nishimura, T.; Saniabadi, A. R.; Poland, D. C.; van Dijk, W.; Kuwano, H.; Kochibe, N.; Yazawa, S., alpha1-acid glycoprotein fucosylation as a marker of carcinoma progression and prognosis. *Cancer* **2004**, *101* (12), 2825-36.
- [169] Amon, R.; Reuven, E. M.; Leviatan Ben-Arye, S.; Padler-Karavani, V., Glycans in immune recognition and response. *Carbohydr. Res.* **2014**, *389*, 115-22.
- [170] Sethi, M. K.; Kim, H.; Park, C. K.; Baker, M. S.; Paik, Y. K.; Packer, N. H.; Hancock, W. S.; Fanayan, S.; Thaysen-Andersen, M., In-depth N-glycome profiling of paired colorectal cancer and non-tumorigenic tissues reveals cancer-, stage- and EGFR-specific protein N-glycosylation. *Glycobiology* **2015**, *25* (10), 1064-78.
- [171] Gilgunn, S.; Conroy, P. J.; Saldova, R.; Rudd, P. M.; O'Kennedy, R. J., Aberrant PSA glycosylation--a sweet predictor of prostate cancer. *Nat Rev Urol* **2013**, *10* (2), 99-107.
- [172] Harvey, D. J.; Rudd, P. M., Fragmentation of negative ions from N-linked carbohydrates. Part 5: Anionic N-linked glycans. *Int. J. Mass spectrom.* **2011**, *305* (2-3), 120-130.
- [173] Mancera-Arteu, M.; Gimenez, E.; Barbosa, J.; Peracaula, R.; Sanz-Nebot, V., Zwitterionic-hydrophilic interaction capillary liquid chromatography coupled to tandem mass spectrometry for the characterization of human alpha-acid-glycoprotein N-glycan isomers. *Anal. Chim. Acta* **2017**, *991*, 76-88.
- [174] Rogerieux, F.; Belaise, M.; Terzidis-Trabelsi, H.; Greffard, A.; Pilatte, Y.; Lambre, C. R., Determination of the sialic acid linkage specificity of sialidases using lectins in a solid phase assay. *Anal. Biochem.* **1993**, *211* (2), 200-4.
- [175] Barroso, A.; Gimenez, E.; Konijnenberg, A.; Sancho, J.; Sanz-Nebot, V.; Sobott, F., Evaluation of ion mobility for the separation of glycoconjugate isomers due to different types of sialic acid linkage, at the intact glycoprotein, glycopeptide and glycan level. *J Proteomics* **2018**, *173*, 22-31.
- [176] Lane, C. S.; McManus, K.; Widdowson, P.; Flowers, S. A.; Powell, G.; Anderson, I.; Campbell, J. L., Separation of Sialylated Glycan Isomers by Differential Mobility Spectrometry. *Anal. Chem.* **2019**, *91* (15), 9916-9924.
- [177] Manz, C.; Grabarics, M.; Hoberg, F.; Pugini, M.; Stuckmann, A.; Struwe, W. B.; Pagel, K., Separation of isomeric glycans by ion mobility spectrometry - the impact of fluorescent labelling. *Analyst* **2019**, *144* (17), 5292-5298.

- [178] Bigge, J. C.; Patel, T. P.; Bruce, J. A.; Goulding, P. N.; Charles, S. M.; Parekh, R. B., Nonselective and efficient fluorescent labeling of glycans using 2-amino benzamide and anthranilic acid. *Anal. Biochem.* **1995**, *230* (2), 229-238.
- [179] Mancera-Arteu, M.; Gimenez, E.; Balmana, M.; Barrabes, S.; Albiol-Quer, M.; Fort, E.; Peracaula, R.; Sanz-Nebot, V., Multivariate data analysis for the detection of human alpha-acid glycoprotein aberrant glycosylation in pancreatic ductal adenocarcinoma. *J Proteomics* **2019**, *195*, 76-87.
- [180] Sarrats, A.; Saldoval, R.; Pla, E.; Fort, E.; Harvey, D. J.; Struwe, W. B.; de Llorens, R.; Rudd, P. M.; Peracaula, R., Glycosylation of liver acute-phase proteins in pancreatic cancer and chronic pancreatitis. *Proteomics Clin Appl* **2010**, *4* (4), 432-48.
- [181] Gornik, O.; Lauc, G., Glycosylation of serum proteins in inflammatory diseases. *Dis Markers* **2008**, *25* (4-5), 267-78.
- [182] Fernandes, C. L.; Ligabue-Braun, R.; Verli, H., Structural glycobiology of human alpha1-acid glycoprotein and its implications for pharmacokinetics and inflammation. *Glycobiology* **2015**, *25* (10), 1125-33.
- [183] Feng, X.; Shu, H.; Zhang, S.; Peng, Y.; Zhang, L.; Cao, X.; Wei, L.; Lu, H., Relative Quantification of N-Glycopeptide Sialic Acid Linkage Isomers by Ion Mobility Mass Spectrometry. *Anal. Chem.* **2021**, *93* (47), 15617-15625.
- [184] Nwosu, C.; Yau, H. K.; Becht, S., Assignment of Core versus Antenna Fucosylation Types in Protein N-Glycosylation via Procainamide Labeling and Tandem Mass Spectrometry. *Anal. Chem.* **2015**, *87* (12), 5905-13.
- [185] Acs, A.; Ozohanics, O.; Vekey, K.; Drahos, L.; Turiak, L., Distinguishing Core and Antenna Fucosylated Glycopeptides Based on Low-Energy Tandem Mass Spectra. *Anal. Chem.* **2018**, *90* (21), 12776-12782.
- [186] Fournier, T.; Medjoubi-N, N.; Porquet, D., Alpha-1-acid glycoprotein. *Biochimica et Biophysica Acta (BBA) - Protein Structure and Molecular Enzymology* **2000**, *1482* (1-2), 157-171.
- [187] McCalley, D. V., A study of column equilibration time in hydrophilic interaction chromatography. *J. Chromatogr. A* **2018**, *1554*, 61-70.
- [188] Wang, N.; Boswell, P. G., Accurate prediction of retention in hydrophilic interaction chromatography by back calculation of high pressure liquid chromatography gradient profiles. *J. Chromatogr. A* **2017**, *1520*, 75-82.
- [189] Hilliard, M.; Alley, W. R., Jr.; McManus, C. A.; Yu, Y. Q.; Hallinan, S.; Gebler, J.; Rudd, P. M., Glycan characterization of the NIST RM monoclonal antibody using a total analytical solution: From sample preparation to data analysis. *MAbs* **2017**, *9* (8), 1349-1359.
- [190] Grabarics, M.; Lettow, M.; Kirk, A. T.; von Helden, G.; Causon, T. J.; Pagel, K., Plate-height model of ion mobility-mass spectrometry. *Analyst* **2020**, *145* (19), 6313-6333.

- [191] Dodds, J. N.; May, J. C.; McLean, J. A., Correlating Resolving Power, Resolution, and Collision Cross Section: Unifying Cross-Platform Assessment of Separation Efficiency in Ion Mobility Spectrometry. *Anal. Chem.* **2017**, *89* (22), 12176-12184.
- [192] Wei, J.; Tang, Y.; Ridgeway, M. E.; Park, M. A.; Costello, C. E.; Lin, C., Accurate Identification of Isomeric Glycans by Trapped Ion Mobility Spectrometry-Electronic Excitation Dissociation Tandem Mass Spectrometry. *Anal. Chem.* **2020**, *92* (19), 13211-13220.
- [193] Sastre Torano, J.; Aizpurua-Olaizola, O.; Wei, N.; Li, T.; Unione, L.; Jimenez-Oses, G.; Corzana, F.; Somovilla, V. J.; Falcon-Perez, J. M.; Boons, G. J., Identification of Isomeric N-Glycans by Conformer Distribution Fingerprinting using Ion Mobility Mass Spectrometry. *Chemistry* **2021**, *27* (6), 2149-2154.
- [194] Yalovenko, N.; Yatsyna, V.; Bansal, P.; AbiKhodr, A. H.; Rizzo, T. R., Analyzing glycans cleaved from a biotherapeutic protein using ultrahigh-resolution ion mobility spectrometry together with cryogenic ion spectroscopy. *Analyst* **2020**, *145* (20), 6493-6499.
- [195] Everest-Dass, A. V.; Abrahams, J. L.; Kolarich, D.; Packer, N. H.; Campbell, M. P., Structural feature ions for distinguishing N- and O-linked glycan isomers by LC-ESI-IT MS/MS. *J. Am. Soc. Mass. Spectrom.* **2013**, *24* (6), 895-906.
- [196] Crispin, M.; Stuart, D. I.; Jones, E. Y., Building meaningful models of glycoproteins. *Nat Struct Mol Biol* **2007**, *14* (5), 354-354.

# Appendix A Sialic Acid and Fucose Determination

## Supporting Information for Chapter 4: Determination of Sialic Acid and Fucose Isomers from Released N-glycans Using Ion Mobility Spectrometry

Table S-1: Observed glycan species in the direct injection approach for the analysis of native, released glycans of hAGP in positive ion mode.

Peak no.	Glycan species	<i>m/z</i>	<i>z</i>	<i>m</i>	Hexose	HexNAc	Fuc	Sia
1	A2G2S1	966.85	2	1931.7	5	4	0	1
2	A2G2S2	1112.39	2	2222.79	5	4	0	2
3	FA2G2S2	1185.43	2	2368.85	5	4	1	2
4	A3G3S2	1294.96	2	2587.92	6	5	0	2
5	A3G3S3	1440.51	2	2879.02	6	5	0	3
6	FA3G3S3	1513.54	2	3025.08	6	5	1	3
7	A4G4S3	1623.08	2	3244.15	7	6	0	3
8	A4G4S4	1768.63	2	3534.60	7	6	0	4
9	FA4G4S4	1841.65	2	3681.31	7	6	1	4

**Table S-2:** Compositional analysis of released and procainamide-labelled N-glycans from hAGP based on LC-MS results.

LC peak no.	Retention time	Glycan species	<i>m/z</i>	<i>z</i>	<i>m</i>	Hexose	HexNAc	Fuc	Sia
1	17.4	A2G2S1	1076.43	2	2150.86	5	4	0	1
2	17.6	A2G2S1	1076.43	2	2150.86	5	4	0	1
3	18.6	A2G2S1	1076.43	2	2150.86	5	4	0	1
4	18.7	A2G2S1	1076.43	2	2150.86	5	4	0	1
5	20.3	FA2G2S2	1294.99	2	2587.98	5	4	1	2
6	21.3	FA2G2S2	1294.99	2	2587.98	5	4	1	2
7	22.3	FA2G2S2	1294.99	2	2587.98	5	4	1	2
8	22.5	FA2G2S2	1294.99	2	2587.98	5	4	1	2
9	20.6	A2G2S2	1221.98	2	2441.96	5	4	0	2
10	21.7	A2G2S2	1221.98	2	2441.96	5	4	0	2
11	22.2	A3G3S2	1404.54	2	2807.08	6	5	0	2
12	23.2	A3G3S2	1404.54	2	2807.08	6	5	0	2
13	24.1	A3G3S2	1404.54	2	2807.08	6	5	0	2
14	24.7	A3G3S3	1550.07	2	3098.14	6	5	0	3
15	25.6	A3G3S3	1550.07	2	3098.14	6	5	0	3
16	26.5	A3G3S3	1550.07	2	3098.14	6	5	0	3
17	25.7	FA3G3S3	1623.08	2	3244.16	6	5	1	3
18	26.2	FA3G3S3	1623.08	2	3244.16	6	5	1	3
19	26.6	FA3G3S3	1623.08	2	3244.16	6	5	1	3
20	26.1	A4G4S3	1732.60	2	3463.2	7	6	0	3
21	27.0	A4G4S3	1732.60	2	3463.2	7	6	0	3
22	27.6	A4G4S3	1732.60	2	3463.2	7	6	0	3
23	28.2	A4G4S4	1878.12	2	3754.24	7	6	0	4
24	28.9	A4G4S4	1878.12	2	3754.24	7	6	0	4
25	28.9	FA4G4S4	1951.11	2	3900.22	7	6	1	4
26	29.3	FA4G4S4	1951.11	2	3900.22	7	6	1	4
27	29.7	FA4G4S4	1951.11	2	3900.22	7	6	1	4

**Table S-3:** LC-IM-MS analysis of procainamide-labelled N-glycans from hAGP. Sialic acid linkage ratio is derived by the peak area of the characteristic B<sub>3</sub> fragment in percent for each glycan species. This percentage ratio is normalized to the number of sialic acids and then rounded to absolute integers.

Peak no.	ATD ratio	(rel. in %)	ATD ratio	(norm.in %)	Abs. ratio	
	$\alpha$ 2,6	$\alpha$ 2,3	$\alpha$ 2,6	$\alpha$ 2,3	$\alpha$ 2,6	$\alpha$ 2,3
1	0	100	0,0	1,0	0	1
2	0	100	0,0	1,0	0	1
3	100	0	1,0	0,0	1	0
4	100	0	1,0	0,0	1	0
5	0	100	0,0	2,0	0	2
6	46	54	0,9	1,1	1	1
7	54	46	1,1	0,9	1	1
8	100	0	2,0	0,0	2	0
9	46	54	0,9	1,1	1	1
10	100	0	2,0	0,0	2	0
11	0	100	0,0	2,0	0	2
12	43	57	0,9	1,1	1	1
13	100	0	2,0	0,0	2	0
14	30	70	0,9	2,1	1	2
15	63	37	1,9	1,1	2	1
16	100	0	3,0	0,0	3	0
17	36	64	1,1	1,9	1	2
18	59	41	1,8	1,2	2	1
19	90	10	2,7	0,3	3	0
20	0	100	0,0	3,0	0	3
21	40	60	1,2	1,8	1	2
22	83	17	2,5	0,5	3	0
23	0	100	0,0	4,0	0	4
24	28	72	1,1	2,9	1	3
25	11	89	0,4	3,6	0	4
26	24	76	1,0	3,0	1	3
27	47	53	1,9	2,1	2	2

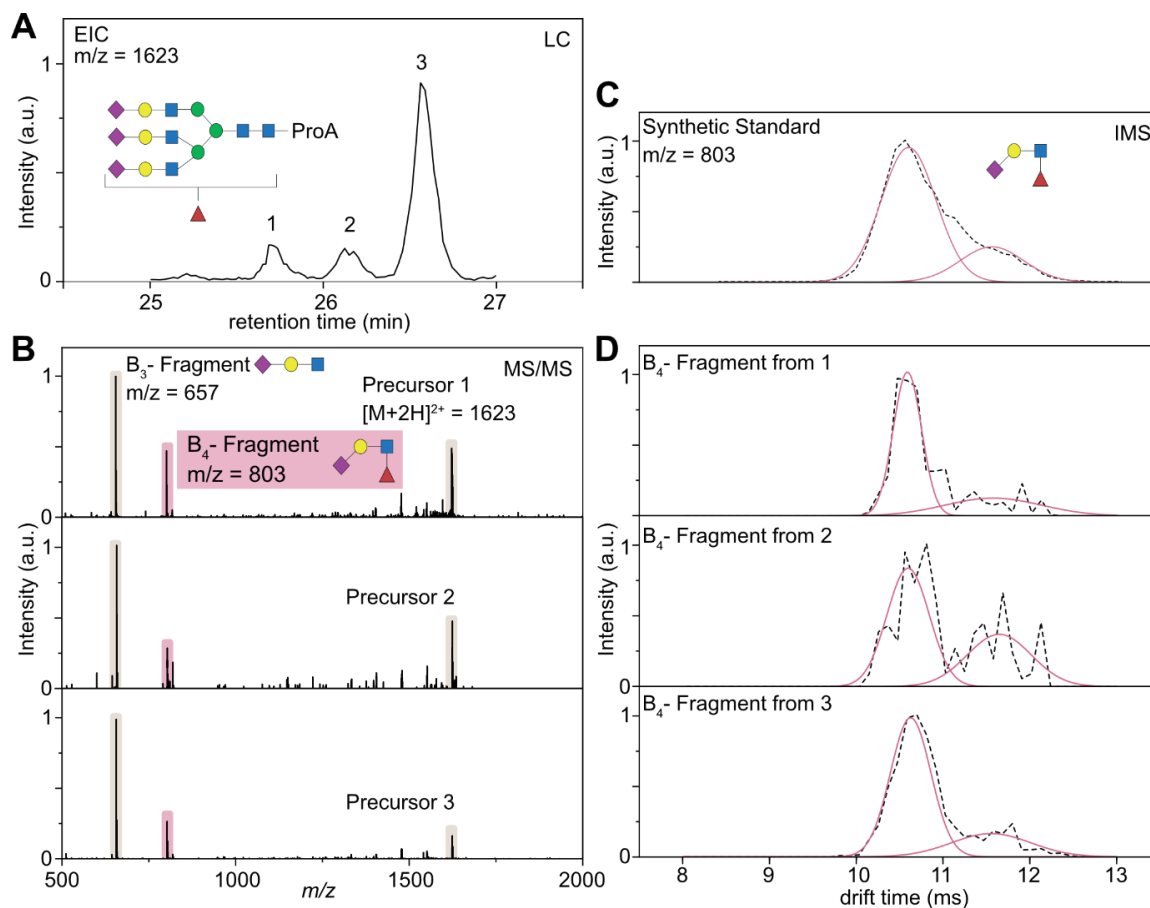


**Figure S-4:** Determination of fucosylation pattern for triantennary species. (a) Extracted ion chromatogram (EIC) of a triply sialylated triantennary glycan with one fucose attached ( $m/z = 1623$ ). (b) MS/MS spectra of the precursor ions 1 to 3 which are almost identical and show the dominant  $B_3$  trisaccharide fragment. In addition, all three species show the characteristic  $B_4$  fragmentation (highlighted in red) which indicates antenna fucosylation. (c) Mobilogram of a synthetic standard (3'-Sialyl-Lewis-X). (d) Mobilograms of the  $B_4$  fragment generated from all precursor ions. Comparison with the synthetic standard allows to identify the fucose isoforms and confirm the native state of the fucosylation. As the fucosylated species are generally low in intensity (especially in positive ion mode) the right shoulder of the ATD at  $\sim 11.6$  ms exhibits a very low S/N ratio. The main signal at 10.5 ms, however, can still be used for unambiguous assignment of the ATD.

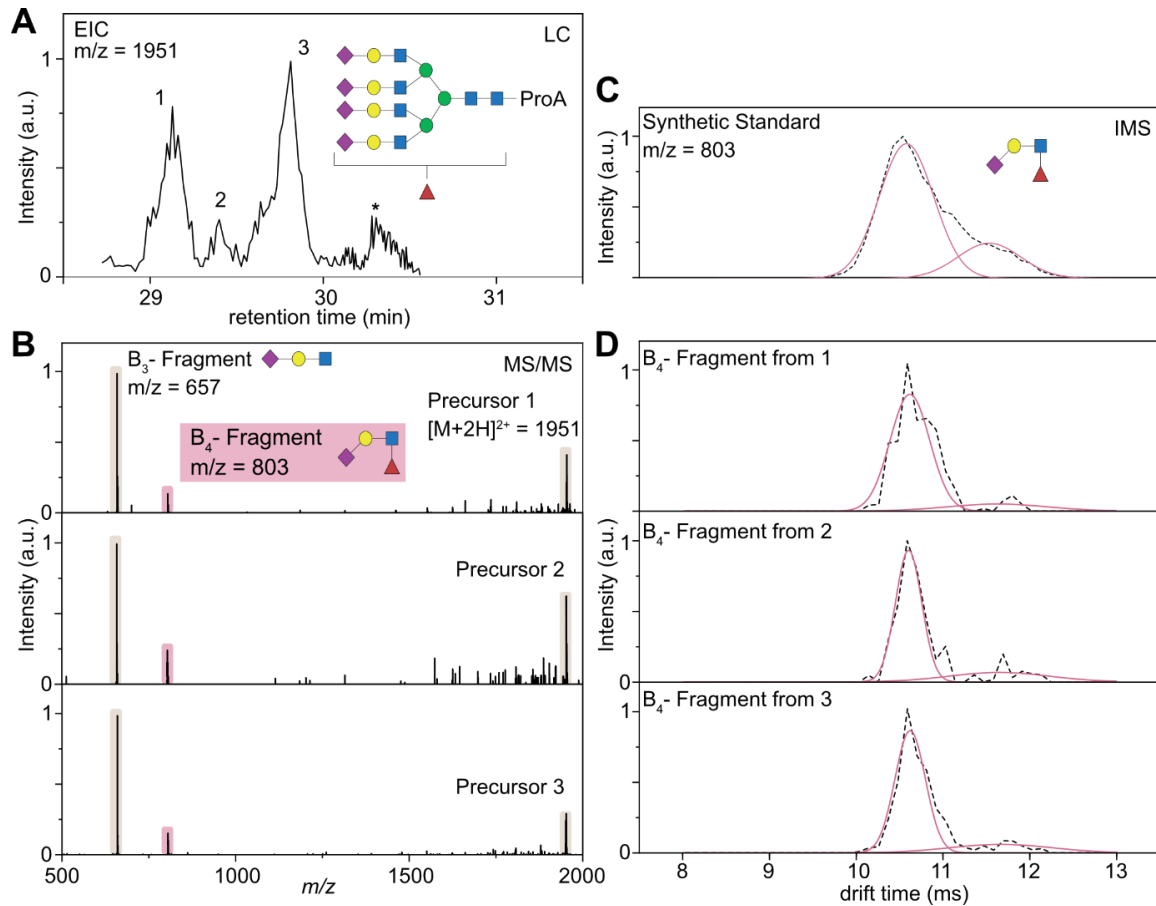


**Figure S-5:** Determination of fucosylation pattern for tetraantennary species. (a) Extracted ion chromatogram (EIC) of a quadruply sialylated tetraantennary glycan with one fucose attached ( $m/z = 1951$ ). (b) MS/MS spectra of the precursor ions 1 to 3 which are almost identical and show the dominant B<sub>3</sub> trisaccharide fragment. In addition, all three species show the characteristic B<sub>4</sub> fragmentation (highlighted in red) which indicates antennary fucosylation. (c) Mobilogram of a synthetic standard (3'-Sialyl-Lewis-X). (d) Mobilograms of the B<sub>4</sub> fragment generated from all precursor ions. The intensity of the large tetraantennary species is very low in positive ion mode and therefore the fragment intensity is even lower. Therefore, the shoulder on the right-hand side of the ATD at ~11.6 ms is almost non-existent. The main signal at 10.5 ms, however, can still be used for unambiguous assignment of the ATD.

## Appendix B Internal Dextran Calibration

### Supporting Information for Chapter 5: Dextran as Universal Calibrant for N-Glycan Analysis by Liquid Chromatography Coupled to Ion Mobility-Mass Spectrometry

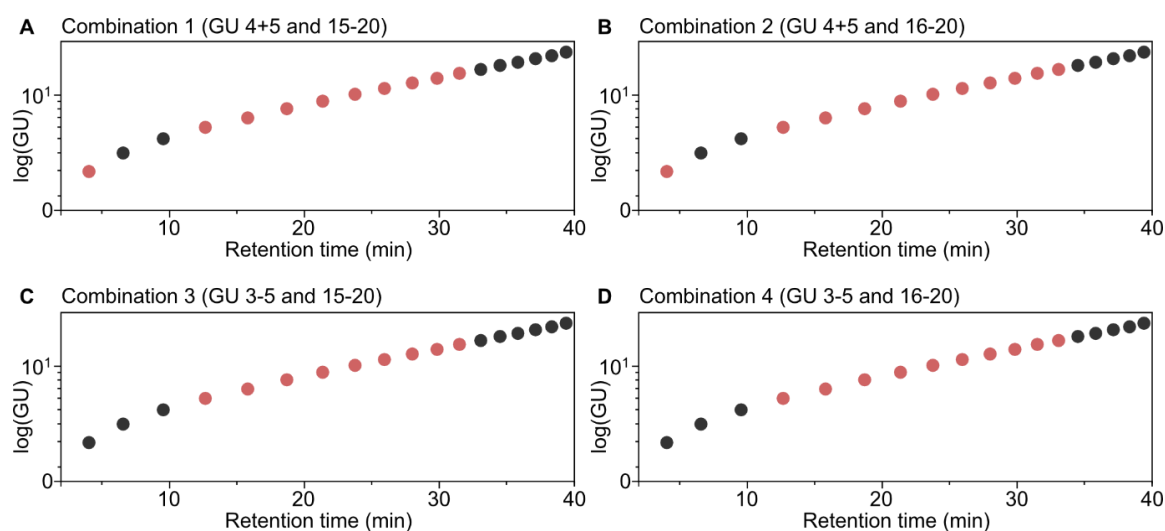


**Figure S-6:** Generation of polynomial fits for different combinations of minimized dextran ladder. GU 1 and GU 2 (dextran mono- and disaccharides) are ignored in all cases, as they elute early together with access label and salts and therefore are impractical to use for accurate calibration curves. As described in the main manuscript, GU 6-14 are also left out to leave an N-glycan elution window. Only GU 3-5 and 15-20 are therefore considered for an accurate fit. To determine the accuracy of the respective fit, we generate a polynomial of fifth grade only based on the reduced number of data points (individual for each combination) and used the resulting equation to generate absolute GU values (see table S-2). (a) Combination 1 utilizes 8 data points (GU 4+5 and 15-20). (b) Combination 2 utilizes 7 data points (GU 4+5 and 16-20). (c) Combination 3 utilizes 9 data points (GU 3-5 and 15-20). and (d) Combination 4 utilizes 8 data points (GU 3-5 and 16-20).

**Table S-7:** Calculated GU values for the different combinations of the minimized dextran ladder. Gu values are calculated based on the polynomial fit generated in figure S-1. The theoretical GU values serve as reference to evaluate the calculated GU values for the different combinations. The GU values in the range of 6-14 are highlighted as the majority of N-glycans should elute in this time frame. The calculated GU values in this range should therefore be as accurate as possible to calibrate for actual samples. Combination 1 shows the highest accuracy in this range (deviations <0.02) and exhibits very similar values to the theoretical GU values and the external GU calibration which utilizes all data points. Combinations 2-4 show larger deviations up to 0.1 GU, especially in the smaller GU range of 6-11. Therefore, less data points than the ones used in combination 1 seem impractical and were not further tested.

<b>Retention time (min)</b>	<b>GU theo</b>	<b>GU all data points</b>	<b>Combi 1</b>	<b>Combi 2</b>	<b>Combi 3</b>	<b>Combi 4</b>
3.88	3	29.3	3.08	3.04	3.00	3.00
6.25	4	3.99	4.00	4.00	4.00	4.00
9.20	5	5.04	5.00	5.00	5.00	5.00
12.37	6	<b>6.03</b>	<b>6.00</b>	<b>5.98</b>	<b>5.96</b>	<b>5.95</b>
15.49	7	<b>6.99</b>	<b>7.00</b>	<b>6.95</b>	<b>6.91</b>	<b>6.90</b>
18.39	8	<b>7.98</b>	<b>7.99</b>	<b>7.93</b>	<b>7.83</b>	<b>7.87</b>
21.05	9	<b>8.98</b>	<b>8.98</b>	<b>8.93</b>	<b>8.88</b>	<b>8.86</b>
23.48	10	<b>9.99</b>	<b>9.98</b>	<b>9.94</b>	<b>9.89</b>	<b>9.88</b>
25.69	11	<b>11.01</b>	<b>10.99</b>	<b>10.95</b>	<b>10.92</b>	<b>10.91</b>
27.71	12	<b>12.02</b>	<b>11.99</b>	<b>11.97</b>	<b>11.95</b>	<b>11.94</b>
29.55	13	<b>13.02</b>	<b>12.99</b>	<b>12.98</b>	<b>12.97</b>	<b>12.96</b>
31.26	14	<b>14.01</b>	<b>14.00</b>	<b>13.99</b>	<b>13.99</b>	<b>13.98</b>
32.83	15	15.00	15.00	15.00	15.00	14.99
34.28	16	15.99	16.00	16.00	16.00	16.00
35.62	17	16.98	17.00	17.00	17.00	17.00
36.88	18	17.98	18.00	18.00	18.00	18.00
38.06	19	19.00	19.00	19.00	19.00	19.00
39.16	20	20.02	20.00	20.00	20.00	20.00

**Table S-8:** GU deviation between external and internal dextran calibration for the released glycans of IgG. The differences in absolute GU values (between external and internal calibration) and the difference relative to the GU value from the external calibration are broken down for each glycan species of human IgG.

<b>LC peak no.</b>	<b>Glycan</b>	<b>GU int</b>	<b>GU ext</b>	<b>Deviation (abs.)</b>	<b>Deviation (in %)</b>
1	FA2	5.66	5.70	0.04	0.70
2	FA2B	6.05	6.07	0.02	0.33
3	FA2G1	6.41	6.42	0.01	0.16
3	FA2G1	6.52	6.53	0.01	0.15
4	FA2BG1	6.71	6.71	0.00	0.00
5	FA2G2	7.21	7.25	0.04	0.55
6	FA2BG2	7.47	7.46	0.01	0.13
7	FA2G2S1	8.28	8.29	0.01	0.12
8	FA2BG2S1	8.41	8.40	0.01	0.12
9	FA2G2S2	9.55	9.59	0.04	0.42
10	FA2BG2S2	9.73	9.77	0.04	0.41
			<b>Avg. deviation</b>	<b>0.02 GU</b>	<b>0.28%</b>

**Table S-9:** Comparison of calculated internal and external GU values of IgG with database values. The calculated values of the internal dextran ladder (8 data points) are in very good agreement with reference GU values from glycostore. The biggest deviation is 0.21 GU for FA2BG2S1, while the average deviations is around 0.106 GU. The error is therefore well below 1.5% for all identified glycans from IgG. A similar picture can be seen for the external calibration. Although the largest deviation is a little bit bigger with 0.23 GU for the largest glycan FA2BG2S2, the general trends for deviations are very similar and the average deviation is roughly the same with 0.114 GU.

<b>Glycan</b>	<b>GU ref</b>	<b>GU int</b>	<b>deviation (abs)</b>	<b>deviation (%)</b>	<b>GU ex</b>	<b>deviation (abs)</b>	<b>deviation (%)</b>
FA2	5.66	5.66	0.00	0.00	5.70	0.04	0.71
FA2B	6.06	6.05	0.01	0.17	6.07	0.01	0.17
FA2G1	6.48	6.41	0.07	1.08	6.42	0.06	0.93
FA2G1	6.60	6.52	0.08	1.21	6.53	0.07	1.06
FA2BG1	n.A.	6.71	n.A.	n.A.	6.71	n.A.	n.A.
FA2G2	7.35	7.21	0.14	1.90	7.25	0.10	1.36
FA2BG2	7.56	7.47	0.09	1.19	7.46	0.10	1.32
FA2G2S1	8.39	8.28	0.11	1.31	8.29	0.10	1.19
FA2BG2S1	8.62	8.41	0.21	2.44	8.40	0.22	2.55
FA2G2S2	9.39	9.55	0.16	1.70	9.59	0.20	2.13
FA2BG2S2	9.54	9.73	0.19	1.99	9.77	0.23	2.41
	<b>Avg. dev.</b>		<b>0.11 GU</b>	<b>1.30%</b>		<b>0.11 GU</b>	<b>1.38%</b>

**Table S-10:** Absolute CCS values of the dextran ladder obtained by direct infusion IM-MS. All CCS values are measured in nitrogen in positive ion mode for the singly protonated (1+) or doubly protonated (2+) species. The singly charged species of dextran can be seen up to the 7-mer, while the doubly charged species almost cover a range from GU 3 to GU 20. This list of absolute  $^{DT}CCS_{N_2}$  is used to generate the calibration curve for estimating  $^{TW}CCS_{N_2}$  values.

Glycan	m/z	z	m	CCS (in Å <sup>2</sup> )
Dextran GU 1	400.24	1	400.24	212.64
Dextran GU 2	562.29	1	562.30	228.05
Dextran GU 3	724.34	1	724.35	256.11
Dextran GU 4	886.39	1	886.40	283.82
Dextran GU 5	1048.45	1	1048.45	308.92
Dextran GU 6	1210.50	1	1210.50	329.58
Dextran GU 7	1372.56	1	1372.56	352.46
Dextran GU 3	362.67	2	724.35	325.01
Dextran GU 4	443.70	2	886.40	327.72
Dextran GU 5	524.72	2	1048.45	331.75
Dextran GU 6	605.75	2	1210.50	354.02
Dextran GU 7	686.78	2	1372.56	373.15
Dextran GU 8	767.80	2	1534.61	392.75
Dextran GU 9	848.83	2	1696.66	411.96
Dextran GU 10	929.85	2	1858.72	430.14
Dextran GU 11	1010.88	2	2020.77	444.69
Dextran GU 12	1091.91	2	2182.82	461.99
Dextran GU 13	1172.93	2	2344.87	478.73
Dextran GU 14	1253.96	2	2506.93	498.37
Dextran GU 15	1334.99	2	2668.98	517.84
Dextran GU 16	1416.02	2	2831.03	534.17
Dextran GU 17	1497.04	2	2993.08	550.28
Dextran GU 18	1578.07	2	3155.14	566.94
Dextran GU 19	1659.10	2	3317.19	582.57
Dextran GU 20	1740.12	2	3479.24	593.90

**Table S-11:** Comparison of calculated and theoretical CCS from human IgG. All CCS values are given in Å<sup>2</sup> and measured in nitrogen in positive ion mode as doubly protonated (2+) species. The absolute <sup>DT</sup>CCS<sub>N<sub>2</sub></sub> of IgG were measured *via* direct injection IM-MS and are used here to evaluate the accuracy of the external and internal calibration. The estimated <sup>TW</sup>CCS<sub>N<sub>2</sub></sub> are generated *via* a calibration excel sheet created in the working group. \* In short, the absolute CCS from dextran (**Table S-10**) and the measured TWIMS drift times of each dextran oligosaccharide are used to generate a calibration curve. By using the TWIMS drift time of the IgG glycan, the CCS of the sample can be estimated with help of the calibration curve.

Glycan	MS peak no.	m/z	z	<sup>DT</sup> CCS <sub>N<sub>2</sub></sub>	<sup>TW</sup> CCS <sub>N<sub>2</sub></sub> internal	Devi. (in %)	<sup>TW</sup> CCS <sub>N<sub>2</sub></sub> external	Dev. (in %)
FA2	1	841.89	2	424.56	420.16	1.04	420.33	1.00
FA2B	3	943.43	2	448.41	454.90	1.45	454.92	1.45
FA2G1	2	922.92	2	446.58	440.34	1.40	440.43	1.38
FA2G2	4	1003.94	2	467.16	468.73	0.34	468.69	0.33
FA2BG1	5	1024.46	2	461.20	453.73	1.62	453.76	1.61
FA2BG2	6	1105.48	2	491.71	490.91	0.16	490.76	0.19
FA2G2S1	7	1149.49	2	479.72	481.5	0.37	481.4	0.35
FA2BG2S1	8	1251.03	2	494.34	490.61	0.75	490.47	0.78
FA2G2S2	9	1295.04	2	520.13	518.21	0.37	517.93	0.42
FA2BG2S2	10	1396.58	2	530.22	530.26	0.01	529.92	0.06
					<b>Avg. dev.</b>	<b>0.75%</b>		<b>0.76%</b>

\*The calibration process in general and the utilized excel spreadsheet can be found here: [www.bcp.fu-berlin.de/en/chemie/chemie/forschung/OrgChem/pagel/research/carbohydrates/index.html](http://www.bcp.fu-berlin.de/en/chemie/chemie/forschung/OrgChem/pagel/research/carbohydrates/index.html)

For further information see: Hofmann, J.; Struwe, W. B.; Scarff, C. A.; Scrivens, J. H.; Harvey, D. J.; Pagel, K. Estimating Collision Cross Sections of Negatively Charged N-Glycans Using Traveling Wave Ion Mobility-Mass Spectrometry. *Anal. Chem.* **2014**, *86*, 10789-10795.

## List of Publications

1. C. Manz, K. Pagel; Glycan analysis by ion mobility-mass spectrometry and gas-phase spectroscopy, *Current Opinion in Chemical Biology* **2018**, 42, 16-24.
2. M. Lettow, E. Mucha, C. Manz, D. A. Thomas, M. Marianski, G. Meijer, G. von Helden, K. Pagel; The role of the mobile proton in fucose migration, *Analytical and Bioanalytical Chemistry* **2019**, 411, 4637-4645.
3. C. Manz, K. Pagel; Ionenmobilitätsmassenspektrometrie zur Strukturaufklärung von Milchzuckern, *chrom+food FORUM* **2019**, 3, 24-26, Sonderedition zur ANAKON 2019 Münster.
4. C. Manz, M. Grabarics, F. Hohberg, M. Pugini, A. Stuckmann, K. Pagel; Ion mobility-mass spectrometry of isomeric glycans – the impact of reducing end modifications, *Analyst* **2019**, 144, 5292-5298.
5. T. Wiglenda, N. Groenke, W. Hoffmann, C. Manz, L. Diez; A. Buntru, L. Brusendorf, N. Neuendorf, S. Schnoegl, P. Schmieder, K. Pagel, E.E. Wanker; Sclerotiorin Stabilizes the Assembly of Nonfibrillar Abeta42 Oligomers with Low Toxicity, Seeding Activity, and Beta-sheet Content, *Journal of Molecular Biology* **2020**, 432, 2080-2098.
6. L. Urner, M. Schulze, Y. Maier, W. Hoffmann, S. Warnke, I. Liko, K. Folmert, C. Manz, C. Robinson, R. Haag, K. Pagel; A new azobenzene-based design strategy for detergents in membrane protein research, *Chemical Science*. **2020**, 11, 3538-3546.
7. C. Manz, K. Pagel, Fluoreszenzmarkierung isomerer Zucker - Kombination von Flüssigkeitschromatographie und Ionenmobilitätsmassenspektrometrie zur Analyse von Glykanen, *GIT Laborfachzeitschrift* **2020**, 3/20, 20–21.
8. R. Miller, S. Guimond, R. Schwörer, O. Zubkova, P. Tyler, Y. Xu, J. Liu, P. Chopra, G.J. Boons, M. Grabarics, C. Manz, J. Hofmann, N. Karlsson, J. Turnbull, W. Struwe, K. Pagel, Shotgun ion mobility mass spectrometry sequencing of heparan sulfate saccharides, *Nature Communication* **2020**, 11, 1481.
9. C. Pappas, P. Mandal, B. Liu, B. Kauffmann, X. Miao, D. Komaromy, W. Hoffmann, C. Manz, R. Chang, K. Liu, K. Pagel, I. Huc, S. Otto, Emergence of low-symmetry foldamers from single monomers, *Nature Chemistry* **2020**, 12, 1180-1186.

10. M. Grabarics, M. Lettow, C. Kirschbaum, K. Greis, C. Manz, K. Pagel, Mass Spectrometry-Based Techniques to Elucidate the Sugar Code, *Chemical Reviews* **2022**, 122, 8, 7840–7908.
11. C. Manz, M. Mancera-Arteu, A. Zappe, E. Hanozin, L. Polewski, E. Giménez, V. Sanz-Nebot, K. Pagel, Determination of Sialic Acid Isomers from Released N-Glycans Using Ion Mobility Spectrometry, *Analytical Chemistry* **2022**, 94, 39, 13323–13331.
12. C. Manz, C. Frank, A. Zappe, M. Götze, K. Pagel, Dextran as internal calibrant for N-glycan analysis by liquid chromatography coupled to ion mobility-mass spectrometry, *Analytical and Bioanalytical Chemistry* **2022**, 414, 5023–5031.